AD648400

RADIATIVE TRANSFER IN A GAS OF UNIFORM PROPERTIES IN LOCAL THERMODYNAMIC EQUILIBRIUM

PART 3: A DETAILED CALCULATION FOR NITROGEN

B. L. HUNT and M. SIBULKIN

D D C

MAR 1 7 1967

B

Report No.
Nonr-562 (35)/18

December 1966

RADIATIVE TRANSFER IN A GAS OF UNIFORM PROPERTIES

IN LOCAL THERMODYNAMIC EQUILIBRIUM

PART 3: A DETAILED CALCULATION FOR NITROGEN

by

Brian L. Hunt and Merwin Sibulkin

Division of Engineering
Brown University
Providence, Rhode Island

December 1966

This report describes a calculation of radiative transfer in nitrogen.
The gas is uniform and in local thermodynamic equilibrium. The temperatures
and densities used in the calculations range from 5,000°K to 35,000°K and
from 10^{-5} atmospheres to 10^{-1} atmospheres respectively.

Radiative transfer due to the lines is computed by techniques developed
in Part 1 of this series of reports. Between 150 and 250 small clusters
of nonhydrogenic lines are treated individually (the exact number depends
on the conditions); each cluster contains, on the average, 3 or 4 lines.
The remaining lines are treated as hydrogenic or accounted for by the use
of extensions of the continuum absorption coefficients. The lines are
classified into various groups and the contribution of each group to the
overall radiation from the gas is distinguished. The reduction in line
intensity due to the background continuum is allowed for. The intensity
due to a combination of up to 18 types of continuum and pseudo-continuum
processes is computed with exact allowance for self-absorption. The results
for the total intensity and the relative contributions of selected groups
of contributors are presented graphically. In addition, an equivalent
gray gas absorption coefficient is defined and the values presented.

The results of the calculation demonstrate that, in most cases, the
atomic and ionic lines are the most important contributors. The exceptions
to this occur at high densities (10^{-1} atmospheres), where the bound-free
continua dominate, and at low temperatures (c. 5000°K), where molecular bands
are most important. When the gas is highly ionized, the dominant contributors
are a few strong lines arising from same-shell transitions which have low-
lying initial energy levels and are situated in the near ultra violet. A
further interesting and unexpected result is that the intensities of the

strongest lines are often significantly influenced by Doppler broadening
of the line profiles.

TABLE OF CONTENTS

LIST OF TABLES

PRINCIPAL SYMBOLS

a	constant used in the directionally approximate flux equation (see Appendix I)
A	line wwdth constant for Stark broadening
A_{res}	line width constant for resonance broadening
b	constant used in the directionally approximate flux equation (see Appendix I)
B	frequency integrated Planck function
B_ν	Planck function
c	velocity of light in a vacuum
D	width of a group of lines
e	charge of electron
E_i	energy of the ith electronic level
E_T	ionization energy
$f_{\ell u}$	absorption oscillator strength for a transition form state ℓ to state u
g_i	statistical weight of state i
$g_{n\ell}(\nu)$	bound-free Gaunt factor
$g_{ff}(\nu,kT)$	free-free Gaunt factor
h	Planck's constant
I_ν	specific intensity of radiation
I	frequency integrated specific intensity of radiation, $\int_0^\infty I_\nu d\nu$.
J	inner quantum number
k	Boltzmann's constant

K_ν linear spectral absorption coefficient

$\bar{K}$ equivalent gray gas absorption coefficient (see Eq. (4.8))

$\bar{K}_p$ Planck mean absorption coefficient

ℓ orbital angular momentum quantum number

ℓ slab thickness

L total orbital angular momentum quantum number

m lower state principal quantum number

$\bar{m}$ m corresponding to the first high series which is completely merged according to effective widths or is completely optically thin

m_e mass of electron

M^* effective number of clusters in a group of lines

n principal quantum number

$\bar{n}$ upper state principal quantum number of the first high line which is either merged according to its effective width or optically thin

N^* effective number of lines in a group

N_e number density of electrons

N_L Loschmidt number $(2.6871 \times 10^{19} \text{ cm}^{-3})$

N_S number density of species S

$\bar{N}_S$ N_S/N_L

NI,NII, etc.   first, second, etc. spectrum of nitrogen (i.e. spectra associated with N, N^+, etc. respectively)

q_ν^+, q_ν^- half-range radiative fluxes defined in Appendix I

Q_S electronic partition function of species S

Ry Rydberg energy constant

s path length

S	total spin angular momentum quantum number
T	temperature
w	Stark line width parameter
w_D	line semi-half-width due to Doppler broadening
z	number of charges
η_ν	optical depth in a plane slab measured perpendicular to the slab faces
λ	wavelength
ν	frequency
ν_o	central frequency of a line
ν_T	frequency of an ionization threshold
ρ	density
ρ_o	$m_{N_2} N_L$ $(1.25 \times 10^{-3}$ gm cm$^{-3})$
σ	radial matrix element for a bound-bound transition
σ_ν	spectral absorption coefficient
$\mathcal{S}(\cdot)$	relative strength of a line within a multiplet
$\mathcal{S}(\cdots)$	relative strength of a multiplet within a transition array
ψ_{core}	factor accounting for the radiation from high series, see Eq. (3.5)

1. INTRODUCTION

This part of the work is concerned with the calculation of the specific intensity of radiation in a volume of nitrogen gas where the properties are uniform and the gas is in local thermodynamic equilibrium. It is shown in Section 4.1 that the results presented can easily be rescaled to give the flux from a uniform, plane slab of nitrogen which has transparent boundaries and no incident radiation. The range of thermodynamic states of the gas and path lengths were chosen to approximately correspond to conditions produced by a space vehicle reentering the earth's atmosphere. Particular interest was taken in the atomic and ionic line radiation because the importance of lines as a mechanism for transporting energy under these conditions has been debated.

Relevant previous work which included line radiation is that of Vorobyov and Norman[13] or nitrogen and of Allen[14] on air.

The calculations presented here are based on the techniques developed in Parts 1 and 2. Chapter 2 discusses and presents tables of the data used to represent the lines. Chapter 3 discusses the data used for the continuum processes. Finally, Chapter 4 describes and presents the calculation and its results.

2. SPECTRAL LINE DATA

2.1 Introduction

In a hydrogenic gas (i.e. where a single electron experiences a Coulomb potential) the spectral lines have distributions in both frequency and oscillator strength which may be expressed as simple analytic expressions. In a non-hydrogenic gas, however, the electron fields interact and, except close to a photoionization edge, the hydrogenic distributions do not even approximately describe the line spectrum. Since it is the non-analytic lines which are of most importance in radiative transfer, the treatment of lines has to be based on the spectrum as obtained from experiment or predicted by approximate theoretical methods.

The frequency distribution of lines is determined by the arrangement of energy levels of the atom and ions. Section 2.2 is therefore devoted to describing the energy level structure of nitrogen with the aid of a number of diagrams.

Section 2.3 discusses the method used to obtain oscillator strengths and derives expressions for the relative multiplet strengths in some cases for which values have not previously been tabulated.

Section 2.4 considers the application of the methods developed in Part 2 to the weak lines of nitrogen.

The treatment of line profiles which was discussed at length in Part 1, Chap. 4 is summarized in Section 2.5.

Section 2.6 describes the calculation of the data necessary for computing the intensity of a group of closely spaced lines.

The detailed line spectrum of nitrogen is extremely complicated and in order to carry out radiative transfer calculations it is necessary to reduce the number of lines by combining them into groups wherever possible. This process has been carried out for the first four spectra of nitrogen. Whenever

approximations have been made by combining lines into groups, the aim has been to restrict the resulting error in the total specific intensity of the gas to a few percent, both under optically thin and self-absorbed conditions. Comments on the approximations are to be found in Section 2.7 for lines of NI, in Section 2.8 for lines of NII, in Section 2.9 for lines of NIII and in Section 2.10 for lines of NIV. Detailed tabulations of the data assembled for the grouped lines is collected in Tables 2.3 to 2.14 at the end of this chapter. The sources of this data are given in Section 2.11.

Lines which are not listed individually in the Tables at the end of this Chapter and which are not part of the pseudo-continua (see Section 2.4) were treated either by approximate extensions of the line series to which they belong (used for the high lines of low-lying series, see Section 2.3) or by the use of hydrogenic formulae (used for lines from highly excited initial states, again see Section 2.3).

2.2 Energy Levels

The energy level diagrams of the radiating particles are of great importance in line radiative transfer because the energy transferred in each transition depends on the lower energy level through the occupation number and on the difference in energy levels (i.e. the frequency) through the oscillator strength and the Planck function. In addition, the energy level structure determines (for a given line width) whether or not the line overlaps its neighbors (see Part 1. Section 3 4).

The energy levels of hydrogen are distributed in a very regular manner such that differences in spin and angular momentum cause splitting which is much less than the energy differences due to the principal quantum number, n (i.e. total momentum). For example, states with $n = 2$ suffer the greatest separation which is about 5×10^{-5} eV compared to a difference

of 1.9 eV between the $n = 2$ and $n = 3$ states. In contrast, the lower
levels of a non-hydrogenic material are widely split by differences in spin
and angular momentum. The order of increasing effectiveness in splitting
levels for a given electron configuration is J, L and S, ℓ and the core
term. This can be seen for nitrogen by referring to Fig. 1 which shows the
energy levels of atomic nitrogen over the range 10 eV to 13.5 eV and to
Figs. 2, 3 and 4 which apply to N, N^+ and N^{++} respectively over
wider ranges. These diagrams will be of assistance in the detailed discus-
sion of the next paragraph.

Differences in values of J produce very small differences in energy
(typical splitting is 10^{-3} eV to 10^{-1} eV). The width of the resulting
multiplet is so small that the Planck function and Boltzmann distribution
function are essentially constant across the width. At low densities, the
line half-width is much smaller than the multiplet splitting and the lines
are effectively isolated. At high densities, however, the effective line
width can be considerably larger than the multiplet splitting and the whole
multiplet behaves like a single degenerate line (see the discussion in
Part 1, Section 3.4). At high values of ℓ (and of n) the term splitting
can be almost as small as the multiplet splitting but at lower values it is
larger and then the resulting differences in Planck and Boltzmann functions
must be taken into account.

Differences in ℓ can produce enough splitting to span the gap between
energies with different values of n, the effect being greatest for low
values of ℓ (and n). Finally, the splitting due to different core terms
can be very large; each core term corresponds to a term of the ion which
results when the jumping electron is removed so that the core term splitting
is of the order of the term splitting of the residual ion. Unlike the other
forms of splitting discussed above, core term splitting does not decrease

with increasing n.

The values of energy level used in this report were obtained either from experimental values compiled by Moore[1] or from the approximate predictions of Gilmore,[2] occasionally supplemented by other sources or approximate methods, these are indicated in Section 2.11.

2.3 Calculation of Oscillator Strengths

A general discussion of the methods available for calculating oscillator strengths has been given earlier (Part 1, Section 3.2). This section gives further details of the method chosen.

We recall from Part 1, Section 3.2 that the oscillator strength for a line is

$$g_J f_{JJ'} = \mathcal{J}(\mathcal{L}) \, g_L f_{LL'}$$

$$= 2.45 \times 10^{-2} (h\nu \text{ eV}) \mathcal{J}(\mathcal{L}) \, \mathcal{J}(\mathcal{M}) \, \sigma^2 \tag{2.1}$$

where,

$$g_J = 2J + 1 \quad \text{and} \quad g_L = (2S+1)(2L+1).$$

$\mathcal{J}(\mathcal{L})$ is tabulated for all cases of interest in Ref. 3. In most cases, $\mathcal{J}(\mathcal{M})$ may also be found from Ref. 3 supplemented by Ref. 4. An important exception is the ultraviolet same-shell transition array $s^2 p^3 - s p^4$ (where, for the purposes of obtaining $\mathcal{J}(\mathcal{M})$, the principal quantum numbers of the sub-shells are irrelevant). However, Rohrlich (Ref. 5, p. 446) shows that the values of $\mathcal{J}(\mathcal{M})$ are the same as those of the transition array $p^3 - s p^2$, which is included in Allen's tabulation.

Another type of transition array which is not given by Allen is $s^2 p^3 - s p^3 \cdot p$ (where the point indicates that one p-electron is not equivalent because of a difference in principal quantum number). It is not

difficult to demonstrate that the only parentage splitting of s^2p^3 results from the positive or negative spin of the passive s-electron, i.e. each term $(2S+1)_L$ of s^2p^3 has two parent terms $(2S+2)_L$ and $2S_L$ of sp^3. From the paper of Rohrlich[5] an expression for $\int(\mathcal{M})$ can be obtained as follows. Applying Ref. 5 Eq. (17) to the transition

$$p^3\left(^{(2S+1)}L\right)s^{(2S_1+1)}Lnp^{(2S+1)}L' - p^3\left(^{(2S+1)}L\right)s^2(^1S)^{(2S+1)}L$$

where $S_1 = S \pm 1$ and $n > 2$, we get

$$\int(\mathcal{M}) = 2 \times 3 \times (2S+1)(2L'+1)(2S_1+1)(2L+1)(2L+1) \times$$

$$\times W^2(S, \tfrac{1}{2}, S, \tfrac{1}{2}; S_1, 0)W^2(0,0,L,L;0,L)W^2(L,0,L',1;L,1) \quad (2.2)$$

where $W(a,b,c,d;e,f)$ is the Racah coefficient. This latter quantity is tabulated in a number of places, the most extensive of which appears to be that of Nikiforov.[6] In the case where e is zero, the Racah coefficient takes on the simple form (Ref. 6, Eq. (3.2))

$$W(a,b,c,d;0,f) = (-1)^{b+c-f} \frac{\delta_{ab}\,\delta_{cd}}{\sqrt{(2b+1)(2c+1)}} \quad (2.3)$$

where $\delta_{\alpha\beta}$ is the Kronecker delta. The use of certain symmetry properties also given by Nikiforov makes possible the application of Eq. (2.3) to each of the Racah coefficients appearing in Eq. (2.2), after which the expression reduces to

$$\int(\mathcal{M}) = (2L'+1)(2S_1+1) \quad (2.4)$$

A third type of transition array for which no relative multiplet strength is tabulated is $sp^4 - sp^3 \cdot \ell$, here the expressions presented by Armstrong et al.[7] were used, the Jahn coefficient being transformed to a Racah coefficient according to the identity given by Edmonds[8] and values being taken from

Nikiforov's tabulation.[6]

The values of σ^2 available have been discussed in Part 1, Section 3.2. For the most part we have used the Hartree-Fock-Slater values tabulated by Kelly.[9] A comparison between oscillator strengths calculated from these values and the more accurate Hartree-Fock values also calculated by Kelly[10] for multiplets in the ultraviolet of NI is given in Table 2.1, also shown are values calculated by Griem[11] using the Bates-Damgaard method. It can be seen that the Hartree-Fock-Slater values are never more than a factor of 3 from the Hartree-Fock values and are usually much closer. In contrast, the Bates-Damgaard values are frequently low by an order of magnitude and no values are predicted for the strong lines corresponding to transitions within the same shell. Table 2.2 compares a few B-D and H-F-S values in the visible and infrared (no H-F values are available). Here the jumping electron is in a more nearly Coulomb field and both methods give similar values.

In the radiative transfer calculations presented here Hartree-Fock values of oscillator strength were used in the few cases where they were available otherwise lines from low-lying states were evaluated by means of Hartree-Fock-Slater values and lines from highly excited states by the hydrogenic expressions described in the next paragraph.

Where the end states of a transition are highly excited, the potential will be nearly that of a Coulomb field so that the energy levels and oscillator strengths will be approximately given by hydrogenic expressions. In addition, the total radiation from all such lines is usually quite small and any errors caused by using hydrogenic results for these lines will only have a small effect on the overall calculation of intensity. We therefore consider the transition $\gamma(^{(2S_c+1)}L_c)m\ell^{(2S+1)}L - \gamma(^{(2S_c+1)}L_c)n\ell'^{(2S+1)}L'$ where γ stands for the electronic configuration of the core. The hydrogenic

approximations to the initial energy level, frequency and oscillator strength are respectively,

$$E_m = E_T - \frac{Ryz^2}{m^2} \qquad (2.5)$$

$$h\nu = E_n - E_m = z^2 Ry \left(\frac{1}{m^2} - \frac{1}{n^2}\right) \qquad (2.6)$$

and

$$gf = g_{core} \frac{2^6}{3\sqrt{3}\,\pi} \left(\frac{1}{m^2} - \frac{1}{n^2}\right)^{-3} \frac{1}{m^3} \frac{1}{n^3} \qquad (2.7)$$

where z is the number of charges acting on the radiating electron, Ry is the energy of 1 Rydberg unit (= 13.605 eV), E_T is the energy of the ionization threshold above the species ground state, $g = g_{core} 2m^2$ is the statistical weight of the lower level, $g_{core} = (2S_c + 1)(2L_c + 1)$ is the statistical weight of the residual ion and the numerical value of $2^6/3\sqrt{3}\,\pi$ is 3.92.

It can be seen from Eq. (2.7) that as $n \to \infty$ gf becomes proportional to n^{-3}. Since the upper states of the high lines of any series experience a Coulomb field, the n^{-3} dependence is roughly true for all high lines. This provides us with an approximate but convenient method of dealing with the high lines in low series for which Kelly has not calculated any values of σ^2 (in most cases these are lines with $n > 10$). We treat all such lines as occurring at the ionization frequency and having weighted oscillator strengths given by

$$gf = constant/n^3 \qquad (2.8)$$

where the constant is evaluated from the last line for which there is a Hartree-Fock-Slater value of σ^2. It should be observed that the error involved in using Eq. (2.8) is completely negligible since this approximation is only used for the small number of lines for which no Hartree Fock-Slater value exists and which are self-absorbed but isolated.

2.4 Treatment of Weak Lines

In Part 2, Section 3.5 it was shown that all transitions above a certain initial level, $\bar{m}$, in a hydrogenic ion of charge $z+1$ can be accounted for by the expression

$$K_\nu = K_{\nu,ff} \frac{1}{Q_i} [\exp(z^2 Ry/(\bar{m})^2 kT) - 1] \tag{2.9}$$

where $K_{\nu,ff}$ is the absorption coefficient due to free-free transitions (see Section 3.3). The quantity $\bar{m}$ is chosen to be the initial quantum number of the first high series which is either completely merged according to effective widths or entirely optically thin. Since we are using a hydrogenic representation of the upper series and a hydrogenic free-free cross section, we can adopt Eq. (2.9) for the treatment of all high series.

For hydrogen, it has also been shown (Part 2, Section 3.3) that high lines in low series can be treated as extensions of the bound-free continuum provided that they are either optically thick and effectively merged, or optically thin. The same analysis performed on the assumed high-line oscillator strength, Eq. (2.8), would produce the hydrogenic ν^{-3} spectral variation but with a different general level determined by the constant. In most cases, this would not match the (non-hydrogenic) bound-free cross section at the threshold in either magnitude or slope because of the approximate nature of Eq. (2.8). While preserving Eq. (2.8) for any isolated, self-absorbed lines it is probably more accurate to treat other high lines by extending the non-hydrogenic bound-free cross section backwards. The slope of the bound-free cross section at the ionization threshold is only very approximately known from our treatment of the continuum (see Chap. 3) but the experience of calculated non-hydrogenic bound-free cross sections is that the slope at the threshold is usually small. We therefore make the extended continuum constant at its threshold value. In the case of a true

hydrogenic v^{-3} behavior at the $m = 1$ threshold, the use of a constant cross section would be responsible for a 12% underestimate of absorption coefficient at a frequency corresponding to $n = 5$ and for a 3% underestimate at $n = 10$; self-absorption would reduce these small errors even further.

2.5 Line Profiles

The difficult problem of line broadening has been discussed at length in Part 1, Chap. 4. It was shown there that lines with relatively low-lying upper states can be treated as having dispersion profiles with semi-half-widths given by electron impact theory with occasional additional contributions from resonance broadening (in the case of lines of NI) and from Doppler broadening. Part 1, Section 4.6 considers the case of lines with moderate or high energy upper states and concludes that they may be approximately treated as quasi-statically broadened (with the wing profile $L(v) \sim b/[v-v_o]^{2.5}$). Electron impact broadening and quasi-static broadening are both aspects of broadening by charged particles which is called in this report by the commonly accepted name of Stark broadening.

For ease of reference, the expressions for line semi-half-width first given in Part 1, Chap. 4 are repeated again here. The semi-half-width due to electron impact broadening is

$$w(eV) = A \, N_e/N_L [kT(eV)]^{1/6} \tag{2.10}$$

where A is either determined from Grier's results[11] (see Part 1, Section 4.5) or calculated from an adiabatic approximation (Part 1, Eqs. (4.20) and (4.21)).

The semi-half-width due to resonance broadening is given by

$$w(eV) = [(A_{res})_1 \exp(-E_1/kT) + (A_{res})_2 \exp(-E_2/kT)] \frac{N_N}{N_L} \frac{1}{(Q_{el})_N} \tag{2.11}$$

where

$$(A_{res})_i = 0.175 \left(\frac{g_i}{g_n}\right)^{1/2} g_i f_{iu} \frac{1}{h\nu_{iu}(eV)} \tag{2.12}$$

i being the lower state of the perturbing transition. The lower states which are considered to be sufficiently low-lying to contribute are $2s^2 2p^3\ ^4P$, $2s^2 2p^3\ ^2D$ and $2s^2 2p^3\ ^2P$.

The semi-half-width due to Doppler broadening is given in Part 1, Section 4.2. It is

$$w_D = \frac{\nu_0}{c} \sqrt{\frac{2kT}{m_R} \ln 2} \tag{2.13}$$

The line width parameter due to quasi-static broadening is given by

$$w = A(N_e/N_L + \sum_{z_p} z_p^2 N_{z_p}/N_L)^{2/3} \tag{2.14}$$

where

$$A = 0.691 \times 10^{-2}[(n')^2 - n^2]z_r^{-1} \tag{2.15}$$

If the lower state is not quasi-statically broadened, the value of n in Eq. (2.15) is taken to be zero.

Values of A are given in Tables 2.3 to 2.14 while the relation of these values to the formulae of this section is given in Section 2.11.

2.6 Multiplet Growth Parameters

Part 1, Sections 3.4 and 3.5 discussed the curve of growth of a closely-spaced group of lines. Some comments will be made here on three of the parameters introduced by that discussion.

The combined cluster width, D, was obtained by inspection of the energy levels listed by Moore.[1] In the case of states not covered by Moore's table, the width of a similar group of lines was used. No great effort at accuracy was made since the treatment of the transition region in which D plays a role is itself only an approximation.

Values of the effective number of lines, N^*, were calculated with some care for the lower, dispersion profile lines. The values used for the higher states are slightly less accurate for the following reason. Values of N^* for the higher states were first computed on the basis of dispersion profiles. It was subsequently decided to treat these lines as quasi-statically broadened. However, the labor of recalculating correct values of N^* using the revised profile was not felt to be justifiable. It turns out that the values used are slightly greater than the correct values.

The quantity M^*, the number of isolated clusters, is nearly always unity in the case of the quasi-statically broadened lines (where it is not unity, the slight error described in the previous paragraph occurs in this case also). The values of M^* used for the lines with dispersion profiles were calculated correctly but the choice of non-merging clusters is somewhat arbitrary and hence the values of M^* are also somewhat arbitrary.

2.7 Lines of NI

The study of hydrogen presented in Part 2 and the work of Biberman et al.[12,13] have shown that we may expect a few lines from low-lying states to be dominant in an optically thin slab but the higher lines to become of relatively greater importance as the optical thickness increases. When lines are optically thick, the position of the peak of the Planck function is an important parameter and the relative importance of any line from an excited state will be greatest when it is self-absorbed and near the maximum

of the Planck function.

We found for hydrogen that of two corresponding, self-absorbed lines
the one with the higher initial energy level can sometimes transport more
radiant energy because the higher line is at a lower frequency and (at
sufficiently low temperatures) lies nearer to the Planck maximum. In a
non-hydrogenic gas the same effect occurs but, in addition, parentage
splitting gives rise to lines which have high energy levels (and hence low
occupation numbers) but without any compensating reduction in frequency.
Because of this effect, the lines with the lowest energy core
($1s^2 2s^2 2p^2$ ^3P for NI) are the most important. A schematic representation of
the frequency distribution of the lines of NI, NII and NIII is drawn on
Fig. 5.

The expressions used for line widths have been given in Section 2.6.
The various broadening mechanisms were applied as follows to the lines of
NI. Resonance broadening was allowed for in the cases of lines with
$2s2p^4$, $2s^2 2p^2 (^3P)3s$ or $2s^2 2p^2 (^3P)3d$ upper states, details may be found
in Tables 2.3b, 2.4b and 2.5b. Doppler broadening was allowed for on all
2s-2p transitions. Stark broadening was allowed for in all lines.

It remains for us to state at which level the change from dispersion to
quasi-static profiles is considered to occur. In this context, it is unfor-
tunate for us that Griem's calculations[11] cover fewer lines of NI than of
NII and as a consequence we have no direct evidence of how to treat the
states 4d and 4f. Since the energy levels of NI are generally more closely
spaced than those of NII we can expect to find the onset of hydrogenic
behavior at a lower quantum number in NI than in NII. Therefore, for
want of a better method, we treat the 4d and 4f states of NI as quasi-
statically broadened.

A brief discussion of the lines of NI according to initial states now follows and full details of the data values used may be found in Tables 2.3 to 2.9 at the end of this chapter.

Initial Term $1s^2 2s^2 2p^3\ ^4S$

Lines from this term lie in the vacuum ultraviolet and he~ce are of greatest importance at high temperatures. Even at the highest temperature within our range (kT = 3 eV), the Planck maximum lies to the left of these lines (see Fig. 5) and hence, the most important lines tend to be those with the lowest frequencies. For this reason, transitions of the type 2p-nℓ are stronger than those of the type 2s-np. However, estimates indicate that the latter can carry up to 20% as much energy as the 2p-nℓ transitions.

For 2p-nℓ transitions, the pseudo-continuum is restricted to principal quantum numbers higher than 5. All available Hartree-Fock-Slater values of σ^2 have been used.

The 2s-np transitions are relatively weak and can be treated less carefully. Therefore Hartree-Fock-Slater values need be used for the first four lines only and the pseudo-continuum can be allowed to extend back to the leading line if necessary.

A complete list of the allowed transitions is given in Table 3a. Table 3b lists data for all lines for which Hartree-Fock-Slater values of σ^2 were used.

Initial Term $1s^2 2s^2 2p^3\ ^2D$

The comments made about the lines originating on the term $2s^2 2p^3\ ^4S$ also apply to the lines considered here. The treatment is identical with the exception that all multiplets with n = 3 or 4 and the same electronic configuration are grouped together. Lines with a $2s^2 2p^2(^1D)$ core also

occur; these are treated rather less carefully than those of (^{3}P).

Table 2.4a gives general information and a list of allowed transitions. Table 2.4b gives data for all lines for which Hartree-Fock-Slater values of σ^2 were used.

Initial Term $1s^2 2s^2 2p^3 \ ^2$P.

The treatment of the previous two sets of lines is followed. Lines with a ^{1}S core are weak and may be largely combined.

Table 2.5a gives general information and a list of allowed transitions. Table 2.5b gives data for all lines for which Hartree-Fock-Slater values of σ^2 were used.

Initial Term $2s2p^4 \ ^4$P

Lines originating on this state have relatively high values of frequency and hence are most important at high temperatures. The value of initial energy is high and hence these lines tend to be relatively weak. The single same-shell transition (to $2p^5 \ ^2$P) has a very high frequency and may be neglected.

Table 2.6a gives general information and a list of the transitions considered. Table 2.5b gives data for all lines for which Hartree-Fock-Slater values of σ^2 were used.

Initial Configuration $1s^2 2s^2 2p^2 (^{2S_c+1}L_c)3\ell$

There are many states consistent with this configuration and the associated energy levels cannot all be combined. Nevertheless, it is convenient to consider together all the line clusters from this group of initial states.

The set of transitions considered here includes a large number in which the jumping electron remains in the same shell. The lines associated with these transitions tend to have large values of oscillator strength and to lie fairly near (although usually below) the maximum of the Planck function.

Of the transitions involving different shells, by far the strongest are those with $3\ell-4\ell$ jumps. The $3\ell-4\ell$ transitions fall into roughly two classes, those with low values of σ^2 (s-p and p-d) and those with high values of σ^2 (p-s, d-p and d-f). The values of σ^2 of these two groups differ by up to two orders of magnitude but under conditions of self-absorption, estimates suggest that the first group are not completely negligible. However, their relative weakness enables the lines to be lumped into fewer groups. Another factor which frequently helps in the grouping of lines is the decrease of term splitting with rising angular orbital quantum number.

Lines with upper states such that $n \geq 5$ are weak and the upper states can be combined. Another group of relatively weak lines are those with a ^1D core. At most, these lines carry about half as much energy as those with a ^3P core. Another feature of lines with a ^1D core is that, as far as one can estimate, they have the same frequency as similar lines with a ^3P core. They have different initial energies, however, and are listed here separately from the ^3P core lines. In the computation of intensities, we take advantage of the coincidence of frequencies and combine the lines which have a ^1D core with the corresponding lines which have a ^3P core; the difference in initial energies is accounted for in the calculation of the occupation number. Lines with a ^1S core are completely negligible.

Table 2.7a lists the allowed transitions. Table 2.7b gives data for all lines for which Hartree-Fock-Slater values of σ^2 were used; this table classifies the lines into same-shell and different shell transitions.

Initial Configuration $1s^2 2s^2 2p^2 (^{2S_c+1}L_c)4\ell$

We can afford to be somewhat crude about the treatment of these lines since, due to their low occupation numbers and low frequencies they are weak compared to the 3-n transitions. A numerical investigation of the same-shell transitions shows that the 4-4 transitions are at most only about 10% as strong as the 3-3 transitions for temperatures above 0.5 eV. In particular, the very low frequencies of the 4d-4f transitions makes them completely negligible. Kelly does not give values of σ^2 for the 4f to ng transitions and we will neglect them; these transitions are probably comparable to other 4-n transitions but do not on their own give a significant contribution to the total radiation.

The allowed transitions are between the same types of terms as those originating from n = 3 states, the only exception is that 4f - ng transitions also exist. Since we are not including this additional type of transition in our calculation, we will not list the individual multiplets.

Table 2.8 gives details of the data used for all lines whose oscillator strengths were calculated from Hartree-Fock-Slater values of σ^2.

Initial Configurations with $n \geq 5$

All series with $n \geq 5$ are sufficiently weak and sufficiently highly excited to be treated as hydrogenic. We use the following factors to approximately allow for multiplet splitting:

$$N^* = 125 \text{ for } ^3P \text{ core }, \quad N^* = 52.7 \text{ for } ^1D \text{ core}$$

$$\text{and} \quad D = 0.15/n .$$

Same-shell transitions are negligible for $n \geq 7$ due to the very low frequencies and for n = 5 or 6 only the s-p and p-d transitions need

be included. The relevant data is given in Table 2.9.

2.8 Lines of NII

Over an important region of our range of conditions, the majority of
nitrogen particles are singly ionized. We therefore account for the lines
of NII in much the same way as the lines of NI. It is expected that the
relative importance of lines to continuum will decrease as the gas becomes
more highly ionized. This is because the energy levels of the ionic species
are more widely separated than those of the atom with the result that the
occupation numbers of the excited states are low and the frequencies of
transitions from the ground state are high.

Doppler broadening was allowed for on all 2s-2p transitions. States
with $n \geq 5$ were assumed to be quasi-statically broadened.

Initial Configuration $1s^2 2s^2 2p^2$

The lines originating from this configuration are less numerous than
those from the $2s^2 2p^3$ configuration of NI because there is no parentage
splitting when a 2p electron jumps. A further simplification can be made
by neglecting the 2s-np transitions on the grounds that they have extremely
large frequencies (>29 eV) and hence occur where the Planck function is very
small.

In calculating the electron impact line-widths of the same-shell
transitions (by adiabatic theory, see Part 1, Chap. 4), only the perturba-
tion of the lower state was considered because values of σ^2 for the transi-
tions $2s2p^3$-$2p^4$ are not available. In the case of the equivalent
transitions of NI this procedure is approximately correct.

Table 2.10a lists the allowed transitions. Table 2.10b gives detailed
data for all lines for which Hartree-Fock-Slater values of σ^2 were used.

Initial Configuration $2s^2 2p3\ell$

The allowed transitions from these states are the same as those for the ^3P core of NI, except that the multiplicity is always less by unity. The frequencies of these transitions are more widely spaced than those of the corresponding transitions in NI and thus their combination involves a greater percentage error. However, the relatively high values of initial energy level tend to make these lines comparatively weak.

Table 2.11 gives details of the line data for all lines for which Hartree-Fock-Slater values of σ^2 were used.

Initial Configurations with $n \geq 4$

All transitions of NII with $n \geq 4$ are treated as hydrogenic except the $n = 4$ s-p and p-d same-shell transitions which are listed in Table 2.12.

2.9 Lines of NIII

The treatment of these lines is made easier by the fact that they should be quite closely hydrogenic. This occurs because, in the most important transitions, the jumping electron is alone and outside a system of closed subshells.

We therefore use the self-consistent field-function values of σ^2 to calculate only the same-shell transitions and the $2s^2 2p - 2s^2 n\ell$ transitions. Details of these lines may be found in Table 2.13. Doppler broadening was allowed for in all the lines listed in Table 2.13.

2.10 Lines of NIV

There are a significant number of particles of N^{+++} present for conditions of interest to us only when the temperature is high and the density is low. Even under these conditions it seems probable that the lines will

be relatively weak on account of the very large differences between energy values (see the comment in Section 2.8).

This anticipated weakness is fortunate since not many values of σ^2 are available. We use the Hartree-Fock values for the 2s-2p transitions and for the series $2s^{2\,1}S$ - $2snp^1P$. Of higher transitions, only those with a ^2S core are considered and these are treated as hydrogenic.

Details of the more important lines are given in Table 2.14. Doppler broadening was allowed for in all lines listed in Table 2.14.

2.11 Sources of Data

The following symbols identify the sources of the data tabulated in Tables 2.3 to 2.14.

Energy levels and frequencies

G_i Values estimated by Gilmore.[2]

HF   Values calculated by Kelly[10] by the Hartree-Fock method.

      These values are accurate to about 20%.

*   Estimates obtained by interpolation between values in the same line series, where known, or otherwise by drawing a smooth curve from known values (or the estimates of Gilmore[2]) to the hydrogenic values of the high lines.

**   If applied to an energy level, this symbol indicates an estimate obtained from the known energy level of a corresponding term with a different core by adding to the known value the difference between the energy values of the ion terms corresponding to the two core terms. If applied to a value of frequency, this symbol indicates that the value is that of a similar transition with a different core term. This method gives correct values near the ionization limit. At lower energies, comparison of estimated values with known values

indicates a distinct improvement over assuming hydrogenic binding energies.

Unmarked values were obtained from experimental results listed by Moore[1] or, in a few cases, by Gilmore.[2]

Oscillator Strengths

HF   Hartree-Iock values due to Kelly.[10]

Unmarked values were calculated as described in Section 2.3 (see also Part 1, Section 3.2) from Hartree-Fock-Slater values of σ^2 given by Kelly.[9]

Line width constant A for Stark broadening (electron impact or quasi-static broadening)

a   Values calculated from the adiabatic approximation to electron impact theory (Part 1, Eqs. (4.20 and (4.21)). The value corresponding to the strongest line of each group was calculated. The other lines will have the same Stark profile to within the accuracy of the calculation.

G   The accurate results of Griem[11] were matched to the approximate expression, Eq. (2.1C) at 20,000°K.

*   The width of a similar electron impact broadened line with another core term was used.

(unmarked)   These values were obtained from Eq. (2.14) which assumes a quasi-static wing shape.

Line width constants for resonance broadening, A_{res}

All values were obtained from Eq. (2.12).

Line width due to Doppler broadening

This quantity was calculated from the expressi n (2.13) which depends on the line being broadened only through the line center frequency. It is therefore not necessary to list the width of each line in the Tables. The particular lines which were considered to be Doppler broadened are described in Sections 2.7 - 2.10.

Multiplet growth parameters, M^*, N^* and D

The calculation of these quantities is described in Section 2.6.

TABLE 2.1

Comparison of Ultraviolet Multiplet Oscillator Strengths of NI

Subscript H-F-S indicates values of σ^2 from ref. 9
Subscript H-F indicates f values from ref. 10
Subscript B-D indicates f values from ref. 11

Transition	f_{H-F-S}	f_{H-F}	f_{B-D}
$2s^2 2p^3 {}^4S - 2s2p^4 {}^4P$	0.454	0.506	
$2s^2 2p^2 3s {}^4P$	0.183	0.097	0.0048
$2s^2 2p^3 {}^2D - 2s2p^4 {}^2P$	0.403	0.437	
$2s2p^4 {}^2D$	0.290	0.314	
$2s^2 2p^2 3s {}^2P$	0.0742	0.0432	0.0045
$2s^2 2p^2 3s {}^2D$	0.089	0.0584	0.0011
$2s^2 2p^2 ({}^3P) 3d {}^2D$	0.0081	0.0030	0.00032
$2s^2 2p^3 ({}^3P) 3d {}^2F$	0.0451	0.020	0.0089
$2s^2 2p^3 {}^2P - 2s2p^4 {}^2S$	0.137	0.149	
$2s2p^4 {}^2P$	0.364	0.394	
$2s2p^4 {}^2D$	0.139	0.151	
$2s^2 2p^2 ({}^3P) 3s {}^2P$	0.0634	0.0382	0.012
$2s^2 2p^2 ({}^1D) 3s {}^2D$	0.0435	0.0314	0.0139
$2s^2 2p^2 ({}^3P) 3d {}^2P$	0.0119	0.0068	0.00067
$2s^2 2p^2 ({}^3P) 3d {}^2D$	0.0359	0.0144	0.0123

Where no values of f_{B-D} are given, the Bates-Damgaard method is not applicable.

TABLE 2.2

Comparison of Visible Multiplet Oscillator Strengths of NI

Subscript H-F-S indicates σ^2 values from ref. 9
Subscript B-D indicates f values from ref. 11

Transition	f_{H-F-S}	f_{B-D}
$2s^2 2p^2 3s^4 P - 2s^2 2p^2 3p^4 D$	0.594	0.516
$2s^2 2p^2 3p^4 P$	0.377	0.400
$2s^2 2p^2 3p^4 S$	0.139	0.116
$2s^2 2p^2 3s^2 P - 2s^2 2p^2 3p^2 D$	0.550	0.558
$2s^2 2p^2 3p^2 P$	0.370	0.355
$2s^2 2p^2 3p^4 S - 2s^2 2p^2 3d^4 P$	0.779	0.930
$2s^2 2p^2 3p^2 S - 2s^2 2p^2 3d^2 P$	1.057	0.872
$2s^2 2p^2 3p^2 D - 2s^2 2p^2 3d^2 F$	0.642	0.775

A key to the superscripts of Tables 2.3

to 2.14 is given in Section 2.11

TABLE 2.3a

Lines of NI, Initial Term $1s^22s^22p^3{}^4S$

General Data and Allowed Transitions

Initial Energy $= 0$

Ions:	$2s^22p^2{}^3P$	$2s2p^3{}^5S$	$2s2p^3{}^3S$
Ionization Energies eV:	14.548	20.396	33.781

Upper terms to which transitions are allowed:

$1s^22s2p^4{}^4P$ $1s^22s^22p^2(^3P)ns^4P$ $1s^22s2p^3(^5S)np^4P$

$1s^22s^22p^2(^3P)nd^4P$ $1s^22s2p^3(^3S)np^4P$

TABLE 2.3b

Lines of NI, Initial Term $1s^2 2s^2 2p^3\,{}^4S$

Detailed Data

Upper states which are resonance broadened are as follows

Upper states	$(A_{res})_1$	$(A_{res})_2$
$2s2p^4\,{}^4P$	0.019	0
$2s^2 2p^2({}^3P)3s\,{}^4P$	0.004	0
$2s^2 2p^2({}^3P)3d\,{}^4P$	0.002	0

Where $(A_{res})_1$ is associated with the lower state $2s^2 2p^3\,{}^4S$.

Upper State	hv(eV)	gf	N^*	M^*	$D(eV)\times10^3$	A
		2p – nℓ transitions				
$2s^2 2p^2({}^3P)3s\,{}^4P$	10.330	0.386[HF]	2.08	1.0	10	0.018[G]
$4s\,{}^4P$	12.853	0.092[HF]	2.08	1.0	15	0.091[a]
$2s^2 2p^2({}^3P)3d\,{}^4P$	13.008	0.219[HF]	2.08	1.0	11	0.054[a]
$4d\,{}^4P$	13.266	0.360	2.08	1.0	9.6	0.110
5	13.994	0.251	3.0	1.0	21	0.173
6	14.158	0.140	3.0	1.0	20	0.249
7	14.257	0.088	3.0	1.0	20	0.339
8	14.332	0.058	3.0	1.0	15	0.442
9	14.369	0.040	3.0	1.0	15	0.560
10	14.406	0.028	3.0	1.0	10	0.691
		2s – np transitions				
$2s2p^4\,{}^4P$	10.926	2.015[HF]	2.08	1.0	7.9	0.090[a]
$2s2p^3({}^5S)3p\,{}^4P$	18.97[Gi]	0.154	2.08	1.0	10	0.027[*]
$4p\,{}^4P$	19.34[Gi]	0.059	2.08	1.0	10	0.051[*]
$5p\,{}^4P$	19.65[*]	0.026	2.08	1.0	10	0.173
$6p\,{}^4P$	19.93	0.012	2.08	1.0	10	0.249
$2s2p^3({}^3S)3p\,{}^4P$	31.47[*]	0.153	2.08	1.0	10	0.027[*]
$4p\,{}^4P$	32.12[*]	0.059	2.08	1.0	10	0.051[*]
$5p\,{}^4P$	32.92[*]	0.026	2.08	1.0	10	0.173
$6p\,{}^4P$	33.32	0.012	2.08	1.0	10	0.249

TABLE 2.4a

Lines of NI, Initial Term $1s^2 2s^2 2p^3\,^2D$

General Data and Allowed Transitions

Energy = 2.383eV

Ions:	$2s^2 2p^2\,^3P$	$2s^2 2p^2\,^1D$	$2s2p^3\,^3D$	$2s2p^3\,^1D$
Ionization Energies:	12.165	14.063	23.600	30.040

Upper terms to which transitions are allowed:

$2s2p^4\,^2P$	$2s^2 2p^2(^3P)ns\,^2P$	$2s2p^3(^3D)np\,^2P$
^2D	$nd\,^2P$	^2D
	^2D	^2F
	^2F	$2s2p^3(^1D)np\,^2P$
	$2s^2 2p^2(^1D)ns\,^2D$	^2D
	$nd\,^2P$	^2F
	^2D	
	^2F	

TABLE 2.4b

Lines of NI, Initial Term $1s^2 2s^2 2p^3 {}^2D$

Detailed Data

Upper states which are resonance broadened are the following

Upper States	$(A_{res})_1$	$(A_{res})_2$
$2s2p^4 {}^2P$	0.050	0.024
$2s2p^4 {}^2D$	0.039	0.010
$2s^2 2p^2 ({}^3P)3s {}^2P$	0.012	0.005
$3d^2L$	0.003	0

where $(A_{res})_1$ is associated with the lower state $2s^2 2p^3 {}^2D$ and $(A_{res})_2$ is associated with the lower state $2s^2 2p^3 {}^2P$.

Upper State	$h\nu(eV)$	gf	N^*	M^*	$D(eV) \times 10^3$	A
		2p - nℓ	transitions			
$2s^2 2p^2 ({}^3P)3s {}^2P$	8.306	0.432^{HF}	2.60	1.0	11	0.0213^G
$4s {}^2P$	10.538	0.094	2.60	1.0	11	0.153^a
$2s^2 2p^2 ({}^3P)3d {}^2L$	10.620	0.232^{HF}	5.06	1.93	16	0.0530^G
$4d^2L$	11.300	0.404	4.66	1.72	28	0.110
5	11.613	0.261	6.60	1.0	33	0.173
6	11.750	0.147	6.60	1.0	19	0.249
7	11.874	0.091	6.20	1.0	16	0.339
8	11.936	0.059	6.20	1.0	11	0.442
9	11.986	0.041	6.20	1.0	13	0.560
10	12.017	0.029	6.20	1.0	11	0.691
$2s^2 2p^2 ({}^1D)3s {}^2D$	9.972	0.584^{HF}	3.06	1.0	1	0.0213^{**}
$4s {}^2D$	10.872^{**}	0.117	3.06	1.0	1	0.153^*
$2s^2 2p^2 ({}^1D)3d {}^2L$	11.740^{HF}	0.339^{HF}	6.96	2.62	16	0.0525^*
$4d^2L$	13.055^{**}	0.431	7.04	2.69	28	0.110
5	13.377^{**}	0.310	9.10	1.0	23	0.173
6	13.549^{**}	0.175	9.10	1.0	19	0.249
7	13.684^{**}	0.107	9.0	1.0	16	0.339
8	13.775^{**}	0.070	9.0	1.0	11	0.442

TABLE 2.4b (Continued)

Upper State	$h\nu$(eV)	gf	N^*	M^*	D(eV)×10³	A
		$2p \rightarrow n\ell$	transitions			
9	13.857[**]	0.049	9.0	1.0	13	0.560
10	13.914[**]	0.034	9.0	1.0	11	0.691
		$2s \rightarrow np$	transitions			
$2s2p^4{}^2P$	19.38 [HF]	4.37 [HF]	2.59	1.0	2	0.049[a]
^2D	13.95 [HF]	3.14 [HF]	3.06	1.0	2	0.070[a]
$2s2p^3(^3D)3p^2L$	21.419[Gi]	0.514	5.56	2.92	10	0.035[*]
$4p^2L$	22.659[Gi]	0.207	5.56	2.92	10	0.175[*]
$5p^2L$	23.000[*]	0.087	7.84	1.0	8	0.173
$6p^2L$	23.260[*]	0.042	7.84	1.0	8	0.249
$2s2p^3(^1D)3p^2L$	28.435[*]	0.225	5.56	2.92	10	0.035[*]
$4p^2L$	28.800[*]	0.088	5.56	2.92	10	0.175[*]
$5p^2L$	29.200[*]	0.036	7.84	1.0	8	0.173
$6p^2L$	29.589[*]	0.018	7.84	1.0	8	0.249

TABLE 2.5a

Lines of NI, Initial Term $1s^2 2s^2 2p^3{}^2P$

General Data and Allowed Transitions

Initial Energy = 3.575eV

Ions: $2s^2 2p^2{}^3P$ $2s^2 2p^2{}^1D$ $2s^2 2p^2{}^1S$ $2s2p^3{}^3P$ $2s2p^3{}^1P$

Ionization Energies: 10.972   12.871   15.025   24.513   31.648

Upper terms to which transitions are allowed:

$2s2p^4{}^2S$	$2s^2 2p^2({}^3P)ns^2P$	$2s2p^3({}^3P)np^2S$
^2P	nd^2P	^2P
^2D	^2D	^2D
	$2s^2 2p^2({}^1D)ns^2D$	$2s2p^3({}^1P)np^2S$
	nd^2S	^2P
	^2P	^2D
	^2D	
	$2s^2 2p^2({}^1S)ns^2S$	
	nd^2D	

TABLE 2.5b

Lines of NI, Initial Term $1s^22s^22p^3{}^2P$

Detailed Data

Upper states which are resonance broadened are the following

Upper State	$(A_{res})_1$	$(A_{res})_2$
$2s2p^4{}^2S$	0.0	0.018
${}^2P$	0.050	0.024
${}^2D$	0.039	0.010
$2s^22p^2({}^3P)3s^2P$	0.012	0.006
$2s^22p^2({}^3P)3d^2L$	0.0006	0.001

where $(A_{res})_1$ is associated with the lower state $2s^22p^3{}^2D$ and $(A_{res})_2$ is associated with the lower state $2s^22p^3{}^2P$.

Upper State	hν(eV)	gf	N*	M*	D(eV)×10³	A
2p - nℓ transitions						
$2s^22p^2({}^3P)3s^2P$	7.362	0.229^{HF}	3.53	1.0	11	0.0213 G
$4s^2P$	9.346	0.049_{HF}	3.53	1.0	10	0.153 a
$2s^22p^2({}^3P)3d^2L$	9.442	0.127^{HF}	5.71	1.93	7.8	0.053 G
$4d^2L$	10.112	0.200	5.43	1.93	5.6	0.110
5	10.422	0.139	7.35	1.0	28	0.173
6	10.558	0.079	7.35	1.0	23	0.249
7	10.682	0.049	7.19	1.0	14	0.339
8	10.744	0.034	7.00	1.0	12	0.442
9	10.787	0.023	6.89	1.0	12	0.560
10	10.824	0.018	6.75	1.0	10	0.691
$2s^22p^2({}^1D)3s^2D$	8.781_*	0.184^{HF}	2.59	1.0	1	0.0213_*
$4s^2D$	11.302_{HF}	0.035_{HF}	2.59	1.0	1	0.153 a
$2s^22p^2({}^1D)3d^2L$	9.951_{**}	0.095^{HF}	7.95	2.62	7.8	0.041 a
$4d^2L$	11.990_{**}	0.132	8.10	2.62	5.6	0.110
5	12.299_{**}	0.091	9.85	1.0	18	0.173
6	12.460_{**}	0.052	9.85	1.0	23	0.249
7	12.586_{**}	0.032	9.85	1.0	14	0.339
8	12.650_{**}	0.021	9.85	1.0	12	0.442
9	12.703_{**}	0.014	9.85	1.0	12	0.560
10	12.735	0.011	9.85	1.0	10	0.691
$2s^22p^2({}^1S)3$	11.551^{HF}_{**}	0.321^{HF}	4.29	1.96	3	0.053 *
4	14.185_{**}	0.158	4.15	1.63	3	0.110
5	14.466_{**}	0.086	4.15	1 0	3	0.173
6	14.645	0.048	4.15	1.0	1	0.249

TABLE 2.5b (Continued)

Upper State	$h\nu$(eV)	ρf	N^*	M^*	$D(eV)\times10^3$	A
		2s – np		Transitions		
$2s2p^4{}^2S$	14.821	0.892^{HF}	1.93	1.0	1	0.00071^a
^2P	17.529	2.362^{HF}	3.54	1.0	2	0.00055^a
^2D	12.095	0.904^{HF}	2.59	1.0	3	0.00074^a
$2s2p^3(^3P)3p^2L$	22.790	0.319	7.11	2.76	10	0.035^*
$4p^2L$	23.392	0.128	7.11	2.76	10	0.175^*
$5p^2L$	23.796^*	0.027	7.11	1.0	8	0.173
$6p^2L$	24.120	0.015	7.11	1.0	8	0.249
$2s2p^3(^1P)3p^2L$	28.566	0.136	7.55	2.75	10	0.035^*
$4p^2L$	29.731	0.055	7.55	2.75	10	0.175^*
$5p^2L$	30.461	0.024	7.55	1.0	8	0.173
$6p^2L$	31.072	0.011	7.55	1.0	8	0.249

TABLE 2.6a

Lines of NI, Initial Term $1s^2 2s2p^4 \, ^4P$

General Data and Allowed Transitions

Initial Energy $= 10.926$ eV

Ions:	$2s2p^3 \, ^5S$	$2s2p^3 \, ^2D$	$2s2p^3 \, ^2P$	$2s2p^3 \, ^4S$
Ionization Energies:	9.422	15.058	17.162	22.854

Upper terms to which transitions are allowed:

$2s2p^3(^5S)ns \, ^4S$	$2s2p^3(^3D)ns \, ^4D$	$2s2p^3(^3P)ns \, ^4P$	$2s2p^3(^3S)ns \, ^4S$
$nd \, ^4D$	$nd \, ^4D$	$nd \, ^4D$	$nd \, ^4D$
	^4P	^4P	
	$. \, ^4S$		

The transition to upper state $2p^5 \, ^2P$ is neglected.

TABLE 2.6b

Lines of NI, Initial Term $1s^2 2s2p^4 {}^4P$

Detailed Data

Upper State	hν(eV)	σ^f	N^*	M^*	$D(eV) \times 10^3$	A
$2s2p^3(^5S)3$	8.04	3.50	7.4	2.0	10	0.06*
4	8.42	1.25	7.3	1.0	10	0.110
5	8.88	0.71	6.2	1.0	8	0.173
6	9.04	0.42	4.6	1.0	8	0.249
$2s2p^3(^3D)3$	12.85	6.81	40.0	2.0	10	0.06*
4	14.10	2.87	39.0	1.0	10	0.110
5	14.52	1.65	35.3	1.0	8	0.173
6	14.68	0.95	32.0	1.0	8	0.249
$2s2p^3(^3P)3$	15.65	6.66	17.4	2.0	10	0.06*
4	16.31	2.16	17.1	1.0	10	0.110
5	16.62	1.17	14.6	1.0	8	0.173
6	16.78	0.67	12.2	1.0	8	0.249
$2s2p^3(^3S)3$	21.34	2.10	8.3	1.69	10	0.06*
4	22.00	1.25	8.1	1.0	10	0.110
5	22.31	0.76	6.2	1.0	6	0.173
6	22.47	0.44	4.6	1.0	8	0.249

TABLE 2.7a

Lines of NI, Initial Configuration $1s^2 2s^2 2p^2(^{2S_c+1}L_c)3\ell$

Allowed Transitions

^3P Core ($n \geq 3$, $n' \geq 4$)

$3s^4P-np^4S$	$3s^4S-nd^4P$	$3d^4P-n'f^4D$
np^4P	$n's^4P$	$n'p^4S$
np^4D	$3p^4P-nd^4P$	$n'p^4P$
$3s^2P-np^2S$	nd^4D	$n'p^4D$
np^2P	$n's^4P$	$3d^4D-n'f^4D$
np^2D	$3p^4D-nd^4P$	$n'f^4F$
	nd^4D	$n'p^4P$
	nd^4F	$n'p^4D$
	$n's^4P$	$3d^4F-n'f^4D$
	$3p^2S-nd^2P$	$3d^4F-n'f^4F$
	$n's^2P$	$n'f^4G$
	$3p^2P-nd^2P$	$n'p^4D$
	nd^2D	$3d^2P-n'f^2D$
	$n's^2P$	$n'p^2S$
	$3p^2D-nd^2P$	$n'p^2P$
	nd^2D	$n'p^2D$
	nd^2F	$3d^2D-n'f^2D$
	$n's^2P$	$n'f^2F$
		$n'p^2P$
		$n'p^2D$
		$3d^2F-n'f^2D$
		$n'f^2F$
		$n'f^2G$
		$n'p^2D$

^1D Core ($n \geq 3$, $n' \geq 4$)

$3s^2D-np^2P$	$3p^2P-nd^2S$	$3d^2S-n'f^2P$
np^2D	nd^2P	$n'p^2P$
np^2F	nd^2D	$3d^2P-n'f^2P$
	$n's^2D$	$n'f^2D$
	$3p^2D-nd^2P$	$n'p^2P$
	nd^2D	$n'p^2D$
	nd^2F	$3d^2D-n'f^2P$
	$n's^2D$	$n'f^2D$
	$3p^2F-nd^2D$	$n'f^2F$
	nd^2F	$n'p^2P$
	nd^2G	$n'p^2D$
	$n's^2D$	$n'p^2F$
		$3d^2F-n'f^2D$
		$n'f^2F$
		$n'f^2G$
		$n'p^2D$
		$n'p^2F$

TABLE 2.7a (Continued)

$$3d^2G-n'f^2F$$
$$n'f^2G$$
$$n'f^2H$$
$$n'p^2F$$

^1S Core $(n \geq 3,\ n' \geq 4)$

$3s^2S-np^2P$ $\qquad$ $3p^2P-nd^2D$ $\qquad$ $3d^2D-n'f^2F$
$$n's^2S$$ $\qquad\qquad\qquad$ $n'p^2D$

TABLE 2.7b

Lines of NI, Initial Configuration $1s^2 2s^2 2p^2(^{2S_c+1}L_c)3\ell$

Detailed Data

Same-shell transitions

Initial Term	Initial Energy(eV)	Final Term	$h\nu$(eV)	gf	N^*	M^*	D(eV)×10³	A
			^{3}P Core					
$3s^4P$	10.335	$3p^4S$	1.660	1.67	2.07	1.0	10	0.0342[G]
		$3p^4P$	1.509	4.52	6.20	1.0	10	0.0270[G]
		$3p^4D$	1.428	7.14	6.60	1.0	11	0.0248[G]
$3s^2P$	10.689	$3p^2S$	0.913	0.460	1.94	1.0	11	0.0124[a]
		$3p^2P$	1.444	2.22	3.54	1.0	16	0.0404[G]
		$3p^2D$	1.320	3.30	2.60	1.0	11	0.0345[G]
$3p^4S$	11.995	$3d^4P$	1.017	3.12	2.07	1.0	12	0.0540[a]
$3p^2S$	11.602	$3d^2P$	1.368	2.11	1.94	1.0	5	0.0660[G]
$3p^4$?	11.844	$3d^4L$	1.175	10.79	11.8	1.0	19	0.060[a]
$3p^2P$	12.126	$3d^2L$	0.905	4.14	5.39	1.85	8	0.045[a]
$3p^4D$	11.763	$3d^4L$	1.227	18.95	13.9	1.0	44	0.058[a]
$3p^2D$	12.009	$3d^2L$	0.994	7.69	5.10	1.96	16	0.053[a]
			^{1}D Core					
$3s^2D$	12.356	$3p^2L$	1.402	10.63	7.84	2.92	9	0.017[a]
$3p^2L$	13.758	$3d^2L$	1.249	28.7	19.5	2.92	10	0.0525[a]

Different-shell Transitions

Initial Term	Initial Energy(eV)	Final Term	$h\nu$(eV)	gf	N^*	M^*	D(eV)×10³	A
			^{3}P Core					
$3s^4P$	10.335	$4p^4L$	2.926	0.192	15.2	2.76	16	0.18[G]
$3s^2P$	10.689	$4p^2L$	2.641	0.086	7.58	2.72	11	0.175[G]
3s	10.450	5p	3.261	0.230	22.9	1.0	60	0.173
		6p	3.571	0.153	22.9	1.0	60	0.249
		7p	3.737	0.092	22.9	1.0	40	0.339
$3p^4S$	11.995	$4s^4P$	0.855	0.615	2.07	1.0	15	0.091[a]
$3p^4P$	11.844	$4s^4P$	1.017	2.19	6.20	1.0	15	0.091[a]
$3p^4D$	11.763	$4s^4P$	1.097	3.91	6.35	1.0	15	0.091[a]
$3p^4L$	11.815	$4d^4L$	1.368.	1.15	27.5	1.83	22	0.110

TABLE 2.7b (Continued)

Initial Term	Initial Energy	Final Term	$h\nu$(eV)	gf	N^*	M^*	D(eV)$\times10^3$	A
$3p^2S$	11.602	$4s^2P$	1.313	0.097	1.93	1.0	11	0.153[a]
$3p^2P$	12.126	$4s^2P$	0.796	0.86	3.54	1.0	11	0.153[a]
$3p^2D$	12.009	$4s^2P$	0.912	1.65	2.60	1.0	11	0.153[a]
$3p^2L$	12.002	$4d^2L$	1.680	0.54	12.2	1.64	25	0.110
$3p$	11.875	5	1.825	0.796	51.0	1.0	12	0.173
		6	2.145	0.268	51.0	1.0	12	0.249
		7	2.306	0.150	51.0	1.0	11	0.339
$3d^4P$	13.012	$4p^4L$	0.309	2.85	9.6	1.0	84	0.180[G]
$3d^4D$	13.020	$4p^4L$	0.234	3.58	7.7	1.0	37	0.177[G]
$3d^4F$	12.989	$4p^4D$	0.261	6.93	6.5	1.0	14	0.170[G]
$3d^2L$	13.005	$4p^2L$	0.198	4.58	12.3	2.66	12	0.175[G]
$3d$	13.000	$4f$	0.692	86.0	33.3	1.0	62	0.110
		5	0.957	13.95	44.1	1.0	62	0.173
		6	1.158	4.41	44.1	1.0	62	0.249
		7	1.257	1.62	44.1	1.0	62	0.339
		^1D Core						
$3s^2D$	12.356	$4p^2L$	2.641**	0.141	7.7	2.9	3	0.175*
		$5p^2L$	3.261**	0.128	7.7	1.0	3	0.173
		$6p^2L$	3.571**	0.085	7.7	1.0	2	0.249
		$7p^2L$	3.737**	0.051	7.7	1.0	2	0.339
$3p$	13.758	4	1.600**	9.5	22.5	3.69	20	0.16*
		5	1.825**	0.443	22.5	1.0	12	0.173
		6	2.145**	0.149	22.5	1.0	12	0.249
		7	2.306**	0.084	22.5	1.0	12	0.339
$3d$	15.001	$4p$	0.248**	91.5	19.5	1.0	25	0.18*
		$4f$	0.692**	48.0	23.2	1.0	60	0.110
		5	0.957**	7.79	25.0	1.0	60	0.173
		6	1.158**	2.45	25.0	1.0	60	0.249
		7	1.257**	0.90	25.0	1.0	60	0.339

TABLE 2.8

Lines of NI, Initial Configuration $1s^2 2s^2 2p^2 ({}^{2S_c+1}L_c)4\ell$

Same-shell transitions

Initial State	Initial Energy(eV)	Final State	$h\nu$(eV)	gf	N^*	M^*	D(eV)×10^3	A
$({}^3P)4s$	12.876	4p	0.441	25.0	13.6	1.0	62	0.180^G
$({}^3P)4p$	13.318	4d	0.360	54.1	39.0	1.0	124	0.110
$({}^3P)4d$	13.677	4f	0.016	5.48	33.2	1.0	33	0.110
$({}^1D)4$	15.448	4	0.372**	39.1	30.0	1.0	62	0.110

Different-shell transitions

Initial State	Initial Energy(eV)	Final State	$h\nu$(eV)	gf	N^*	M^*	D(eV)×10^3	A
$({}^3P)4s$	12.876	5p	1.009	0.0124	22.9	1.0	6	0.173
$({}^3P)4p$	13.318	5s	0.320	13.4	21.0	1.0	6	0.173
		5d	0.667	3.16	39.0	1.0	12	0.173
$({}^3P)4d$	13.677	5p	0.209	59.0	34.0	1.0	31	0.173
$({}^3P)4d,f$	13.687	5f,d	0.310	58.5	52.1	1.0	31	0.173
$({}^3P)4$	13.550	6	0.607	22.3	125	1.0	50	0.249
		7	0.707	7.8	125	1.0	37	0.339
		8	0.769	4.0	125	1.0	37	0.442
$({}^1D)4$	15.448	5	0.310	84.5	68.0	1.0	37	0.173
		6	0.620	48.9	68.0	1.0	31	0.249

TABLE 2.9

Lines of NI, Same-Shell Transitions with n = 5 or 6

Initial State	Initial Energy(eV)	hν(eV)	gf	N^*	M^*	D(eV)$\times 10^3$	A
(^{3}P)5	13.700	0.174	82	51.2	1.0	37	0.173
(^{1}D)5	15.60[**]	0.174[**]	46	30.0	1.0	30	0.173
(^{3}P)6	13.980[**]	0.10	118	51.2	1.0	30	0.249
(^{1}D)6	15.88[**]	0.10[**]	66	30.0	1.0	25	0.249

TABLE 2.10a

Lines of NII, Initial Configuration $1s^2 2s^2 2p^2$

Allowed transitions

Lower term $2s^2 2p^2\,^3P$

Upper terms

$2s2p^3\,^3S$	$2s^2 2pns\,^3P$	$2s2p^2(^4P)np\,^5S$
^3P	$nd\,^3P$	$np\,^3S$
^3D	$nd\,^3D$	$np\,^5P$
		$np\,^3P$
		$np\,^5D$
		$np\,^3D$
		$2s2p^2(^2P)np\,^3S$
		$np\,^1S$
		$np\,^3P$
		$np\,^1P$
		$np\,^3D$
		$np\,^1D$

Lower term $2s^2 2p^2\,^1D$

Upper terms

$2s2p^3\,^1P$	$2s^2 2pns\,^1P$	$2s2p^2(^2D)np\,^1P$
^1D	$nd\,^1P$	$np\,^1D$
	$nd\,^1D$	$np\,^1F$
	$nd\,^1F$	

Lower term $2s^2 2p^2\,^1S$

Upper terms

$2s2p^3\,^1P$	$2s^2 2pns\,^1P$	$2s2p^2(^2S)np\,^1P$
	$nd\,^1P$	

TABLE 2.10b

Lines of NII, Initial Configuration $1s^2 2s^2 2p^2$

Detailed Data

Same-shell transitions

Initial Configu-ration	Initial Energy(eV)	Final Configu-ration	$h\nu(eV)$	gf	N^*	M^*	$D(eV)\times 10^3$	A
$2s^2 2p^2{}^3P$	0	$2s2p^3{}^3S$	19.232	3.03^{HF}	2.74	1.0	16	0.060^a
		^3P	13.541	1.54^{HF}	2.19	1.0	16	0.060^a
		^3D	11.435	2.13^{HF}	4.71	1.0	16	0.060^a
$2s^2 2p^2{}^1D$	1.899	$2s2p^3{}^1P$	18.776	1.23^{HF}	1.0	1.0	0	0.067^a
		^1D	15.977	3.26^{HF}	1.0	1.0	0	0.067^a
$2s^2 2p^2{}^1S$	4.052	$2s2p^3{}^1D$	16.623	0.818^{HF}	1.0	1.0	0	0.057^a

Different -shell transitions

Initial Configu-ration	Initial Energy(eV)	Final Configu-ration	$h\nu(eV)$	gf	N^*	M^*	$D(eV)\times 10^3$	A
$2s^2 2p^2{}^3P$	0	$2s^2 2p3s{}^3P$	18.466	0.797^{HF}	2.69	1.0	23	0.009^c
		$4s{}^3P$	24.371	0.16	2.69	1.0	20	0.051^c
		$3d$	23.297	3.028^{HF}	7.84	1.85	18	0.0085^c
		$4d$	26.085	1.785	7.84	1.85	16	0.135^c
		5	27.275	0.720	9.79	1.0	30	0.087
		6	28.068	0.325	9.79	1.0	25	0.125
$2s^2 2p^2{}^1D$	1.899	$2s^2 2p3s{}^1P$	16.597	0.503^{HF}	1.0	1.0	0	0.0065^c
		$4s{}^1P$	22.632	0.083	1.0	1.0	0	0.043^c
		$3d$	21.473	1.492^{HF}	2.07	2.07	0	0.01^c
		$4d$	24.262	0.915	2.07	2.07	0	0.18^c
		5	25.514	0.374	2.69	1.0	0	0.087
		6	26.172	0.169	2.69	1.0	0	0.125
$2s^2 2p^2{}^1S$	4.052	$2s^2 2p3s{}^1P$	14.444	0.108^{HF}	1.0	1.0	0	0.0065^c
		$4s{}^1P$	20.478	0.015	1.0	1.0	0	0.043^c
		$3d{}^1P$	20.758	0.296^{HF}	1.0	1.0	0	0.011^c
		$4d{}^1P$	22.148	0.167	1.0	1.0	0	0.216^c
		5	23.308	0.068	1.59	1.0	0	0.087
		6	24.023	0.031	1.59	1.0	0	0.125

TABLE 2.11

Lines of NII, Initial Configuration $1s^2 2s^2 2p3\ell$

Same-shell transitions

Initial States	Initial Energy(eV)	Final States	$h\nu$(eV)	gf	N^*	M^*	D(eV)×10³	A
$3s\,^3P$	18.482	$3p\,^3L$	2.393	7.97	9.74	2.79	53	0.0078
$3s\,^1P$	18.496	$3p\,^1L$	2.901	3.086	2.72	2.72	0	0.0123
$3p\,^3S$	20.939	$3d\,^3P$	2.485	2.25	2.74	1.0	10	0.0088
^3P	21.158	$3d$	2.132	5.79	7.29	1.88	21	0.0085
^3D	20.663	$3d$	2.492	11.28	8.35	1.91	48	0.0075
^1S	22.102	$3d\,^1P$	1.469	0.433	1.0	1.0	0	0.011
^1P	20.408	$3d$	2.926	2.61	1.88	1.88	0	0.0089
^1D	21.598	$3d$	1.847	2.77	1.93	1.93	0	0.0092

Different-shell transitions

Initial States	Initial Energy(eV)	Final States	$h\nu$(eV)	gf	N^*	M^*	D(eV)×10³	A
$3s$	18.479	$4p$	6.695	1.03	12.0	5.11	29	0.051
$3p\,^3S$	20.939	$4s\,^3P$	3.449	0.414	2.74	1.0	21	0.051
$3p\,^3P$	21.159	$4s\,^3P$	3.229	1.161	2.59	1.0	21	0.051
$3p\,^3D$	23.245	$4s\,^3P$	1.143	0.685	4.7	1.0	21	0.051
$3p\,^1S$	22.102	$4s\,^1P$	2.428	0.097	1.0	1.0	0	0.0434
$3p\,^1P$	20.408	$4s\,^1P$	4.122	0.495	1.0	1.0	0	0.0434
$3p\,^1D$	21.598	$4s\,^1P$	2.932	0.586	1.0	1.0	0	0.0434
$3p\,^3L$	20.865	$4d\,^3L$	5.182	1.964	42 3	2.25	124	0.135
$3p\,^1L$	21.262	$4d\,^1L$	5.108	0.611	4.0	2.72	124	0.183
$3d$	23.270	$4p$	1.934	9.9	19.9	1.0	372	0.051
		$4f$	2.920	52.1	19.4	1.0	186	0.114
$3s$	18.479	$5p$	8.430	0.52	11.9	1.0	25	0.087
		$6p$	9.422	0.28	11.9	1.0	25	0.125
$3p$	20.955	5	6.199	2.77	32.0	1.0	80	0.087
		6	7.091	1.42	32.0	1.0	80	0.125
$3d$	23.270	5	4.153	10.72	30.0	1.0	80	0.087
		6	4.810	3.58	30.0	1.0	80	0.125

TABLE 2.12

Lines of NII. Same-Shell Transitions with n = 4

Initial States	Initial Energy (eV)	Final States	$h\nu$(eV)	gf	N^*	M^*	D(eV)$\times 10^3$	A
4s	24.423	4p	0.744	13.2	12.5	1.0	371	0.05[G]
4p	25.167	4d	0.930	39.4	22.6	1.0	124	0.15[G]

TABLE 2.13

Lines of NIII

Same-shell transitions

Initial States	Initial Energy(eV)	Final States	$h\nu$(eV)	gf	N^{*}	M^{*}	D(eV)$\times 10^{3}$	A
$2s^{2}2p\,^{2}P$	0	$2s2p^{2}\,^{2}S$	16.24	0.340^{HF}	1.93	1.0	22	2.37×10^{-4} a
		^{2}P	18.08	3.48^{HF}	3.54	1.0	16	2.5×10^{-4} a
		^{2}D	12.52	1.28^{HF}	2.59	1.0	19	2.68×10^{-4} a
$2s2p^{2}\,^{4}P$	7.09	$2p^{3}\,^{4}S$	16.03	2.053^{HF}	2.08	1.0	17	1.72×10^{-4} a
^{2}D	12.5	^{2}P	16.02	0.843^{HF}	2.59	1.0	1	2.15×10^{-4} a
		^{2}D	12.7	2.124^{HF}	3.06	1.0	1	3.21×10^{-4} a
^{2}P	18.0	^{2}P	10.44	0.961^{HF}	3.53	1.0	13	3.86×10^{-4} a
		^{2}D	7.08	1.184^{HF}	2.59	1.0	13	4.74×10^{-4} a
^{2}S	16.2	^{2}P	12.3	0.518^{HF}	1.93	1.0	0.5	2.48×10^{-4} a
$2s^{2}3s\,^{2}S$	27.44	$2s^{2}3p\,^{2}P$	3.03	1.47	1.93	1.0	4	14.4×10^{-4} a
$2s^{2}3p\,^{2}P$	30.46	$3d\,^{2}D$	2.42	2.29	2.59	1.0	2	14.6×10^{-4} a
$2s^{2}4s\,^{2}S$	37.33	$4p\,^{2}P$	1.32	2.36	1.93	1.0	3	0.907×10^{-2} a
$4p\,^{2}P$	38.65	$4d\,^{2}D$	0.75	2.83	2.59	1.0	3	1.0×10^{-2} a
$4d\,^{2}D$	39.4	$4f\,^{2}F$	0.31	1.39	2.42	1.0	3	1.1×10^{-2} a

Different-shell transitions

Initial States	Initial Energy(eV)	Final States	$h\nu$(eV)	gf	N^{*}	M^{*}	D(eV)$\times 10^{3}$	A
$2s^{2}2p\,^{2}P$	0	$3s\,^{2}S$	27.4	0.280^{HF}	1.93	1.0	22	23.1×10^{-4} a
		$3d\,^{2}D$	33.1	2.33^{HF}	2.6	1.0	22	14.6×10^{-4} a
		4	39.0	0.74	3.72	1.0	20	1.0×10^{-2} a
		5	42.2	0.228	2.82	1.0	20	5.75×10^{-2}

TABLE 2.14

Lines of NIV

Same-shell transitions

Initial States	Initial Energy(eV)	Final States	hν(eV)	$g_i f$	N^*	M^*	D(eV)×10^3	A
$2s^2$ ^1S	0	$2s2p$ ^1P	16.15	0.845^{HF}	1.0	1.0	0	2.15×10^{-4} a
$2s2p$ ^3P	8.32	$2p^2$ ^3P	13.41	2.214^{HF}	2.69	1.0	0	2.47×10^{-4} a
$2s2p$ ^1P	16.15	^1D	7.21	0.670^{HF}	1.0	1.0	0	4.55×10^{-4} a
		^1S	13.07	0.213^{HF}	1.0	1.0	0	3.32×10^{-4} a

Different-shell transitions

Initial States	Initial Energy(eV)	Final States	hν(eV)	$g_i f$	N^*	M^*	D(eV)×10^3	A
$2s^2$ ^1S	0	$2s3p$ ^1P	48.1	0.845^{HF}	1.0	1.0	0	16.0 ×10^{-4} *
		$2s4p$ ^1P	62.8	0.148	1.0	1.0	0	1.0 ×10^{-2} *
		$2s5p$ ^1P	68.1	0.060	1.0	1.0	0	4.31×10^{-2}

3. CONTINUUM CROSS SECTIONS

3.1 Introduction

The processes which we consider in the continuum are bound-free transitions of NI, NII, NIII and NIV, free-free transitions in the fields of N^+, N^{++}, N^{+++} and N^{++++} and molecular band radiation from N_2 and N_2^+. Other processes which occur but have been shown by previous work[13,14] to be negligible are free-free transitions in the fields of N and N_2 and bound-free transitions of the N^- ion. A paper by Norman[15] suggests that the latter effect can be significant at certain wavelengths and so, when more reliable cross sections are available, it will probably be worthwhile to check its contribution to the overall radiative energy transfer.

As mentioned in Part 1, Chap. 5, data for these continuum processes is more widely available in the literature than data for the corresponding bound-bound transitions and it has not been necessary to calculate any continuum cross sections for this work.

Section 3.2 discusses the sources of data used for bound-free transitions. Section 3.3 presents the expressions used for the free-free cross sections and Section 3.4 describes the approximate treatment of the molecular bands.

3.2 Bound-Free Cross Sections

Sherman and Kulander[16] have used the Burgess-Seaton method to calculate cross sections of 18 atom → ion transitions from low-lying states of N. These include all the important transitions from the $2p^3$ states and all transitions from $2s^2 2p^2 (^3P)3s$ and $2s^2 2p^2 (^3P)3p$ states, the cross section are given for each frequency at which a photoionization threshold occurs. In our calculations, the photoionization edges belonging to all terms with

with a $(^3P)3s$ configuration are combined at a single, average frequency and all terms with a $(^3P)3p$ configuration are combined at another frequency. This procedure involves little error and is consistent with the treatment of the corresponding line series. In addition, the configurations $(^1D)3s$ and $(^1D)3p$ are assumed to have the same cross sections as $(^3P)3s$ and $(^3P)3p$ respectively. The bound-free absorption coefficients of both cores can then be calculated for these configurations by summing the two occupation numbers.

We treat all other bound-free transitions of NI by the hydrogenic expression

$$\sigma_v = \frac{2^3}{3\sqrt{3}} \frac{h^3}{\pi^2 c} \frac{1}{m_e^2 e^2} \left(\frac{v_T}{v}\right)^3 \cdot \frac{1}{z^2} n\, g_{n\ell}(v) \tag{3.1}$$

where $g_{n\ell}(v)$ is the bound-free Gaunt factor associated with the initial state n,ℓ. Values of $g_{n\ell}(v)$ are tabulated by Karzas and Latter[17]. There exists an approximate expression due to Menzel and Pekeris[18] and corrected by Burgess[19] for the shell averaged Gaunt factor g_n which is good out to an electron energy of about 10eV from the photoionization threshold, thereafter it is poor but the cross section itself is very low so that it is adequate for our purposes. In the form given by Peach[20] it is

$$g_n(v) = 1 + \alpha\left(\frac{v}{v_T}\right)^{1/3} + \beta\left(\frac{v}{v_T}\right)^{2/3} + 1/n^2 \left[-2\alpha\left(\frac{v}{v_T}\right)^{-2/3} - 2/3\,\beta\left(\frac{v}{v_T}\right)^{-1/3}\right]$$
$$\tag{3.2}$$
$$+ 1/n^4\, 2/3\, \beta\left(\frac{v}{v_T}\right)^{-4/3}$$

where $\alpha = 0.1728$, $\beta = -0.0496$ and v_T is the threshold frequency.

For the 3d initial states, an examination of the results of Karzas and Latter[17] shows that the shell-averaged expression is seriously in error but the following simple expression is within about 10% for free electron

energies less than about 15eV

$$
g(\nu) = \begin{cases} 0.7626 & (h\nu-h\nu_T)/Ry \le 0.131 \\ \\ [10(h\nu-h\nu_T)/Ry]^{-1} & (h\nu-h\nu_T)/Ry > 0.131 \end{cases} \tag{3.3}
$$

No Burgess-Seaton calculations appear to be available for NII or higher spectra (except for one transition of NII[21]) but in any case, the ionic bound-free radiation occurs where the Planck function is small. It will therefore be sufficiently accurate to use Seaton's approximate formula[22] for the $2p^q$ states (this is claimed to be correct to 20% for positive ions) and hydrogenic results for more highly excited states. The lowest energy configuration of N^{+++} is $1s^2 2s^2$ and hence is not covered by Seaton's formula. The corresponding photoionization is not expected to be very important and is therefore also accounted for by the hydrogenic formula.

It is worth remarking that more accurate cross sections have been calculated by Johnston and his colleagues at Lockheed Missiles and Space Company[21,7] these calculations are, over a very wide temperature range, the best predictions which the current state of knowledge allows (without going to Hartree-Fock wave functions). Unfortunately, the only forms in which these results are available are mean absorption coefficients[7] and spectral absorption coefficients (to 10eV photon energy) in air.[23] The latter cannot be reduced to an absorption cross section per particle since the bound-free transitions of nitrogen and all its ions are lumped together and hence depend on the species concentrations in air.

3.3 Free-Free Cross Sections

Although the free-free radiation is often not negligible, it is never dominant and it is therefore not necessary to use the relatively elaborate method of Peach[24] to calculate the free-free cross sections. We therefore use for each ionic species the hydrogenic expression

$$K_{\nu,ff} = \frac{16\pi^2 e^6}{3\sqrt{3}\ ch} \frac{z^2 N_e N_z}{(2\pi m_e)^{3/2} kT^{1/2}\nu^3}\ g_{ff}(\nu,kT) \qquad (3.4)$$

where $g_{ff}(\nu,kT)$ is the free-free Gaunt factor which, for temperatures of interest to use, is close to unity over the important frequency range 0.1eV to 10eV. We therefore use Eq. (3.4) with unit Gaunt factor.

A remark on the accuracy of Eq. (3.4) is to be found in Part 1, Section 5.3. In the same section it was noted that an effective value of z^2 is often used to account, approximately, for non-hydrogenic effects. Following Allen[14] we adopt the value $z^2_{eff} = 1.5$ for singly ionized nitrogen, as suggested by the experimental results of Allen et al.[25] obtained in air. For the higher ions we use $z^2_{eff} = z^2$.

The inclusion of the high, merged (or thin) series into the free-free absorption coefficient is accomplished (see Section 2.4) by multiplying Eq. (3.4) by the factor

$$\phi_{core} = 1 + \frac{g_{core}}{Q_i} \{\exp(z^2 Ry/[(\bar{m})^2 kT]) - 1\} \qquad (3.5)$$

where $\bar{m}$ is the initial quantum number of the first completely merged (or thin) series (see Part 2, Section 3.5). Multiplying Eq. (3.4) by ϕ_{core}, summing over the ionic species considered and inserting values for z^2, we obtain for the absorption coefficient due to free-free and pseudo free-free

transitions

$$K_{\nu,ff} = \frac{16\pi^2 e^6}{3\sqrt{3}\ ch} \frac{N_e}{(2\pi m_e)^{3/2}(kT)^{1/2}} \frac{1}{\nu^3} g_{ff}(\nu,kT)$$

$$(1.5\ N_{N^+}\phi_{3_{P+^1D}} + 4N_{N^{++}}\phi_{2_P} + 9N_{N^{+++}}\phi_{1_S} + 16N_{N^{++++}}\phi_{2_S}). \qquad (3.6)$$

Numerically, $K_{\nu,ff}$ can be written

$$K_{\nu,ff} = 1.75 \times 10^2 \frac{\tilde{N}_e}{(kT)^{1/2}} \frac{1}{(h\nu)^3} g_{ff}(1.5\tilde{N}_{N^+}\phi_{3_{P+^1D}}$$

$$(3.7)$$

$$+ 4\tilde{N}_{N^{++}}\phi_{2_P} + 9\tilde{N}_{N^{+++}}\phi_{1_S} + 16\tilde{N}_{N^{++++}}\phi_{2_S})$$

where kT and hν are in eV and $\tilde{N}_S$ is the number density of species S divided by the Loschmidt number.

3.4 Molecular Bands

For densities less than about 1 atmosphere, radiation from molecular bands is not significant above about 10,000°K due to the dissociation of the molecules. Below this temperature, both N_2 and N_2^+ contribute molecular band radiation. The determination of molecular band absorption coefficients has been the object of continuing work, both theoretical and experimental. In particular the work of Churchill and his colleagues[23] at the Lockheed Missiles and Space Company and of Keck, Allen and others[26,27] at the AVCO Everett Research Laboratory should be mentioned.

The detailed structure of a band absorption coefficient is extremely complex but fortunately need not be considered within the accuracy of these calculations. We therefore look for a representation which contains the

gross features of the band shapes according to some frequency-averaging
procedure. Churchill et al.[23] have published tables of absorption coeffi-
cients for 4 bands of N_2 and N_2^+ in air. These are conveniently fre-
quency averaged and, once the concentrations of N_2 and N_2^+ in air are
known,[*] can be reduced to temperature and frequency-dependent cross sec-
tions per molecule. Allen[26] has published tables and graphs of the spectral
content of the local emission coefficient (i.e. of $K_\nu B_\nu$) these give more
details than we require but cover 7 bands of N_2 and N_2^+. (However, only
enough additional information is available to obtain the absorption coeffi-
cient of 6 of these bands and one of these is of negligible strength.)
Allen's results can be used to obtain a very simple, approximate representa-
tion and for this reason they were adopted, the details are discussed next.

Allen[26] presents the spectral content of 7 band systems but, due to
lack of an f-number, the absorption coefficient of the N_2 (Birge-Hopfield
#1) cannot be obtained from his report. Churchill[23] presents results for
this system but, since his value of f-number is only tentative, it was not
considered worthwhile to combine it with Allen's spectral predictions; in
any case molecular transitions are represented in the same frequency inter-
val by the related N_2 (Birge-Hopfield #2) system. It is easy to check
that the very low value of f-number belonging to the N_2 (Lyman Birge-
Hopfield) system implies an absorption coefficient more than 4 orders of
magnitude smaller than that of the N_2 (Birge-Hopfield) system which occu-
pies the same frequency interval, the former system may therefore be
neglected. The five systems represented in these calculations are shown
in Table 3.1.

TABLE 3.1

Molecular Band Systems Included in the Calculations

System	Transition in Spectroscopic Notation	Approximate photon energy range (eV)
N_2 (First Positive)	$A^3\Sigma^+ - B^3\pi$	0.3 - 2.7
N_2 (Second Positive)	$B^3\pi - C^3\pi$	1.8 - 5.4
N_2 (Birge-Hopfield #2)	$X^1\Sigma^+ - b^1\Sigma^+$	5.5 - 14.1
N_2^+ (First Negative)	$X^2\Sigma^+ - B^2\Sigma^+$	1.5 - 5.0
N_2^+ (Meinel)	$X^2\Sigma^+ - A^2\pi$	0.3 - 2.25

The absorption coefficient implied in Allen's results is the "smeared rotational line" model of Keck et al.[27] which has been shown by Patch et al.[28] to be equivalent to a "just overlapping line" model. Although, as indicated by the name, the rotational lines are not distinguished, considerable detail of the vibrational structure is given. The linear (true) absorption coefficient has the form[28]

$$K'_\nu = \frac{\pi e^2}{m_e c^2} \frac{hc}{3Py} \frac{h\nu}{kT} \left|\frac{R(\bar{r})}{ea_o}\right|^2 N \phi \exp[- h/kT(\nu_{oo}-\nu)]$$

$$= 8.96 \times 10^{-3} \frac{(\lambda cm)^{-1}}{(kT\ eV)} \left|\frac{R(\bar{r})}{ea_o}\right|^2 \frac{N}{N_L} \phi \exp[- h/kT(\nu_{oo}-\nu)]cm^{-1}$$

(3.8)

where N is the number of molecules per unit volume which are in the lower electronic state of the transition, ϕ is a dimensionless function which contains the vibrational-rotational structure of the band system and $\left|\frac{R(\bar{r})}{ea_o}\right|^2$ and ν_{oo} are spectroscopic constants.

Allen's graphical presentation is of the quantity $\phi\lambda^{-6}$ which is the spectral variation of the local emission coefficient. Now, the general shape of the curves can in each case be approximated by three straight lines on Allen's (semi-logarithmic) plots. This approximation loses the detailed vibrational-rotational structure but preserves the overall band-shape; it is better at high temperatures than at low temperatures and better for some band systems (e.g. N_2 B-H #2) than for others (e.g. N_2^+ Meinel). The curves were fitted by eye to obtain the constants a and b in the following equation for each band-system and temperature:

$$\phi\lambda^{-6} = \begin{cases} a_1 e^{-b_1\lambda} & \lambda_o \leq \lambda \leq \lambda_1 \\ a_2 e^{-b_2\lambda} & \lambda_1 \leq \lambda \leq \lambda_2 \\ a_3 e^{-b_3\lambda} & \lambda_2 \leq \lambda \leq \lambda_3 \end{cases} \tag{3.9}$$

The spectral content of the absorption coefficient (see Eq. (3.8)) is given by $\phi \times \lambda^{-1} \propto \phi\lambda^{-6}/(h\nu)^5$. The constants in Eq. (3.9) are therefore redefined so that we obtain a quantity η such that

$$\phi\lambda^{-1}cm^{-1} = \eta/(h\nu)^5 \tag{3.10}$$

and

$$\eta = \begin{cases} \alpha_1 e^{-\beta_1/h\nu} & h\nu_o \geq h\nu \geq h\nu_1 \\ \alpha_2 e^{-\beta_2/h\nu} & h\nu_1 \geq h\nu \geq h\nu_2 \\ \alpha_3 e^{-\beta_3/h\nu} & h\nu_2 > h\nu \geq h\nu_3 \end{cases} \tag{3.11}$$

where $h\nu$ is in eV and $h\nu_i = hc/\lambda_i$. The constants α_i and β_i are presented in Table 3.2.

TABLE 3.2

Values of α_i and β_i

$N_2(1+)$

T °K	i	0	1	2	3
11,000	α		0	5.57×10^6	7.32×10^4
	β		0	7.177	4.04
	hν	2.695	2.695	0.838	0.310
8,000	α		0	1.981×10^6	3.60×10^4
	β		0	6.621	3.69
	hν	2.695	2.695	0.838	0.310
5,000	α		0	3.98×10^5	1.16×10^4
	β		0	5.53	2.57
	hν	2.695	2.695	0.838	0.310

$N_2(2+)$

T °K	i	0	1	2	3
11,000	α		9.588×10^{-18}	1.011×10^8	1.88×10^{13}
	β		-243.1	10.19	50.8
	hν	5.39	4.396	3.351	1.771
8,000	α		1.573×10^{-34}	2.452×10^7	1.799×10^{13}
	β		-417.3	5.761	51.1
	hν	5.39	4.460	3.351	1.771
5,000	α		1.787×10^{-56}	2.35×10^7	7.660×10^{12}
	β		-647.8	7.565	57.1
	hν	5.39	4.508	3.351	1.771

TABLE 3.2 (Continued)

N_2 (B-H#2)

T °K	i	0	1	2	3
11,000	α		1.213×10^6	1.752×10^{11}	1.963×10^{19}
	β		-106.85	41.97	181.3
	hν	14.121	12.523	7.514	5.5
8,000	α		1.889×10^4	1.181×10^{11}	3.632×10^{23}
	β		-157.8	39.95	255.4
	hν	14.121	12.638	7.491	5.5
5,000	α		5.595×10^3	4.453×10^{10}	2.212×10^{30}
	β		-164.3	33.92	371.89
	hν	14.121	12.473	7.451	5.5

N_2 (1-)

T °K	i	0	1	2	3
11,000	α		3.662×10^{-28}	3.046×10^7	1.183×10^{11}
	β		-315.2	6.020	31.781
	hν	5.00	3.999	3.115	1.5
8,000	α		2.021×10^{-43}	2.929×10^6	7.645×10^{10}
	β		-454.3	0	32.007
	hν	5.00	4.012	3.147	1.5
5,000	α		1.948×10^{-32}	2.171×10^5	4.863×10^8
	β		-348.9	-4.301	19.435
	hν	5.00	4.038	3.076	1.5

TABLE 3.2 (Continued)

T °K	$N_2^+(M)$ i	0	1	2	3
11,000	α		2.885×10^5	0	0
	β		3.933	0	0
	$h\nu$	2.246	0.300	0.300	0.300
8,000	α		2.080×10^5	0	0
	β		3.812	0	0
	$h\nu$	2.246	0.300	0.300	0.300
5,000	α		3.134×10^4	0	0
	β		3.878	0	0
	$h\nu$	2.246	0.300	0.300	0.300

4. CALCULATION OF RADIATIVE ENERGY IN NITROGEN

4.1 Introduction

The previous chapters of this part have described the calculation and assembly of data for the calculation to be discussed in this chapter.

The basic problem solved is as follows. It consists of finding the specific intensity of radiation at a point in a volume of nitrogen gas which is in local thermodynamic equilibrium and has the same thermodynamic state and species composition at all points. The path on which the specific intensity is defined originates on a transparent boundary and there is no radiation incident on this boundary from outside. Under these conditions, the equations of radiative transfer (Part 1, Eq. 1.1) can be reduced to the quadrature

$$I(s) = \int_0^\infty B_\nu [1 - \exp(-K_\nu s)] d\nu \qquad (4.1)$$

where the origin of coordinate s lies on the boundary.

The calculation and results will be discussed and interpreted in terms of the problem stated above. It is important to observe, however, that they are also relevant to the radiative flux emerging from a homogeneous plane slab of nitrogen gas. This may be seen as follows. Approximate, half-range equations can be obtained in a number of ways; their most general form is (see Appendix I),

$$\frac{dq_\nu^+}{d\eta_\nu} = 2\pi a \, B_\nu - bq_\nu^+ \qquad \bullet \quad (4.2a)$$

$$\frac{dq_\nu^-}{d\eta_\nu} = 2\pi a \, B_\nu + bq_\nu^- \qquad (4.2b)$$

where q_ν^+ and q_ν^- are the half-range fluxes, $d\eta_\nu \equiv K_\nu(x)dx$ is the increment in optical depth and a and b are constants. Solving Eq. (4.2a) for

the frequency integrated flux emerging from a homogeneous plane slab of thickness ℓ with transparent walls one gets

$$q^+(\ell) = 2\pi \frac{a}{b} \int_0^\infty B_\nu [1 - \exp(-K_\nu b\ell)]d\nu. \qquad (4.3)$$

Comparing Eqs. (4.3) and (4.1), one can see that

$$q^+(\ell) = 2\pi \frac{a}{b} I(b\ell). \qquad (4.4)$$

It is shown in Appendix I that if the approximate equations, Eqs. (4.2a) and (4.2b) are to be correct in the optically thick and optically thin limits, then a and b must take the values 1 and 2 respectively. Eq. (4.4) then becomes

$$q^+(\ell) = \pi I(2\ell). \qquad (4.5)$$

Eq. (4.5) therefore provides a means of obtaining a flux from the results presented in this chapter. Alternative values of a and b can be used if desired.

Earlier chapters of this work have discussed at length the calculation of K_ν for Eq. (4.1) and have developed techniques for dealing with the various difficulties which arise. Besides computing I(s), we examine the contributions of the various processes to determine which are the most important under any given condition. This was done by first dividing the lines of each spectrum into three classes: Class A containing a relatively small number of strong lines, Class B containing the isolated, self-absorbed lines of low-lying series and Class C containing the isolated, self-absorbed lines of all other series (if any). The detailed composition of these classes is given in Table 4.1 which also acts as the key to the symbols of Figs. 9 to 11.

Section 4.2 gives an outline of the method of calculation (some further details are to be found in Appendix II). Section 4.3 presents and discusses the results.

4.2 The Method of Calculation

The calculation was programmed in FORTRAN IV (E-Level) for the IBM 360 computer at Brown University. The program consists of a main program and sixteen subprograms. A short description of these is given in Appendix II. It is the purpose of this section to give an outline of the method of computation and the form of the output.

For given temperature and density, the program first calculates the species composition according to the method described in Part 1, Section 2.3. The species composition is consistent with Figs. 4 to 7 of Part 1 and Fig. 13 of this part. The program then calculates the radiative transfer for each of a number of path lengths according to the following procedure.

The program first deals with the lines of each of the first four spectra. It finds the initial quantum number, $\bar{m}$, of the first merged (or thin), high series (see Part 2, Section 3.5). Values of $\bar{m}$ are limited to $\bar{m} \geq 9$. Next, it treats the class B lines, finding for each series the first merged or thin high line, $\bar{n}$, (see Part 2, Section 3.3) and calculating the intensity due to self-absorbed or isolated low lines. The quantity $\bar{n}$ is limited to a minimum value which depends on the series. The influence of the background continuum (excluding the high lines, see Appendix II) on each low-line intensity is allowed for by the factor $\exp(-K_{\nu_0,c} s)$, where $K_{\nu_0,c}$ is the continuum absorption coefficient at the line center; the justification of this procedure may be found in Section 3.1 of Part 1. A computation similar to that described above for the Class B lines is now performed on the Class C lines (in this case $\bar{n} \geq 9$). In the treatment of each series of

either class, the pseudo-threshold frequency defined by the first thin or
merged high line is stored according to a parameter which relates it to the
corresponding photoionization transition. Finally for the lines, the inten-
sities due to the Class A lines are computed. Here, the effect of high lines
is included in the background continuum. The line intensities are calculated
by the methods developed in Sections 3.4, 3.5 and 4.7 of Part 1.

After calculating line intensities and finding the pseudo-continuum
thresholds, the program then finds the contribution of all the continuum
and pseudo-continuum processes. It does this by performing a Simpson's rule
integration with respect to ν over the quantity $B_\nu[1-\exp(-K_{\nu,c}s)]$ where
$K_{\nu,c}$ is the total absorption coefficient due to all continuum and pseudo-
continuum processes.

The contributions from extremely low and extremely high frequency
continua are found analytically. For sufficiently low frequencies, the free-
free absorption coefficient will be large enough to produce black-body radia-
tion. Therefore, if ν_{ir} is the largest value for which $K_{\nu_{ir}}s \gg 1$ and
$h\nu_{ir}/kT \ll 1$, then the intensity I_{ir} due to frequencies in the range
$0 \leq \nu \leq \nu_{ir}$ is found by setting $\exp(h\nu/kT)-1 \cong h\nu/kT$ in the Planck func-
tion and integrating from 0 to ν_{ir}

$$I_{ir} = 1.67 \times 10^{10}kT(h\nu_{ir})^3 \text{erg sec}^{-1}\text{cm}^{-2} \qquad (4.6)$$

where kT and $h\nu_{ir}$ are in eV. For sufficiently large frequencies, the
continuum absorption coefficient (which is dominated at large frequencies
by the bound-free coefficient) will fall off and the gas will become opti-
cally thin. We choose an absorption coefficient fall-off of the form
$K_\nu \propto \nu^{-2}$ for these high frequencies (this decay law approximately represents
the behavior of nonhydrogenic bound-free transitions). Then, if ν_{uv} is
the start of this optically thin region and we also require $h\nu_{uv}/kT \gg 1$,

we can obtain the intensity I_{uv} due to frequencies in the range $\nu_{uv} \leq \nu \leq \infty$ by putting $\exp(h\nu/kT)-1 \stackrel{\sim}{=} \exp(h\nu/kT)$ in the Planck function, using the optically thin result

$$I_{uv} = \int_{\nu_{uv}}^{\infty} B_\nu K_\nu \, d\nu$$

and setting $K_\nu \stackrel{\sim}{=} \kappa/\nu^2$ where κ is the constant of proportionality. The result is

$$I_{uv} = 5.02 \times 10^{10} \kappa s kT(h\nu_{uv}+kT)\exp(-h\nu/kT) \text{ erg sec}^{-1}\text{cm}^{-2} \qquad (4.7)$$

where $h\nu_{uv}$ and kT are in eV.

The quantities ν_{ir} and ν_{uv} having been found, it remains to compute the Simpson's rule integration from ν_{ir} to ν_{uv}. However, this is not completely straightforward since the interval ν_{ir} to ν_{uv} is usually large and the integrand is usually uneven so that an extremely large number of intervals are required to achieve an acceptable accuracy. In order to avoid this, the interval is divided into a number of sections, each section being treated only as accurately as the size of its contribution to the overall integral warrants. An overall accuracy of approximately 1% is aimed at. Full details are given in Appendix II in the description of subprogram CONT.

After calculating the overall continuum intensity, the program computes the contribution of each individual continuum process. Since it is the contribution in the presence of all the other processes which is required, this is done in each case by integrating the continuum intensity in the absence of the process concerned and subtracting this value from the total continuum intensity. Because of the tolerance on the integration procedure, each individual contribution is accurate to only about 2% of the total continuum intensity.

The output of the program consists of the total intensity in various forms. The individual contributions of groups of lines (see Table 4.1) and of the continuum and pseudo-continuum processes are all expressed as fractions of the total intensity. Additional information which is given is the ratio of the intensity of each group of lines to the intensity of the same group in the absence of a background continuum and the quantum numbers corresponding to the start of pseudo-bound-free continuum absorption coefficients. A typical output of the program is presented as Table 4.2.

Finally, we discuss the steps taken to check out the program. In the first place, it must be said that to exhaustively check the operation of every possible path in such a complex computation is not feasible. The following tests were made, however. The operation of every subprogram was checked against hand calculations by a series of specially designed test programs. Diagnostic output instructions were included to check most intermediate steps. Inevitably, when the subprograms were incorporated into the main calculation, changes were found to be necessary. In the event of extensive alterations, a subprogram was retested by means of the appropriate test program. The calculated composition was compared with the results of Drellishak et al.[29], as described in Part 1, Chapter 2, and the agreement was satisfactory. Random selections of line intensities calculated by the subprograms within the main calculation were checked against hand calculations. The overall continuum absorption coefficient and the overall energy at low temperatures were checked for order of magnitude agreement with the results for air of Churchill et al.[23] and Allen[14] respectively. Finally, by using a very low value of path-length, it was possible to use the program to find values of the Planck mean absorption coefficient. Values calculated at $kT = 1eV$ and $kT = 2eV$ were compared with the Planck mean absorption

coefficients calculated by Armstrong et al.[7] which are the most accurate currently available. Table 4.3 shows this comparison. It can be seen that our results are within 25% of Armstrong's. This agreement can be considered as satisfactory.

4.3 Presentation and Discussion of Results

The results are shown on Figs. 6 to 12 while Figs. 13 and 14 show additional information. Figures 6 to 12 contain the following information. Figures 6a, 6b and 6c show the quantity I/B as a function of path length, s, for each of the temperatures $5,000^\circ K$, $11,000^\circ K$, $15,000^\circ K$, $20,000^\circ K$, $30,000^\circ K$ and $35,000^\circ K$ at the three densities 10^{-1}, 10^{-3} and 10^{-5} times atmospheric. (A temperature of $11,000^\circ K$ had to be used rather than $10,000^\circ K$ because of the availability of molecular band data, see section 3.4.) The figures consist of curves drawn through values calculated at six equally spaced (on a logarithmic scale) path lengths over the range 0.1 cm to 35 cm. The case of $s = 10$ cm has been cross-plotted: Fig. 7 shows I/B as a function of temperature while Fig. 8 shows I/B as a function of density. Calculations for Fig. 7 were performed at temperatures of $5,000^\circ K$, $8,000^\circ K$, $11,000^\circ K$, $15,000^\circ K$, $20,000^\circ K$, $25,000^\circ K$, $30,000^\circ K$ and $35,000^\circ K$. Calculations for Fig. 8 were performed at values of ρ/ρ_o which are powers of 10 in the range 10^{-5} to 10^{-1}.

Figures 9 to 11 display the distribution of radiative intensity over the individual contributors. On these plots, each contributor is represented by an area; the value of the intensity due to any individual contributor to a given value of the abscissa may be found from the vertical extent of the appropriate area. The lines of the various spectra are highlighted by distinctive cross-hatching. The distribution of intensity is shown on Figs. 9a to 9e as a function of path length, on Fig. 10 as a function of temperature

and on Fig. 11 as a function of density. The curves were drawn through

values calculated at the same points as used for the corresponding plots of

ι/B (see preceding paragraph). The symbols used on Figs. 9 to 11 are

listed in Table 4.1. However, the following comment is necessary regard-

ing the continuum contributors. As described in Section 4.2, the radiation

due to each continuum contributor was calculated as the difference between

the continuum radiation due to all contributors and the continuum radiation

due to all contributors except the individual process in question. When

the gas is optically thin, this is the same as calculating the radiation

due to each contributor alone. However, when self-absorption occurs, the

problem becomes nonlinear with the result that the sum of the individual

continuum contributions is less than the total continuum value. The

difference appears as part of the unlabelled area at the top of the higher

density plots of Figs. 9 to 11. By virtue of the method of calculation,

the values presented for each individual contributor represent the errors

incurred by neglecting that contributor.

The last set of figures, Figs. 12a, 12b and 12c present the equivalent

gray-gas absorption coefficient, $\bar{K}$. This quantity is defined such that

$$1 - e^{-\bar{K}s} = \frac{I}{B} .$$ (4.6)

Before discussing Figs. 6-12, we briefly recapitulate the factors

which govern the intensity of a radiating process (a more detailed discus-

sion may be found in Part 2). The occupation number of the initial state

is determined by the total number of particles of the atom or ion which

are present and by the Boltzmann factor (which favors states of low energy).

The cross section of a bound-free continuum process is independent of the

thermodynamic state but that of a line is not, due to the line profile.

Increasing temperature and density tend to increase the line width, hence

increasing the radiation from a self-absorbed line. Finally, the frequency

of a transition is important since it determines the local value of the

Planck function; it was demonstrated in Part 2 that for some lines, this

can be the dominant effect.

Figures 6 to 8, The Frequency Integrated Intensity

Figures 6 to 8 present I/B, the radiant energy as a fraction of

balck-body intensity. This quantity is the sum over a large number of

intensities, the rates of change of which can be different; it is there-

fore not surprising that curves of I/B exhibit a variety of forms. The

complexity of the calculation of I/B makes it difficult to interpret any

but the gross features of its behavior; such an interpretation is all that

is attempted here.

As a function of path length, I/B must always increase although the

rate of growth can be small when Doppler broadened lines dominate (see

Fig. 6c) or where black-body radiation is approached (see Fig. 6a). Black-

body radiation is achieved only at the highest density, $\rho/\rho_o = 10^{-1}$, and

then only for relatively high temperatures and path lengths. The intensity

at 5,000°K (which, it may be noted, has been multiplied by a factor of 10^4)

grows linearly with s because optically thin molecular bands dominate

the radiation. (Atomic lines occur but are self-absorbed and negligible

compared to the molecular bands.) The intensity curves for higher

temperatures grow less rapidly due to self-absorption.

Figure 7 shows the quantity $(I/B)/(\rho/\rho_o)$ as a function of

temperature. The factor $(\rho/\rho_o)^{-1}$ eliminates some of the density

dependence of these curves which would coincide in the absence of self-absorption and change of species. In general, the curves of Fig. 7 exhibit an increase of intensity with temperature. At $\rho/\rho_0 = 10^{-1}$ this rise is due to an increase in the bound-free continuum produced by the increasing importance of transitions from excited states. At lower densities, the following explanation for the increase of intensity with temperature is offered. At $\rho/\rho_0 = 10^{-5}$, the lines are not heavily self-absorbed. As the temperature increases, each line spectrum in turn becomes important and then dies away (see Fig. 10). Now, the dominant lines in each of the second and third spectra (namely IIA1, IIIA1 and IIIA2) have approximately the same frequencies and total oscillator strengths but at temperatures where the third spectrum is dominant, the Planck maximum is nearer to the line positions than at temperatures for which the second spectrum is dominant. Consequently, the intensity can increase with temperature. At $\rho/\rho_0 = 10^{-3}$, on the other hand, the same effect is obscured by the occurrence of considerable self-absorption which favors the lines of the lower ionized species (because Stark broadening is more important for such lines). It seems likely that the local minimum of the $\rho/\rho_0 = 10^{-3}$ curve (which does not occur at $\rho/\rho_0 = 10^{-5}$) is due to the increased self-absorption of the higher species lines.

Figure 8 shows the intensity as a function of density. The rise in intensity with increasing density is due to the accompanying increase in optical thickness.

Figures 9 to 11, The Distribution of Radiation Among Individual Contributors

Figures 9a-9e show the effect of changes in path length s for a variety of conditions. In general, one can see that the importance of

lines with respect to continuum decreases with increasing s. This is due to one or both of the following two effects. At low densities, the continuum is optically thin while many of the stronger lines are self-absorbed. In this case, the energy carried by the continuum grows linearly with s but the line intensities grow only as $s^{1/2}$, or more slowly. This effect is mainly responsible for the decrease in relative line intensity at $\rho/\rho_o = 10^{-3}$. The second effect occurs at higher densities where the continuum experiences some self-absorption. When this occurs, the continuum reduces the intensity of each line by the factor $\exp(-K_{\nu_o,c}s)$ (see Part 1, Section 3.1), hence reducing the relative importance of the lines. As an illustration of the magnitude of this effect, for the case $T = 20,000^{\circ}K$, $\rho/\rho_o = 10^{-1}$ and $s = 10cm$, the factor $\exp(-K_{\nu_o,c}s)$ is, on the average, 0.1. It is this effect which is responsible for the dramatic fall of the line contribution with s at $\rho/\rho_o = 10^{-1}$. In addition to this change in the balance of energy between lines and continuum, the distribution over line contributors changes due, primarily, to a decrease in importance as s increases of the Doppler broadened lines. For example, if two or more species are contributing line radiation, the relative importance of the atom or lowest ion tends to increase with s. This occurs because the lines of higher ions are predominantly Doppler broadened and hence the associated line intensity grows more slowly than that due to the dispersion profiles of the atomic (or first ion) lines.

Figure 10 shows the influence of temperature on the distribution of radiation. At $\rho/\rho_o = 10^{-1}$, only the first spectrum makes any substantial contribution to the radiation. The lines contribute only 15% or less of the total except between $9,000^{\circ}K$ and $15,000^{\circ}K$ where the line radiation contribution rises to a maximum of 30%. This maximum is caused by the

local importance of the IA3 group and this importance follows from the relatively large widths of these lines. At higher temperatures, they become insignificant due to a rise in continuum absorption coefficient at the frequencies of these lines. The plot for $\rho/\rho_o = 10^{-3}$ shows the contribution of many different groups. After the initial dominance of the molecular bands, first the lines and continuum of the first spectrum and then the lines and continuum of the second spectrum become dominant. In each case, the lines rise into prominence first and then, at slightly higher temperatures, the bound-free continuum rises with the result that the relative importance of the lines shows a number of maxima and minima. That the lines of a spectrum should become important at lower temperatures than the continuum is presumably caused by the movement of the maximum of the Planck function in the direction of higher frequencies as the tempera- ture rises. The plot for $\rho/\rho_o = 10^{-5}$ shows many of the features of that for $\rho/\rho_o = 10^{-3}$ but the lines are not so heavily self-absorbed with the result that the continuum is unimportant except at low temperatures. This decrease in self-absorption also results in the 2s-2p same-shell transi- tions making an appearance in the first spectrum (group IA1) and becoming dominant in the second spectrum (group IIA1). These lines have large f- numbers and moderate frequencies but suffer from small Stark widths so that they tend to be heavily self-absorbed at all but the lowest densities. A comparison can be made between Fig. 10 and Fig. 13. Figure 13 shows the distribution of radiating particles (i.e. molecules, atoms and molecular and atomic ions) in a manner similar to that used in Fig. 10 for the distribution of radiative energy. The comparison of these two figures shows that the relative importance of radiative transfer by atoms and the lower ions tends to lag (in terms of increasing temperature) behind the

relative importance in number densities. In the case of higher ions, the temperature at which each ion is dominant in the transfer of radiative energy approximately coincides with the temperature at which it is numerically dominant. We may also point out that whereas N_2^+ is not sufficiently abundant to appear on Fig. 13, it can be the dominant contributor to radiative energy transfer as shown on Fig. 10; an explanation for this behavior is included in the next paragraph.

The influence of varying density is shown on Figs. 11a to 11d. Increasing density has two general effects, it increases the number density of each species (and hence the optical depths) and it changes the composition of the gas, making the less highly ionized particles more abundant. In the case of lines, both these effects favor the lower spectra. (The increase in optical depth favors the lower spectra because, as pointed out previously, such lines tend to have broader profiles and hence a more rapidly rising intensity than lines of higher spectra.) Figure 11 shows a fall in the importance of lines with density due to self-absorption and the increase in importance of the lower spectra which has just been discussed.

The 5,000°K plot of Fig. 11a shows the interesting result that the intensity from the N_2^+ molecular bands exceed the intensity from the N_2 molecular bands at low densities. This occurs despite the number of particles of N_2^+ being less than the number of particles of N_2 by several orders of magnitude (compare Fig. 13). The reason for this behavior is as follows. Both bands of N_2^+ originate from the ground state and have frequencies which put them at or near the maximum of the Planck function at a temperature of 5,000°K. On the other hand, two bands of N_2 originate from excited states which have low occupation numbers at this temperature. The remaining band of N_2, the Birge-Hopfield #2 band, originates from the ground state but occurs at high frequencies where values of the Planck

function are low.

We will now draw attention to some additional conclusions which can be drawn from Figs. 9, 10 and 11 and make some general comments. From these figures it can be seen that whereas the contribution from the lines of the first spectrum is scattered over many different groups, one or occasionally (in the case of the second spectrum) two groups transport all the significant line energy for the ions. This is because most of the ion lines have either very high energy levels or very high frequencies (which puts them in the tail of the Planck function) and hence are very weak. The few strong lines of each spectrum are the same-shell transitions from the ground state. The balance in importance between lines and continua is maintained for these spectra (and if anything, shifted in favor of the lines) because although few lines are important, the bound-free continua occur at very high frequencies and are thus poor carriers of radiation.

From Figs. 9 to 11 it can be seen that for temperatures above $10,000^{\circ}K$, molecular bands are not significant. At temperatures above $10,000^{\circ}K$, the lines are dominant for densities below approximately 10^{-4} times atmospheric, a balance between lines and continua exists for densities of 10^{-4} to 10^{-2} while at higher densities the continuum processes are the most important, although lines are not negligible.

In the range of conditions examined, all the first four line spectra can be important but only the continuum processes of the first two spectra need be accounted for. Class C lines are never significant while the only important continuum and pseudo-continuum mechanisms (apart from molecular bands) are the bound-free and high lines of the first and second spectra.

Finally, it can be seen that the continuum is approximately optically thin for densities below 10^{-2} times atmospheric while at least some of the

lines suffer self-absorption at all conditions (evidence for this statement
will be given in the discussion of the equivalent gray-gas absorption
coefficient).

Figure 12. The Equivalent Gray Gas Absorption Coefficient

When the gas is optically thin with respect to every contributor, $\bar{K}$,
defined by (see Eq. (4.8))

$$\bar{K} \equiv - \ln(1 - I/B)/s,$$

is equal to $\bar{K}_p$, the Planck mean absorption coefficient. As $I/B \rightarrow 1$,
small errors in the calculation of I cause $\bar{K}$ to become indeterminate.
Because of this indeterminacy, the curves of $\bar{K}$ on Fig. 12a for
$T \geq 20,000°K$ could not be drawn for high values of s and the curve cor-
responding to 15,000°K is not reliable in the dashed region.

It can be seen from Fig. 12 that $\bar{K}$ decreases with increasing path
length except, possibly, where the radiation approaches that of a black-
body and at 5,000°K. In the 5,000°K case, the radiation comes predomi-
nantly from the optically thin molecular bands, hence $\bar{K}$ is independent
of s. Note, however, that the constant value of $\bar{K}$ is not that of the
Planck mean, due to the atomic lines which are self-absorbed and insigni-
ficant contributors to the radiation at the conditions for which the
curves are plotted but are not insignificant in an optically thin medium.
In fact, $\bar{K}$ does not equal $\bar{K}_p$ under any of the conditions presented,
which indicates that the lines are never all optically thin at these
conditions.

An explanation for the fall of $\bar{K}$ with s for the case when the
lines are self-absorbed but the continuum is optically thin (which is
the most common situation) will now be given. Suppose one calculates the

value of $\bar{K}$ at a particular value of s. This value of $\bar{K}$ will always correspond to optically thin, gray radiation (see the values of $\bar{K}$ and s of Figs. 12b and 12c). Thus for increases of path length, the use of a constant value of $\bar{K}$ would predict a radiation intensity which grows linearly with s whereas in the real gas the radiation will grow more slowly due to self-absorption of the lines. Thus, to match the "gray" intensity to the true intensity, $\bar{K}$ must decrease with s.

The Influence of Doppler Broadening

Previous workers did not include Doppler broadening in their calculations of line intensities since preliminary estimates may well lead one to expect its effect to be negligible. Some of our own early calculations also neglected Doppler broadening. However, it turns out from our more accurate calculations that Doppler broadening has a significant influence on the amount of energy radiated at temperatures above approximately 10,000°K provided that the density is not too high. We will therefore discuss the effect of Doppler broadening in some detail.

From the discussion of Part 1, Section 4.7, it can be seen that the influence of Doppler broadening is at its greatest when the dominant lines are low-lying (and hence have significant Doppler broadening) and when these lines are self-absorbed but not strongly self-absorbed. (When strongly self-absorbed, the intensity of a line depends on the Stark width and not on the Doppler width.)

We are able to illustrated the quantitative effect of Doppler broadening on the total intensity under certain conditions because of the early calculations which were performed neglecting Doppler broadening. The ratio of the results from these early calculations to the total intensity obtained from the final calculations is plotted on Fig. 14. Values

are available at 20,000°K for three densities[*] and at 11,000°K for

$\rho/\rho_o = 10^{-5}$. It can be seen from Fig. 14 that even at these moderate tem-

peratures, large errors can be caused by the neglect of Doppler broadening.

In general, the error decreases with path length as self-absorption in-

creases and the controlling part of more and more lines moves into the

Stark-broadened wings. At sufficiently low optical depths, however, the

error increases with increasing s as an increasing number of lines

become self absorbed.

In general, the influence of Doppler broadening will increase with

increasing temperature and with decreasing density for the following rea-

sons. Increasing temperature increases the Doppler line width and the

importance of the Doppler-dominated lines associated with the higher ions.

Decreasing the density lowers the optical depth so that an increasing

number of lines fall in the Doppler-dominated region of their curves of

growth. At the same time, decreasing the density increases the dominance

of the higher ions which are predominantly Doppler broadened.

---

[*] The values plotted for the conditions $T = 20,000°K$ and $\rho/\rho_o = 10^{-5}$ overestimate the correct values of I_{ND}/I since the calculation of line transfer by the third spectrum (NIII) in the absence of Doppler broaden- ing used values of electron impact line width which were too large by a factor of 10.

TABLE 4.1

Line Classification and Symbols Used on Figs. 9 to 11

First Spectrum, NI

Class A Lines

Group	Type of Transition	No. of Transitions Treated Individually	Symbol
1	$2s - 2p$	6	IA1
2	$(^3P)2p - (^3P)3\ell$	6	IA2
3	$3\ell - 3\ell'$	14	IA3
4	$3\ell - 4\ell'$	19	IA4
5	$4\ell - 4\ell'$	4	IA5
6	$4\ell - 5\ell'$	6	IA6
7	$5\ell - 5\ell'$, $6\ell - 6\ell'$	4	IA7

Class B Lines

Group	Type of Transition		No. of Series Treated Individually	Symbol
1	$(^3P)2p-(^3P)n\ell$	$n \geq 4$	3	IB1
2	$(^1D,^1S)2p-(^1D,^1S)n\ell$	$n \geq 3$	3	IB2
3	$\begin{cases} 2s2p^4-2s2p^3n\ell \\ 2s^22p^3-2s2p^3n\ell \end{cases}$	$n \geq 3$	10	IB3
4	$3\ell - n\ell'$	$n \geq 5$	3	IB4
5	$4\ell - n\ell'$	$n \geq 6$	1	IB5

Class C contains all unmerged series with initial quantum numbers $m \geq 5$. The symbol is IC.

Second Spectrum, NII

Class A Lines

Group	Type of Transition	No. of Transitions Treated Individually	Symbol
1	$2s - 2p$	6	IIA1
2	$3\ell - 3\ell'$	8	IIA2
3	$3\ell - 4\ell'$	11	IIA3
4	$4\ell - 4\ell'$	2	IIA4

Class B Lines

Group	Type of Transition		No. of Series Treated Individually	Symbol
1	$2p - n\ell$	$n \geq 3$	3	IIB1
2	$3\ell - n\ell'$	$n \geq 5$	3	IIB2

Class C contains all unmerged series with initial quantum numbers $m \geq 4$. The symbol is IIC.

TABLE 4.1 (Continued)

Third Spectrum, NIII

Class A Lines

Group	Type of Transition	No. of Transitions Treated Individually	Symbol
1	$2s^2 2p - 2s2p^2$	3	IIIA1
2	$2s2p^2 - 2p^3$	6	IIIA2
3	$\{ 3s - 3p, 4s - 4p \}$	5	IIIA3

Class B Lines

Group	Type of Transition	No. of Series Treated Individually	Symbol
1	$2p - n\ell \quad n \geq 3$	1	IIIB1

Class C contains all unmerged series with initial quantum numbers $m \geq 3$. The symbol is IIIC.

Fourth Spectrum, NIV

Class A Lines

Group	Type of Transition	No. of Transitions Treated Individually	Symbol
1	$\{ 2s^2 - 2s2p, 2s2p - 2p^2 \}$	4	IVA1

Class B Lines

Group	Type of Transition	No. of Series Treated Individually	Symbol
1	$2s - np \quad n \geq 3$	1	IVB1

Class C contains all unmerged series with initial quantum numbers $m \geq 3$. The symbol is IVC.

Continuum and Pseudo-Continuum Processes

	Process	Symbol
NI	Bound-Free	IBF
NI	High Lines	IHL
NI	High Series	IHS
NII	Bound-Free	IIBF
NII	High Lines	IIHL
NIII	Bound-Free	IIIBF
NIII	High Lines	IIIHL
NIII	High Series	IIIHS
NIV	Bound-Free	IVBF

TABLE 4.1 (Continued)

	Process	Symbol
NIV	High Lines	IVHL
NIV	High Series	IVHS
N^+	Free-Free	+FF
N^{++}	Free-Free	2+FF
N^{+++}	Free-Free	3+FF
N^{++++}	Free-Free	4+FF
N_2	Molecular Bands	2MB
N_2^+	Molecular Bands	2+MB

Note: A portion of the continuum without a symbol shows the combined effect of various minor contributors plus the influence of self-absorption (see Section 4.3).

Table 4.2

Typical Output of Program RADN

RADIATIVE ENERGY TRANSFER IN ISOTHERMAL NITROGEN

SPECIES COMPOSITION AT TEMPERATURE=15000.0 DEGREES KELVIN, DENSITY= 0.1000E-02 (NONDIMENSIONAL)
        CORRESPONDING PRESSURE= 0.1993E 00 ATMOSPHERES

            VALUES OF PARTICLE DENSITY DIVIDED BY LOSCHMIDT NUMBER (=2.6871E19)
     N2+   N2   N   N+   N++   N+++   N++++   NE
C.3F12TF-CP 0.7CC22F-03 0.37111F-03 0.16289F-02 0.23774E-07 0.10241E-18 0.45359E-39 0.16289E-02

                        PARTITION FUNCTIONS

    CN2+   CN2   CN   CN+   CN++   QN+++   QN++++
C.12U9RE 00 0.25872E 05 0.6817CNF 01 0.10253E 02 0.60493E 01 0.10142E 01 0.20026E 01

                        GAS CONDITIONS

                TEMPERATURE=15000.0 DEGREES KELVIN
                    DENSITY= 0.1000E-02 (NONDIMENSIONAL)
                PATH LENGTH= 0.1000E 02 CM.

                        GENERAL RESULTS

                TOTAL INTENSITY= 0.5779E-04 ERG EV CM-2 STERAD-1
                              = 0.1397E 11 ERG SEC-1 CM-2 STERAD-1
                              = 0.1539E-01 X BLACK-BODY INTENSITY
        FLUX FROM A SLAB OF THICKNESS 0.50E 01 = 0.4390E 04 WATTS CM-2
                    INTENSITY DUE TO LINES= 0.4641E 00 X TOTAL INTENSITY
                    INTENSITY DUE TO CONTINUUM= 0.5359E 00 X TOTAL INTENSITY
        LINE INTENSITY WITH BACKGROUND CONTINUUM
                        DIVIDED BY
        LINE INTENSITY WITHOUT BACKGROUND CONTINUUM = 0.9269E 00
        EQUIVALENT GREY-GAS ABSORPTION COEFFICIENT = 0.1541E-02 CM-1

CCNTINUUM INTENSITIES RELATIVE TO THE TOTAL INTENSITY

```
            ALL CCNTRIBUTORS  0.5355E 00
               NI BOUND-FREE     0.3844E 00
               NI HIGH LINES     0.1205E 00
              NII BOUND-FREE     0.0
              NII HIGH LINES     0.0
             NIII BOUND-FREE     C.0
             NIII HIGH LINES     C.0
              NIV BOUND-FREE     0.0
              NIV HIGH LINES     C.0
                N+ FREE-FREE     0.2651E-01
               NI HIGH SERIES    0.0
               N++ FREE-FREE     0.0
              NII HIGH SERIES    0.0
              N+++ FREE-FREE     C.0
             NIII HIGH SERIES    0.0
             N++++ FREE-FREE     C.0
              NIV HIGH SERIES    0.0
            N2 MOLECULAR BANDS   0.0
           N2+ MOLECULAR BANDS   0.0
           ALL NI CONTRIBUTORS   C.5049E 00
          ALL NII CONTRIBUTORS   C.2651E-01
         ALL NIII CONTRIBUTORS   0.0
          ALL NIV CONTRIBUTORS   0.0
SUM CF INLIVIDUALLY CALCULATED CONTRIBUTORS   0.5315E 00
```

NOTE: VALUES FOR INDIVIDUAL CONTRIBUTORS
ARE ACCURATE TO APPROXIMATELY + OR - 0.11E-01

LINE INTENSITIES

RELATIVE TO THE TOTAL INTENSITY IN THE PRESENCE OF A BACKGROUND CONTINUUM	RELATIVE TO INTENSITIES IN THE ABSENCE OF A BACKGROUND CONTINUUM

FIRST SPECTRUM
ALL LINES RELATIVE TO TOTAL INTENSITY 0.4510E 00

CLASS A LINES

1	0.9072E-02	1	0.9269E 00
2	0.7455E-01	2	0.9798E 00
3	0.5962E-01	3	0.9958E 00
4	0.1201E-01	4	0.9907E 00
5	0.8667E-03	5	0.9626E 00
6	0.5208E-03	6	0.9420E 00
7	0.6325E-04	7	0.7809E 00

CLASS B LINES

GROUP	INTENSITY	GROUP	INTENSITY
1	0.1855E 00	1	0.9174E 00
2	0.1004E 00	2	0.8708E 00
3	0.3200E-02	3	0.9102E 00
4	0.0	4	0.0
5	0.0	5	0.0

CLASS C LINES

INTENSITY	INTENSITY
0.8474E-03	0.8069E 00

SECOND SPECTRUM
ALL LINES RELATIVE TO TOTAL INTENSITY 0.1304E-01

CLASS A LINES

1	0.1215E-01	1	0.9067E 00
2	0.3503E-03	2	0.9972E 00
3	0.7784E-04	3	0.9980E 00
4	0.1215E-05	4	0.9909E 00

CLASS B LINES

GROUP	INTENSITY	GROUP	INTENSITY
1	0.4554E-03	1	0.5408E 00
2	0.0	2	0.0

CLASS C LINES

INTENSITY	INTENSITY
0.5550E-05	0.9944E 00

THIRD SPECTRUM
ALL LINES RELATIVE TO TOTAL INTENSITY 0.4261E-04

CLASS A LINES

1	0.4258E-04	1	0.6988E 00
2	0.3116E-07	2	0.4672E 00
3	0.1105E-11	3	0.9977E 00

CLASS B LINES

GROUP	INTENSITY	GROUP	INTENSITY
1	0.1015E-06	1	0.6333E 00

CLASS C LINES

INTENSITY	INTENSITY
0.8348E-13	0.9984E 00

FOURTH SPECTRUM
ALL LINES RELATIVE TO TOTAL INTENSITY 0.6413E-16

CLASS A LINES

1	0.6413E-16	1	0.4399E 00

CLASS B LINES

GROUP	INTENSITY	GROUP	INTENSITY
1	0.1302E-25	1	0.1877E 00

CLASS C LINES

INTENSITY	INTENSITY
0.1797E-30	0.9922E 00

MISCELLANEOUS LINE INFORMATION

FIRST SPECTRUM

FIRST MERGED SERIES   9
FIRST MERGED LINE
OF NONHYDROGENIC SERIES

GROUP	SERIES	LINE
1	1	9
1	2	6
1	3	6
2	1	6
2	2	6
2	3	5
3	1	6
3	2	6
3	3	5
3	4	5
3	5	5
3	6	4
3	7	4
3	8	4
3	9	4
3	10	4
4	1	5
4	2	5
4	3	5
5	1	6

FIRST MERGED LINE
OF HYDROGENIC SERIES

M	N
5	9
6	9
7	9
8	9

SECOND SPECTRUM

FIRST MERGED SERIES   9
FIRST MERGED LINE
OF NONHYDROGENIC SERIES

GROUP	SERIES	LINE
1	1	11
1	2	10
1	3	6
2	1	5
2	2	5
2	3	5

FIRST MERGED LINE
OF HYDROGENIC SERIES

M	N
4	9
5	9
6	9
7	9
8	9

THIRD SPECTRUM

FIRST MERGED SERIES   9
FIRST MERGED LINE
OF NONHYDROGENIC SERIES

GROUP	SERIES	LINE
1	1	6

FIRST MERGED LINE
OF HYDROGENIC SERIES

M	N
3	9
4	9
5	9
6	9
7	9
8	9

FOURTH SPECTRUM

FIRST MERGED SERIES   9
FIRST MERGED LINE
OF NONHYDROGENIC SERIES

GROUP	SERIES	LINE
1	1	6

FIRST MERGED LINE
OF HYDROGENIC SERIES

M	N
3	9
4	9
5	9
6	9
7	9
8	9

TABLE 4.3

A comparison of the Calculated Planck Mean Absorption

Coefficient with the Results of Armstrong et al.[7]

kT eV	ρ/ρ_o	Planck Mean Absorption Coefficient cm^{-1}	
		Present Calculations	Ref. 7
1	0.98×10^{-1}	1.37	1.74
	10^{-2}	1.35×10^{-1}	1.71×10^{-1}
	10^{-3}	1.16×10^{-2}	1.54×10^{-2}
	10^{-4}	0.78×10^{-3}	1.12×10^{-3}
	10^{-5}	0.51×10^{-4}	0.594×10^{-4}
	10^{-6}	3.8×10^{-6}	3.91×10^{-6}
2	4.35	0.961×10^3	0.965×10^3
	5.88×10^{-2}	6.83	7.01
	6.18×10^{-3}	6.14×10^{-1}	6.13×10^{-1}
	7.16×10^{-4}	6.82×10^{-2}	6.77×10^{-2}
	7.26×10^{-5}	6.26×10^{-3}	6.19×10^{-3}
	7.39×10^{-6}	5.49×10^{-4}	5.41×10^{-4}

APPENDIX I   A Derivation of the Directionally Approximate Flux Equations

Many derivations of directionally approximate equations of radiative transfer may be found in the literature[30,31]. We are interested here in one-dimensional, half-range flux equations. It does not appear to have been pointed out previously that such equations can be derived with two free constants by applying the well-known substitute kernel approximation to the half-range fluxes. This will now be demonstrated.

The half-range fluxes q_ν^+ and q_ν^- at optical thickness η_ν are defined as follows

$$q_\nu^+(\eta_\nu) \equiv 2\pi \int_0^1 I_\nu \mu \, d\mu \qquad (I.1)$$

and

$$q_\nu^- \equiv 2\pi \int_{-1}^0 I_\nu \mu \, d\mu. \qquad (I.2)$$

A formal solution of the equation of radiative transfer for the half-range fluxes in a one-dimensional slab with isotropic wall conditions yields

$$q_\nu^+ = 2q_\nu^+(o)E_3(\eta_\nu) + 2\pi \int_0^{\eta_\nu} B_\nu(y) \, E_2(\eta_\nu-y)dy \qquad (I.3a)$$

and

$$q_\nu^- = 2q_\nu^-(\eta_\nu^L)E_3(\eta_\nu^L-\eta_\nu) - 2\pi \int_{\eta_\nu}^{\eta_\nu^L} B_\nu(y) \, E_2(y-\eta_\nu)dy \qquad (I.3b)$$

where $E_n(x) \equiv \int_0^1 e^{-x/\mu} \mu^{n-2} d\mu$ (see Ref. 32). Making the substitute kernel approximations $E_2(x) \stackrel{\sim}{=} ae^{-bx}$ and $E_3(x) \stackrel{\sim}{=} ce^{-bx}$ and differentiating yields the directionally approximate equations

$$\frac{dq_\nu^+}{dn_\nu} = 2\pi aB_\nu - bq_\nu^+ \tag{I.4a}$$

and

$$\frac{dq_\nu^-}{dn_\nu} = 2\pi aB_\nu + \cdot bq_\nu^- . \tag{I.4b}$$

As is well known, Eqs. (I.4a) and (I.4b) can be combined to produce a second order equation in the full-range flux.

Eqs. (I.4a) and (I.4b) have two free constants a and b. There are a number of ways of choosing these constants but we will mention only one; the constants may be chosen to give the correct expressions for half-range flux in the two limits of optical depth approaching zero and infinity. Matching Eqs. (I.4a) and (I.4b) to the exact expressions in these two limits yields $a = 1$ and $b = 2$. (Note that these values do not satisfy the optically thick limit of the full range flux equation.)

APPENDIX II   Fortran Program RADN

This appendix gives a brief description of the program RADN which calculates the specific intensity at a point in uniform nitrogen gas. The main program (containing 630 statements) and 16 subprograms (containing a total of 920 statements) which comprise RADN are discussed in turn. Each was written in FORTRAN IV (E-level subset) for the IBM 360 computer (Model 50) at Brown University.

Program RADN takes from 3 to 10 minutes to calculate the results for a single point (given temperature, density and path length), depending on the conditions and the number of individual continuum contributions investigated.

Main Program RADN

The main program reads data for the composition calculation, data for Class B lines of NI, NII, NIII and NIV, data for Class A lines of NI, NII, NIII and NIV, data for bound-free transitions of NI, NII, NIII and NIV, one value of temperature, data for molecular bands (if the temperature is 5,000°K, 8,000°K or 11,000°K only), up to ten values of density, up to ten values of path-length and, finally a set of parameters for each density which enable a selection of the individual continuum contributors to be omitted.

The main program then calls and organizes the subprograms to calculate line and continuum intensities. Finally, it processes and writes the results.

Subprograms COMPN, SAHA and SUMO

These three subprograms calculate the composition according to the method described in Part 1, Chapt. 2.

Subprogram MULT

Subprogram MULT calculates the intensity due to a group of closely
spaced lines and indicates whether the group is optically thick or optically
thin. Overlapping of the lines is allowed for as described in Part 1, Sec-
tions 3.4 and 4.7. The line wings have either dispersion or quasi-static
form and, where instructed to, the subprogram allows for a Doppler
broadened core.

Subprogram SOLE

Subprogram SOLE calculates the intensity due to each of several groups
of (Class A) lines. The bulk of the data is given in a two-dimensional
array. For each transition, the subprogram will calculate the occupation
number, the Stark line width and, where necessary, the resonance line
width. These and other necessary values are then fed to subprogram MULT
which returns the corresponding value of intensity (MULT may allow for a
Doppler core if the line data instructs it to). SOLE then calls the
continuum subprograms and finds the total continuum absorption coefficient,
$K_{v_o,c}$ at the line center and calculates an intensity reduced by the factor
$\exp(-K_{v_o,c}s)$. Reduced and unreduced intensities are summed for each group
separately and the sums passed back to the main program.

Subprogram SRIES1

Subprogram SRIES1 finds the position of the pseudo-bound-free
threshold for a number of non-hydrogenic series. Each position is stored
according to a given parameter which enables the position to be related to
the correct photoionization transition.

Data for the non-hydrogenic (Class B) lines is given in a three-
dimensional array. For each transition, starting with the lowest lying,

the subprogram calculates the occupation number and Stark line width. These
and other values are fed to subprogram MULT which returns the corresponding
value of intensity and indicates the optical thickness of the line. For
the line to be considered the start of the pseudo-continuum, it must be
higher up the series than a specified minimum and be either optically thin
or the first of three lines which are merged according to their effective
widths (see Part 2, Section 3.3). (It is necessary to check three lines
to avoid the case where an error in the data results in two lines being
closer together than they should be.) Transitions are only considered for
merging if the entire group of closely spaced lines is itself merged and
behaving like a superline (see Part 1, Section 3.4).

The intensities of all lines not counted in the pseudo-continuum are
added in groups and the sums passed to the main program. As in subprogram
SOLE, the lines are stored both unreduced and reduced by a background con-
tinuum. In this case, however, the high lines are not included in the
continuum (because the extent of the high lines is found within the sub-
program which would have to be called twice for it to be possible to include
high lines in the background continuum).

Subprogram SRIES2

Subprogram SRIES2 performs operations similar to those executed by
SRIES1 but it treats hydrogenic (Class C) series. Since the hydrogenic
data can be calculated within the subprogram, only overall quantities such
as ionization potentials and core statistical weights need be supplied.

Subprogram MERGE

Subprogram MERGE finds the first completely merged or thin series
above a specified minimum (see Part 2, Section 3.5). It treats the

series as hydrogenic and quasi-statically broadened.

Subprogram C1BF

Subprogram C1BF is the first of 6 subprograms for finding the absorption coefficient due to continuum processes. C1BF finds the absorption coefficient due to NI true bound-free transitions. It requires some cross sections in tabular form (we use the Burgess-Seaton calculations of Sherman and Kulander[16], see Section 3.2) at the threshold frequencies which must also be given. Intermediate values are found by linear interpolation. Occupation numbers are calculated in the main program (from given initial energies) and are supplied as data to the subprogram. For higher initial quantum numbers, hydrogenic cross sections, occupation numbers and threshold frequencies are calculated.

Subprogram C2HI

Subprogram C2HI calculates the absorption coefficient due to the merged or thin high lines of NI. It requires the same data as C1BF plus the pseudo-threshold frequencies found by SRIES1. For each initial quantum number for which the given frequency lies between a pseudo-threshold and a true threshold, a value of absorption coefficient is added to a sum. If the initial state is low-lying, the cross section is taken equal to the threshold bound-free value (see Section 2.4). For higher values it is calculated from the hydrogenic bound-free formula.

Subprogram C3BF

Subprogram C3BF calculates the absorption coefficient due to ionic bound-free transitions. The treatment is similar to that of C1BF except that the low-lying cross sections are computed from a formula due to Seaton[22] (see Section 3.2).

Subprogram C4HI

Subprogram C4HI calculates the absorption coefficient due to ionic high lines. The treatment is similar to that of C2HI except that Seaton's formula is used for the low-lying cross sections.

Subprogram C5FF

Subprogram C5FF calculates the absorption coefficient due to free-free transitions and high series (see Section 3.3). Four parameters enable any combination of these contributors to be included.

Subprogram C6MB

Subprogram C6MB calculates the absorption coefficient due to molecular bands. This facility is available at $5,000^{\circ}K$, $8,000^{\circ}K$ and $11,000^{\circ}K$ only. Details of the bands and their treatment may be found in Section 3.4. It is possible to omit either all the bands of N_2 or all the bands of N_2^+ if desired.

Subprogram SIMP

Subprogram SIMP performs a Simpson's rule integration on the quantity $B_\nu [1 - \exp(-K_{\nu,c} s)]$ from $h\nu_1$ to $h\nu_2$. It proceeds as follows. Starting with N intervals, it keeps doubling the number of intervals until the fractional error in two successive integrations is less than a given quantity. If this match is not achieved in 6 attempts, the subprogram accepts the last value but writes a warning message stating the oustanding error, the maximum error at which a match would have been accepted and the value of a parameter which enables one to identify the continuum process being investigated when the unmatched integration occurred. The values of $K_{\nu,c}$ are computed in this subprogram by means of the continuum subprograms (C1BF to C6MB).

Subprogram CONT

Subprogram CONT calculates the intensity due to continuum processes. From 0 to $h\nu_{ir}$ and from $h\nu_{uv}$ to ∞, the intensity is calculated as described in Section 4.2. From $h\nu_1 = 0.35kT$ to $h\nu_2 = 8.9kT$, the intensity is calculated by SIMP with $N = 50$ to a match of 1%; this result we call FINE. From $h\nu_{ir}$ to $h\nu_1$ and from $h\nu_2$ to $h\nu_{uv}$, the photon energy is divided into a number of intervals $h\nu_j$ to $h\nu_{j+1}$ where $\nu_{j+1} = 100 \times \nu_j$. Each interval is calculated by SIMP with $N = 10$ to a match of 10%. If the integrated intensity of any interval exceeds 5% of FINE then the integration over that interval is recomputed with $N = 50$ to a match of 1%. In this way, an overall accuracy of approximately 1% is maintained.

References for Part 3

1. C. E. Moore, "Atomic Energy Levels 1949," NBS Circular 467 (1949).

2. F. R. Gilmore, "Energy Levels, Partition Functions and Fractional Electronic Populations for Nitrogen and Oxygen Atoms and Ions to 25,000°K," RAND Corporation, Memorandum RM-3748-PR.

3. C. W. Allen, Astrophysical Quantities, London University Press, 1963.

4. L. Goldberg, "Relative Multiplet Strengths in LS Coupling," Astrophys. J. 82, 1-25 (1935).

5. F. Rohrlich, "Theoretical Multiplet Strengths," Astrophys. J. 129, 441-448 (1959).

6. A. F. Nikoforov, V. B. Uvarov and Yu. L. Levitan, Tables of Racah Coefficients, Pergamon, 1965.

7. B. H. Armstrong, R. R. Johnston and P. S. Kelly, "Opacity of High-Temperature Air," Air Force Weapons Laboratory Report AFWL-TR-65-17 (1965).

8. A. R. Edmonds, Angular Momentum in Quantum Mechanics, Princeton, 1960.

9. P. S. Kelly, "Transition Probabilities in Nitrogen and Oxygen from Hartree-Fock-Slater Wave Functions," J. Quant. Spectrosc. Radiat. Transfer 4, 117-148 (1964).

10. P. S. Kelly, "Some Analytical Self-Consistent Field Functions and Dipole Transition Matrix Elements for Nitrogen and Oxygen and Their Ions," Astrophys. J. 140, 1247-1268 (1964).

11. H. R. Griem, Plasma Spectroscopy, McGraw-Hill, 1964.

12. L. M. Biberman, V. S. Vorobyov and G. E. Norman, "Energy Emitted in Spectral Lines by a Plasma at Equilibrium," Opt. Spectry. 14, 176-179 (1963).

13. V. S. Vorobyov and G. E. Norman, "Energy Radiated in Spectral Lines by an Equilibrium Plasma II," Opt. Spectry. 17, 96-101 (1964).

14. R. A. Allen, "Air Radiation Graphs: Spectrally Integrated Fluxes Including Line Contributions and Self Absorption," AVCO-Everett Research Laboratory Research Report 230 (1965).

15. G. E. Norman, "The Pole of the Negative Nitrogen Ion N⁻ in the Production of the Continuous Spectrum of Nitrogen and Air Plasmas," Opt. Spectry. 17, 94-96 (1964).

16. M. P. Sherman and J. L. Kulander, "Free-Bound Radiation from Nitrogen, Oxygen and Air," Space Sciences Laboratory, General Electric Co., R65SD15 (1965).

17. W. J. Karzas and R. Latter, "Electron Radiative Transitions in a Coulomb Field," Astrophys. J. Suppl. Series 6, 167-212 (1961).

18. D. H. Menzel and C. L. Pekeris, "Absorption Coefficients and Hydrogen Line Intensities," Mon. Not. Roy. Astron. Soc. 96, 77-111 (1935).

19. A. Burgess, "The Hydrogen Recombination Spectrum," Mon. Not. Roy. Astron. Soc. 118, 477-495 (1958).

20. G. Peach, "Continuous Absorption Coefficients for Non-Hydrogenic Atoms," Mon. Not. Roy. Astron. Soc. 124, 371-381 (1962).

21. R. R. Johnston, B. H. Armstrong and O. R. Platas, "The Photoionization Contribution to the Radiation Absorption Coefficient of Air," Jl. Quant. Spectrosc. Radiat. Transfer 5, 49-53 (1965).

22. M. J. Seaton, "Thermal Elastic Collision Processes," Rev. Mod. Phys. 30, 979-989 (1958).

23. D. P. Churchill, B. H. Armstrong and K. G. Mueller, "Absorption Coefficients of Heated Air: A Compilation to 24,000°K," Air Force Weapons Laboratory Report AFWL-TR-65-132 (1965).

24. G. Peach, "A General Formula for the Calculation of Absorption Cross Sections for Free-Free Transitions in the Field of Positive Ions," Mon. Not. Roy. Astron. Soc. 130, 361-377 (1965).

25. R. A. Allen, A. Textoris and J. Wilson, "Measurements of the Free-Bound and Free-Free Continua of Nitrogen, Oxygen and Air," AVCO-Everett Research Laboratory Research Report 195 (1964).

26. R. A. Allen, "Air Radiation Tables: Spectral Distribution Functions for Molecular Band Systems," AVCO-Everett Research Laboratory Research Report 236 (1966).

27. J. C. Keck, J. C. Camm, B. Kivel and T. Wentink, Jr., "Radiation from Hot Air Part II," AVCO-Everett Research Laboratory Research Report 42 (1959).

28. R. W. Patch, W. L. Shackleford and S. S. Penner," Approximate Spectral Absorption Coefficient Calculations for Electronic Band Systems Belonging to Diatomic Molecules," J. Quant. Spectrosc. Radiat. Transfer 2, 263-271 (1962).

29. K. S. Drellishak, D. P. Aeschliman and A. B. Cambel," Partition Functions and Thermodynamic Properties of Nitrogen and Oxygen Plasmas," Phys. Fluids 8, 1590-1600 (1965).

30. R. Viskanta, "Radiation Transfer and Interaction of Convection with Radiation Heat Transfer," in Advances in Heat Transfer Vol. III, Academic, 1964.

31. S. C. Traugott and K. C. Wang, "On Differential Methods for Radiant Heat Transfer," Int. J. Heat Mass Transfer 7, 269-270 (1964).

32. V. Kourganoff, Basic Methods in Transfer Problems, Dover, 1963.
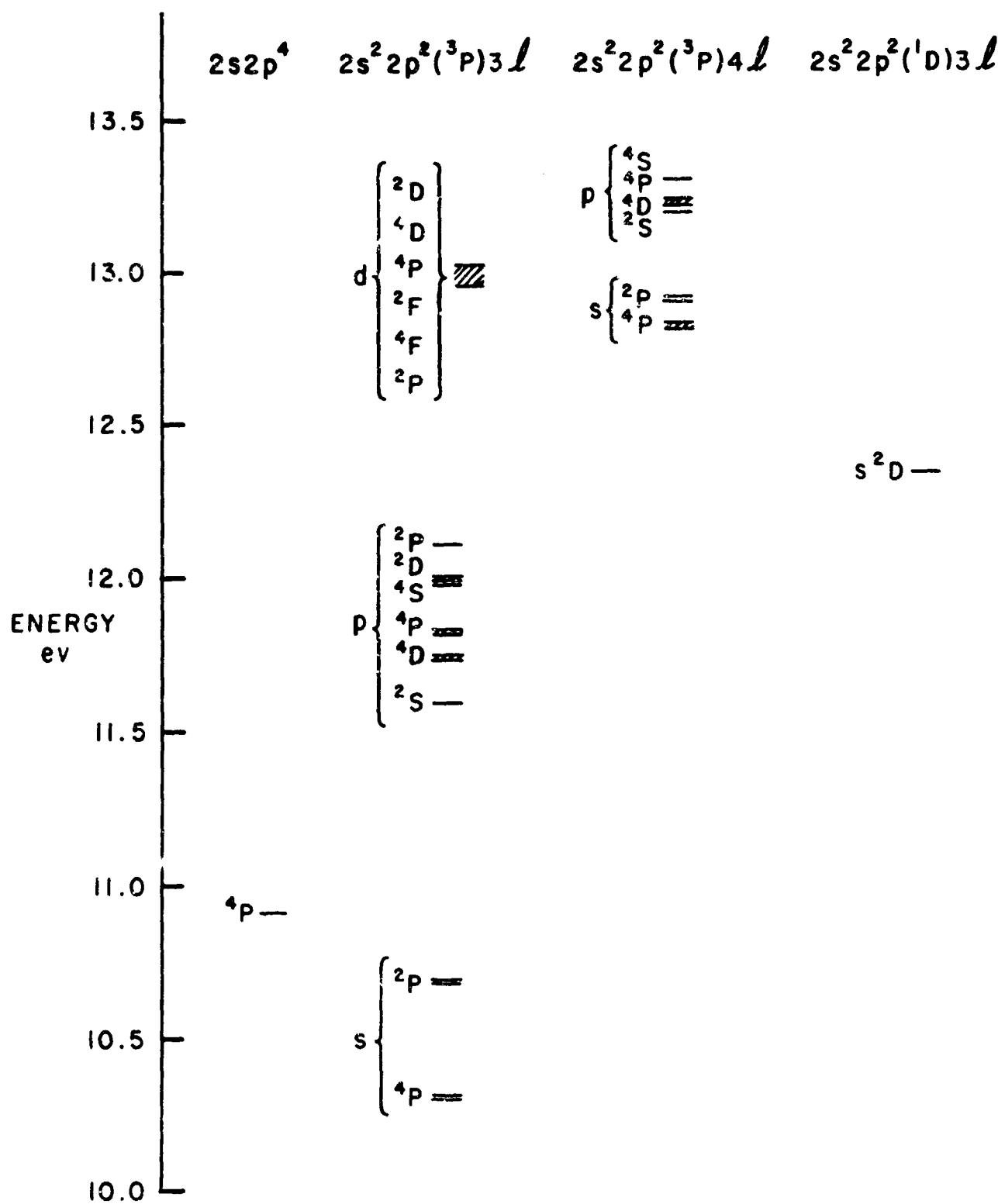
FIG. I SCHEMATIC DIAGRAM SHOWING SOME OF THE
ENERGY LEVELS OF ATOMIC NITROGEN
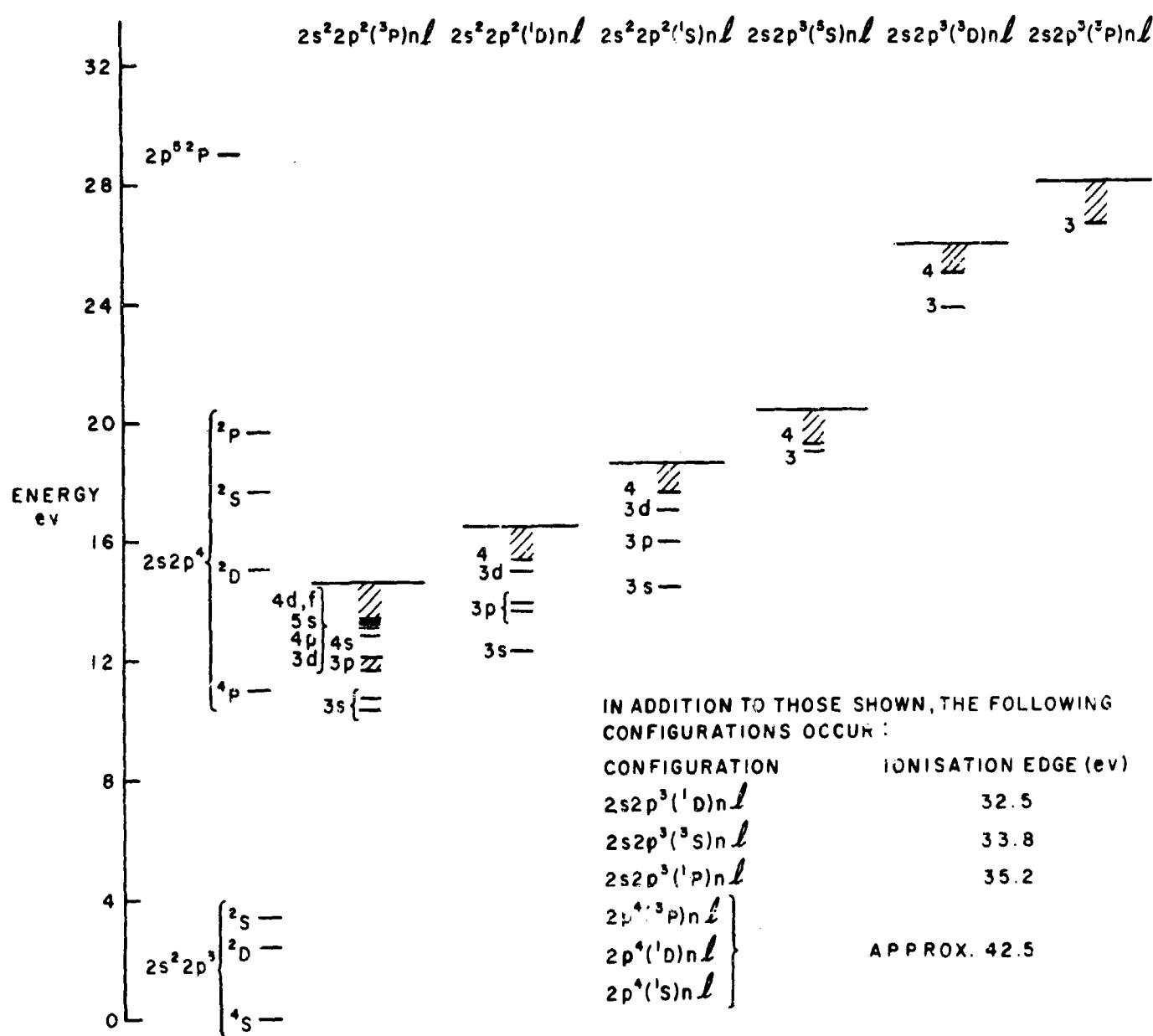
FIG. 2 SCHEMATIC DIAGRAM SHOWING THE MOST IMPORTANT ENERGY LEVELS OF ATOMIC NITROGEN
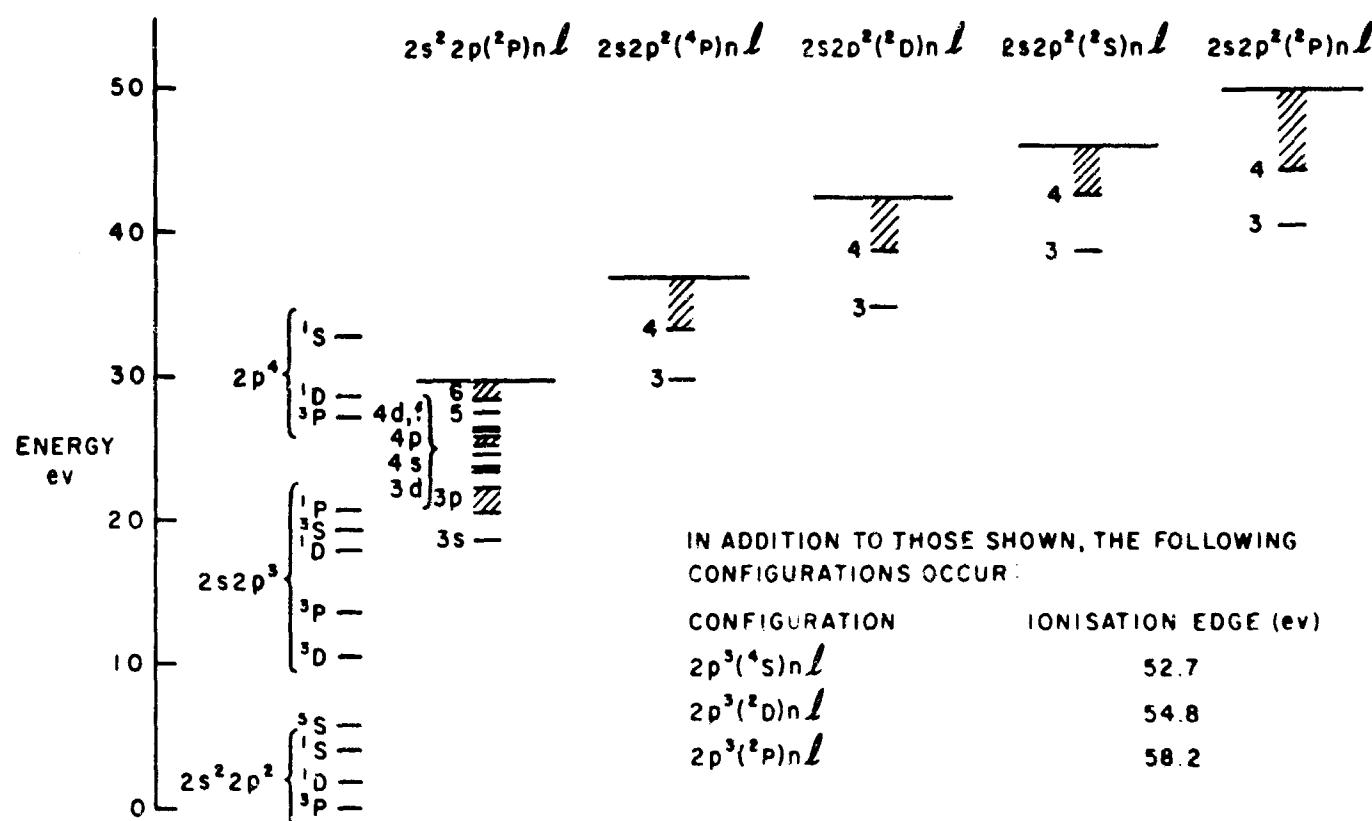
FIG. 3 SCHEMATIC DIAGRAM SHOWING THE MOST IMPORTANT ENERGY LEVELS OF SINGLY IONISED NITROGEN

98
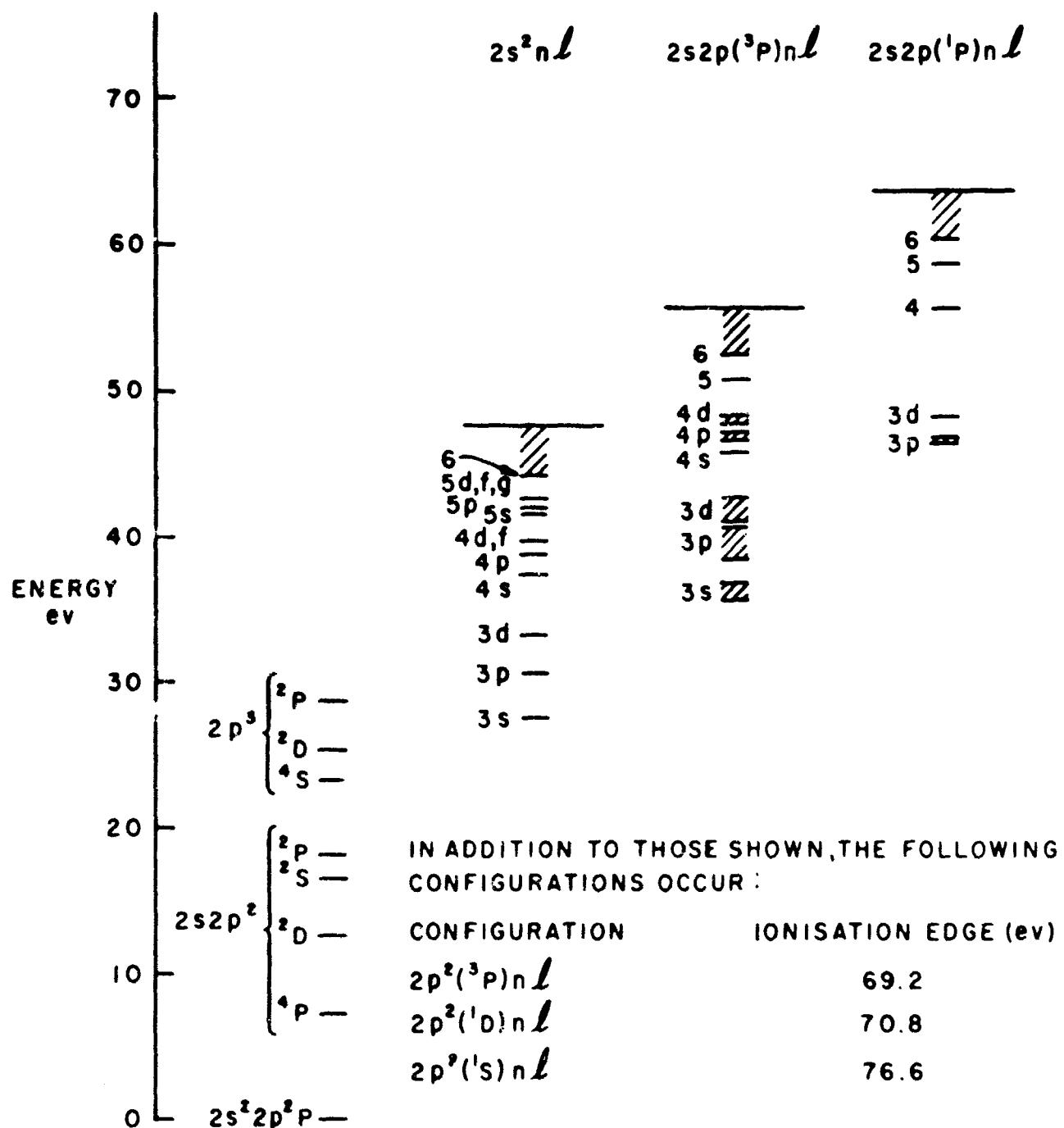
FIG. 4 SCHEMATIC DIAGRAM SHOWING THE MOST IMPORTANT
ENERGY LEVELS OF DOUBLY IONISED NITROGEN

Notes relevant to Fig. 5:

Each horizontal line shows the range of frequencies of a class of spectral lines.

For each class of spectral lines, the type of initial state is shown to the left of the plotted line.

Where parentage splitting can occur, the core term is shown in parentheses to the right of the plotted line.

Both lower and upper states are shown for same-shell transitions.

Within each spectrum, the plotted lines are arranged in vertical order approximately according to the energy of the initial state. Apart from this arrangement, the vertical distribution has no significance.
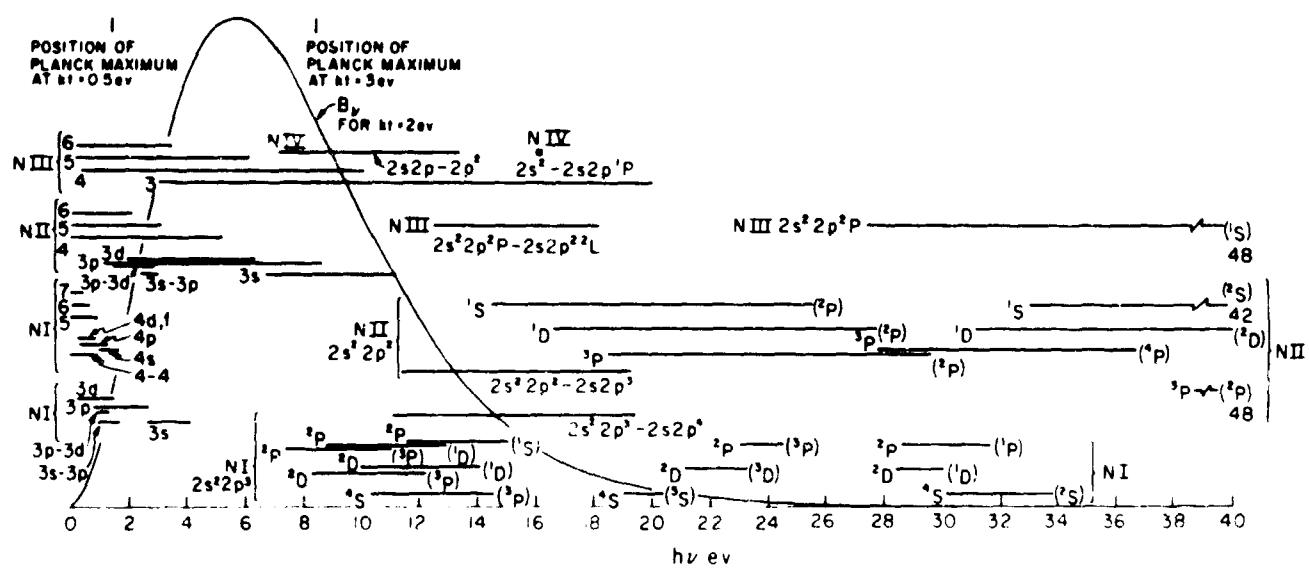
FIG 5 SCHEMATIC DIAGRAM SHOWING THE PLANCK FUNCTION AND THE DISTRIBUTION OVER FREQUENCY OF THE LINES OF THE FIRST FOUR NITROGEN SPECTRA
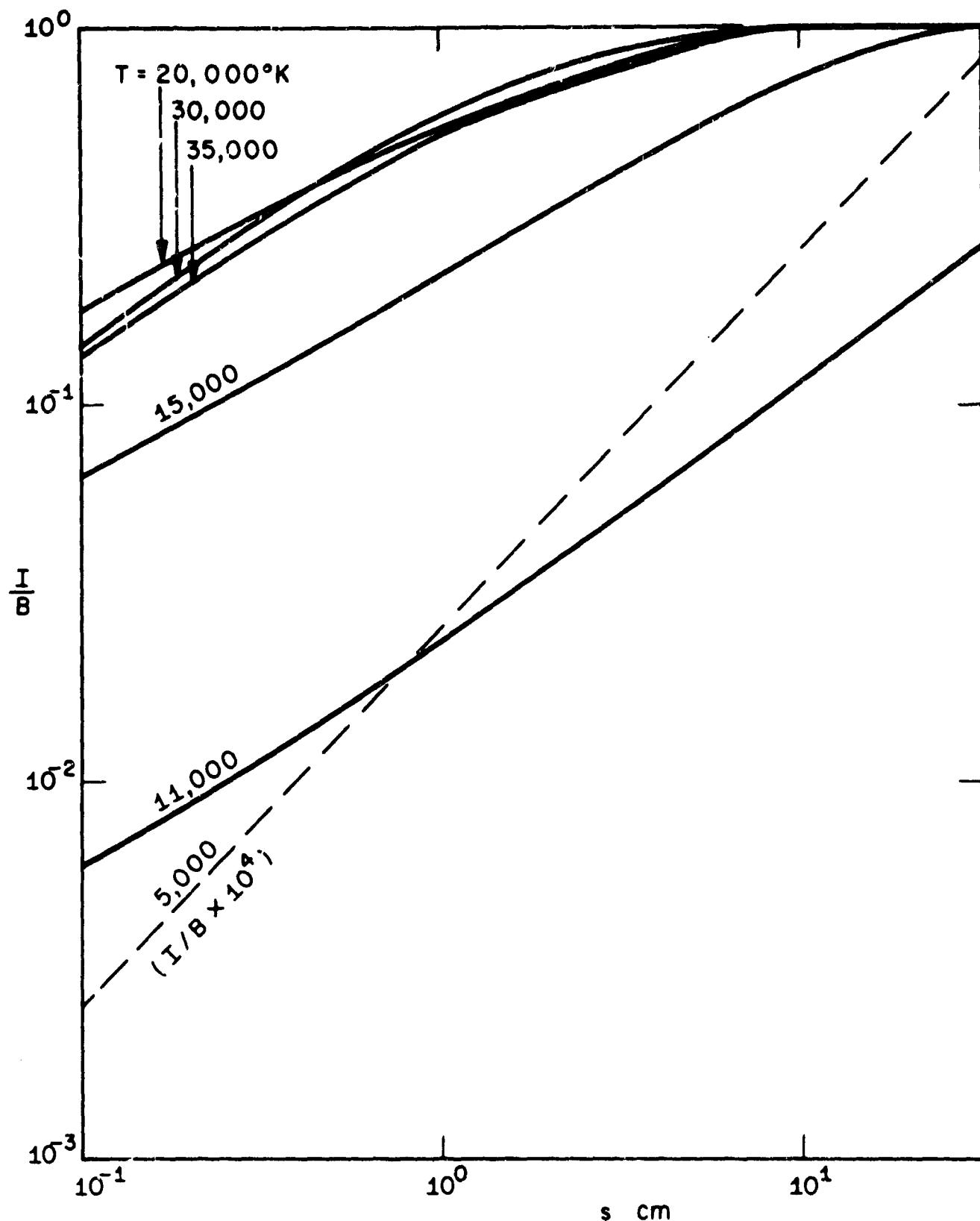
FIG. 6a   RATIO OF FREQUENCY INTEGRATED INTENSITY
TO BLACK-BODY INTENSITY AS A FUNCTION OF
PATH LENGTH

$$\frac{\rho}{\rho_0} = 10^{-1}$$
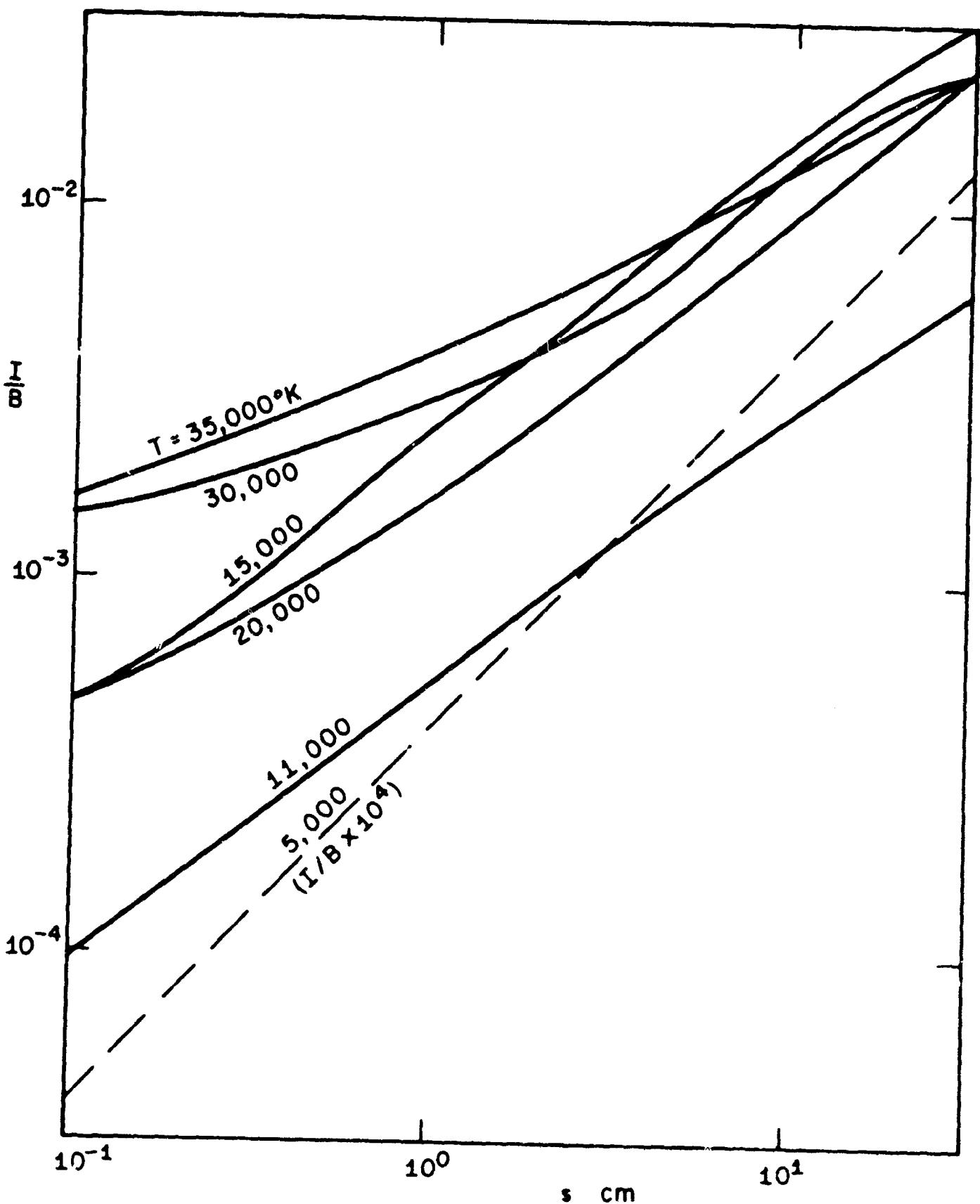
FIG. 6b $\dfrac{\rho}{\rho_0} = 10^{-3}$
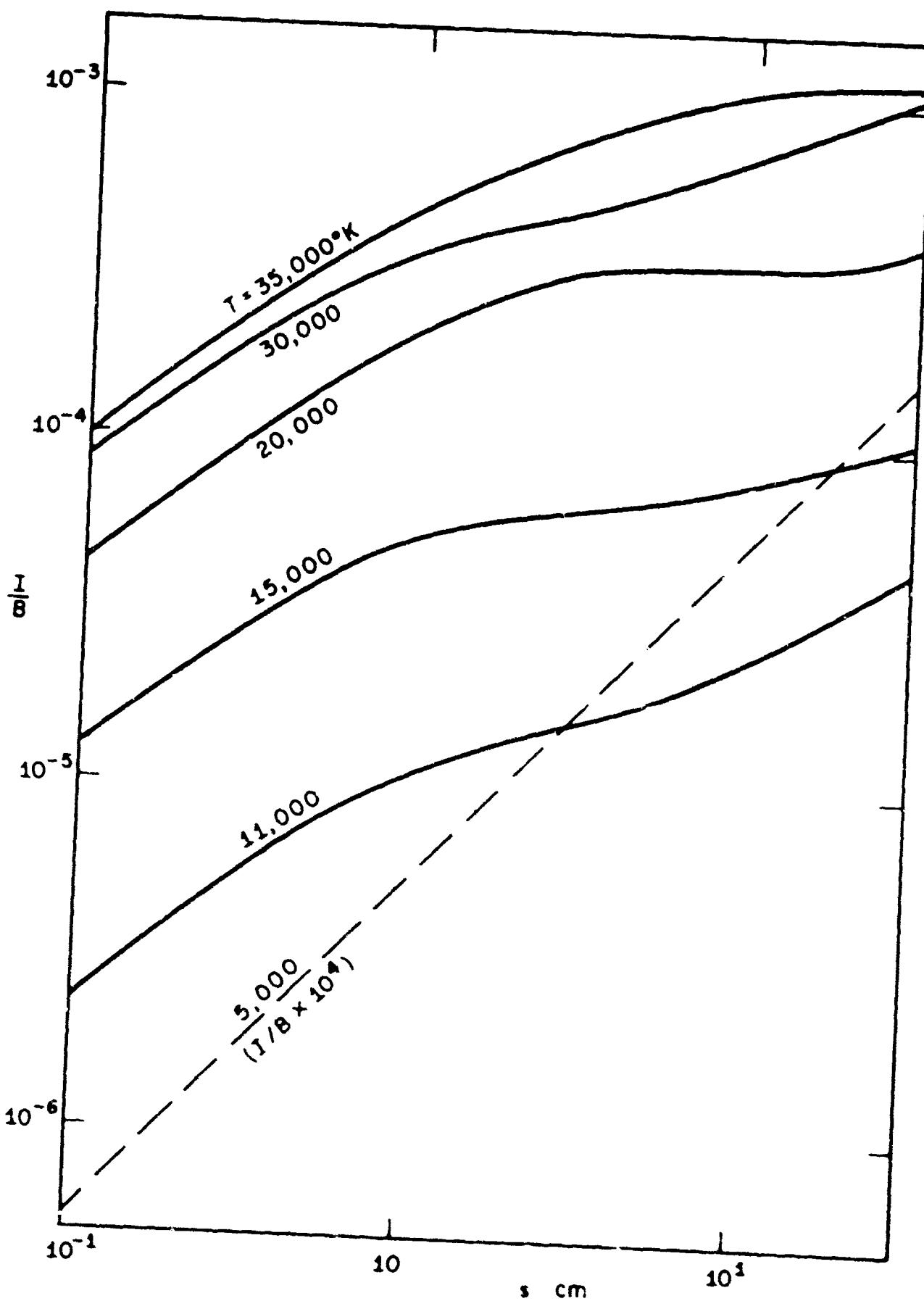
FIG. 6c $\dfrac{\rho}{\rho_0} = 10^{-5}$
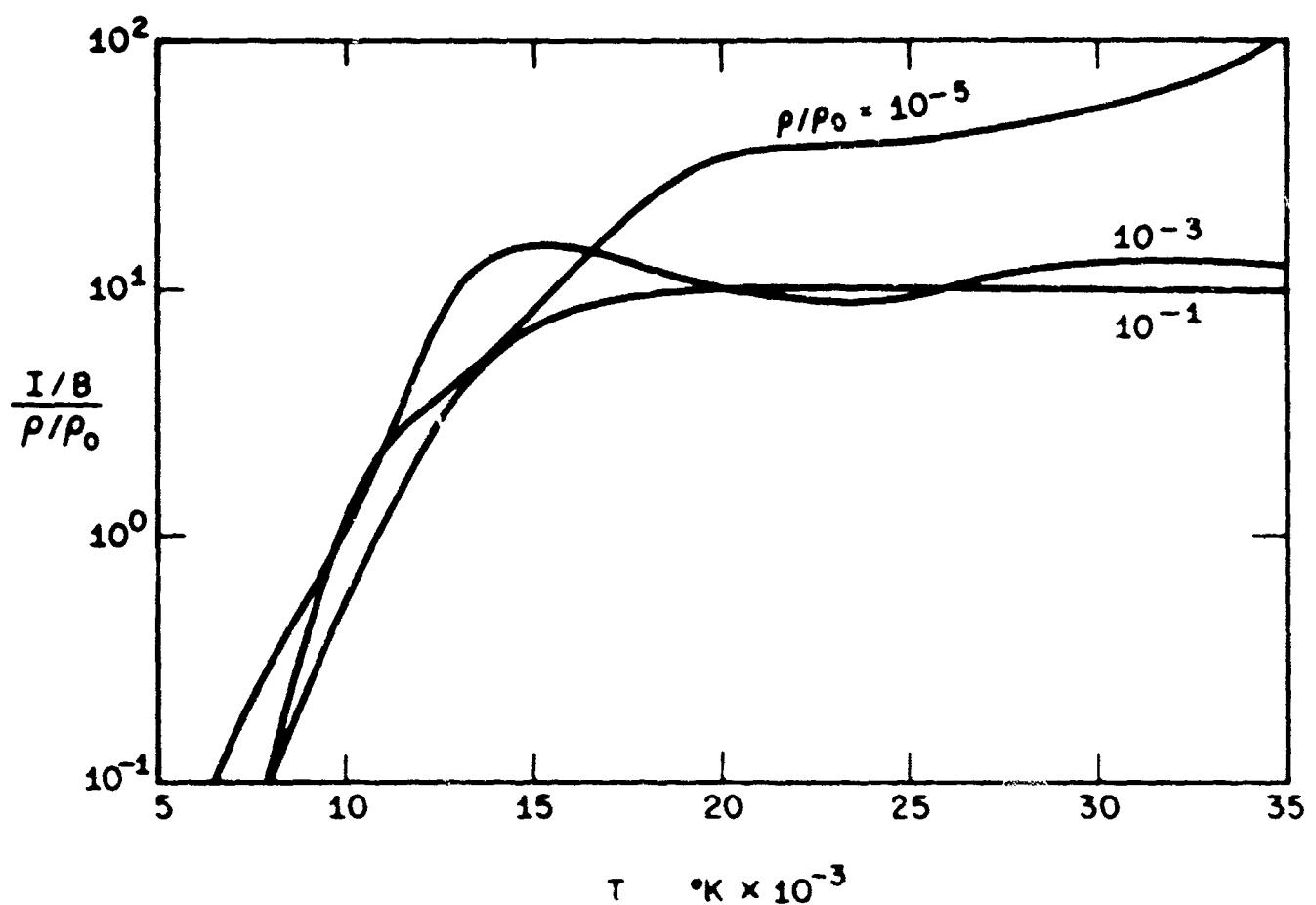
FIG. 7 RATIO OF FREQUENCY INTEGRATED INTENSITY
TO BLACK-BODY INTENSITY DIVIDED BY DENSITY
AS A FUNCTION OF TEMPERATURE FOR
PATH LENGTH = 10 cm
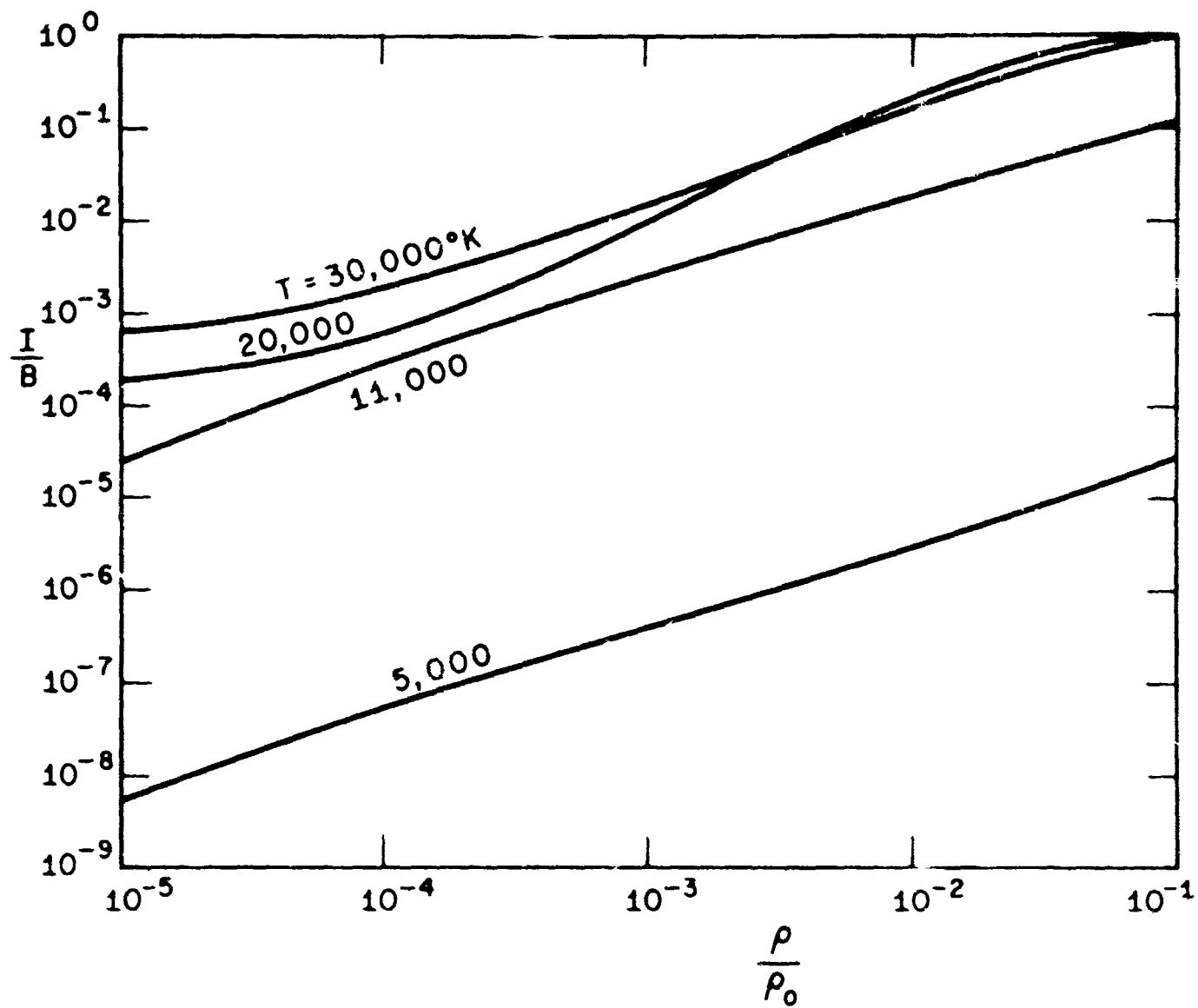
FIG. 8 RATIO OF FREQUENCY INTEGRATED INTENSITY
TO BLACK-BODY INTENSITY AS A FUNCTION OF
DENSITY FOR
PATH LENGTH s = 10 cm

A key to the symbols of Figs. 9 to 11

may be found in Table 4.1
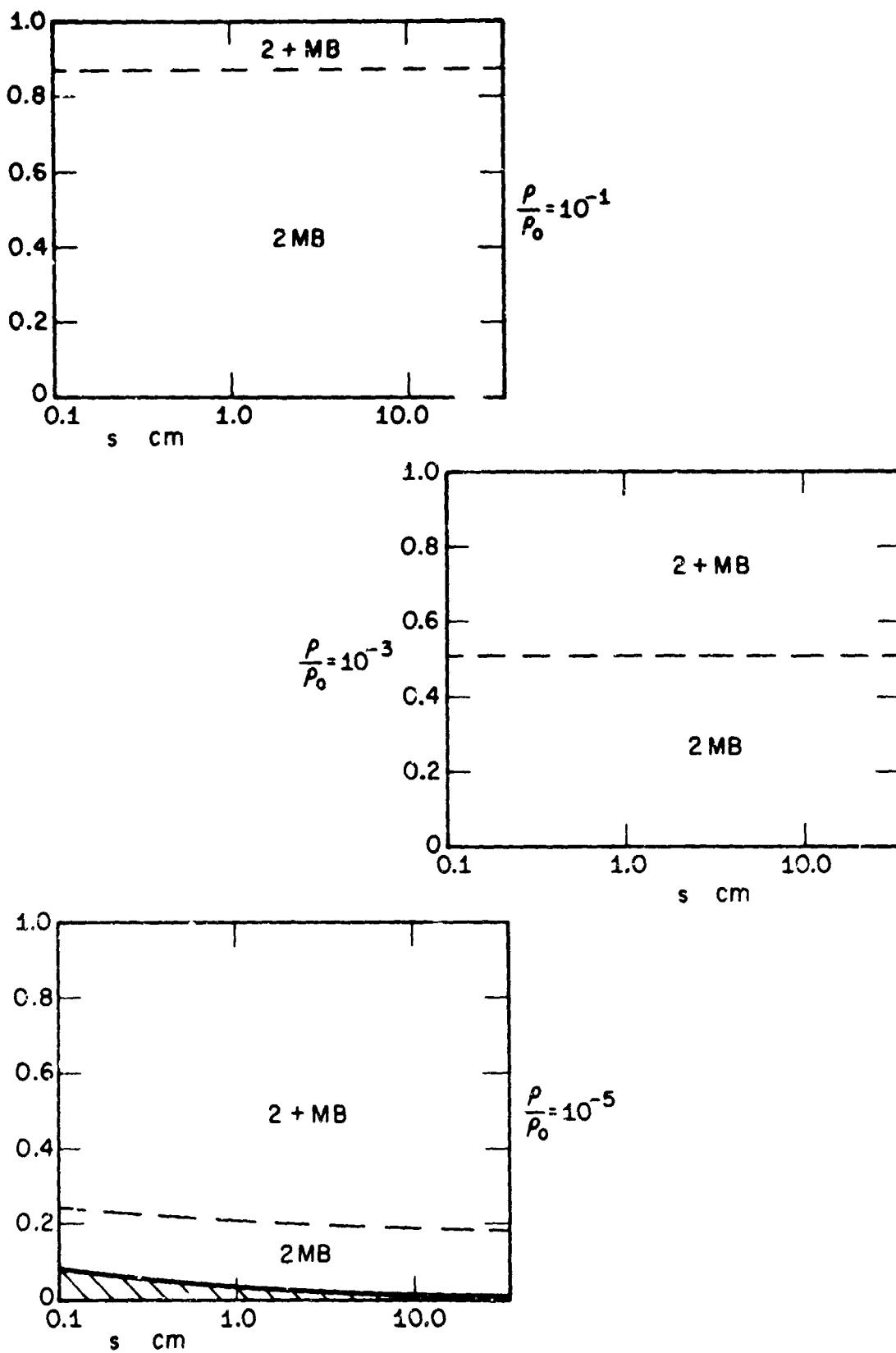
FIG. 9a DISTRIBUTION OF RADIATIVE INTENSITY
OVER INDIVIDUAL CONTRIBUTORS AS A
FUNCTION OF PATH LENGTH FOR
TEMPERATURE, T=5,000°K
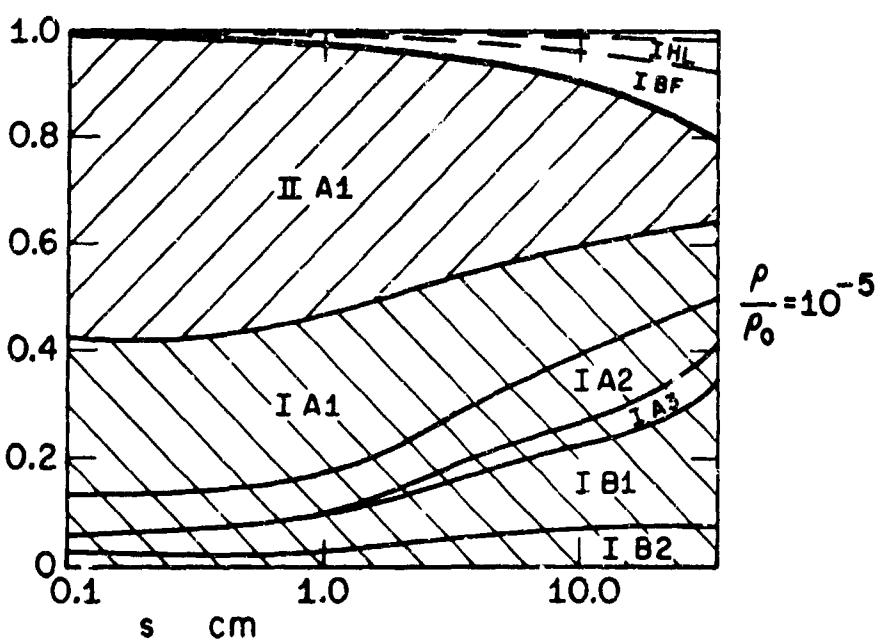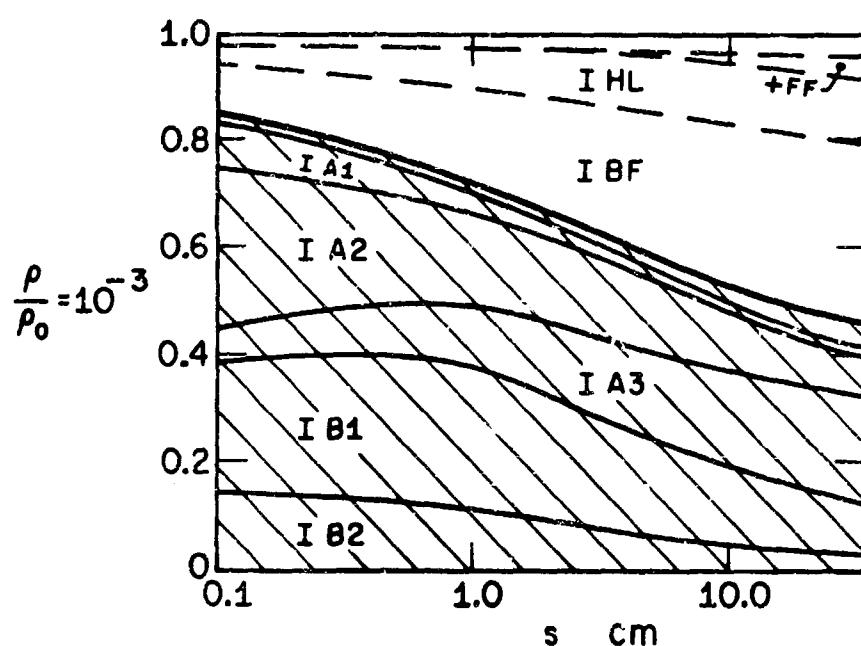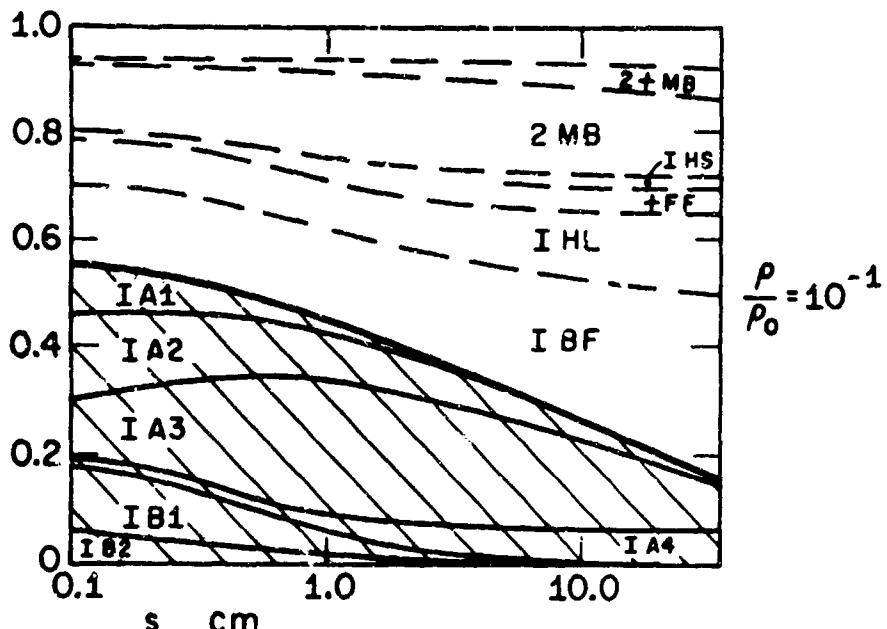
FIG. 9b T=11,000°K
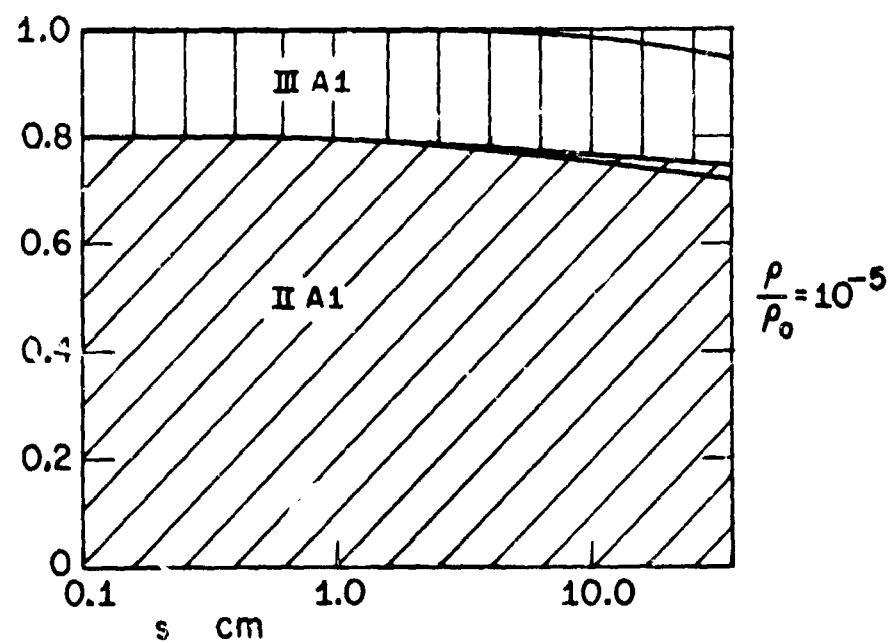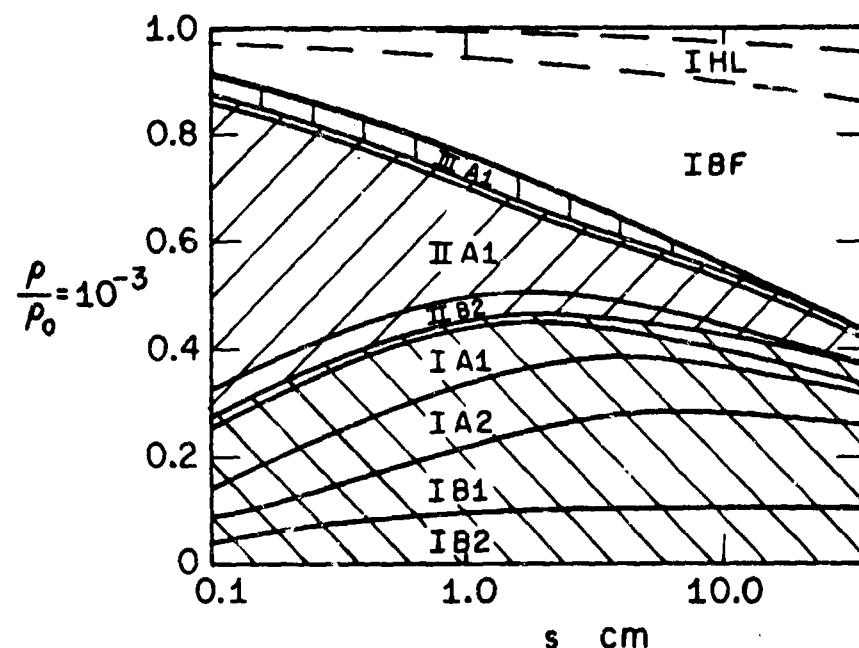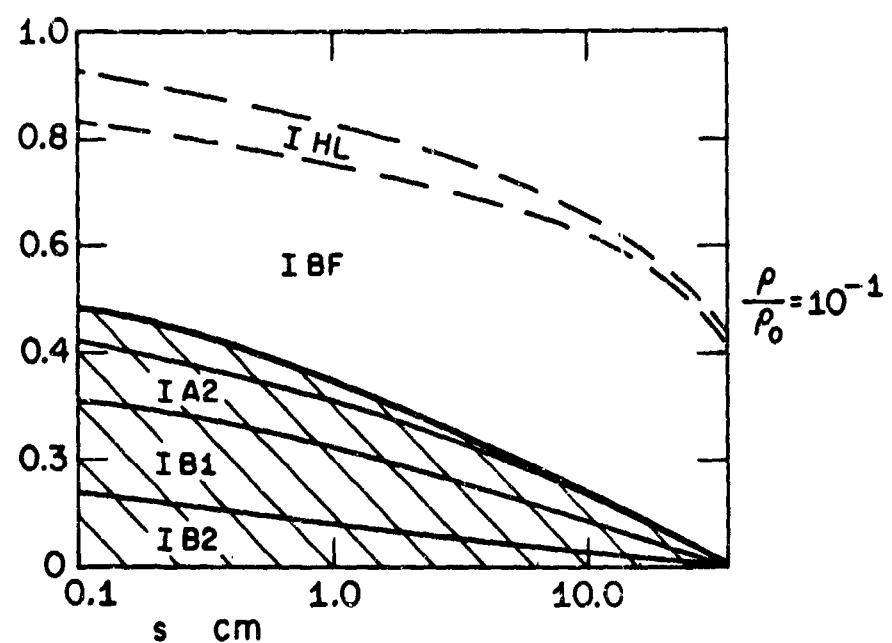
FIG. 9c   T = 20,000 °K
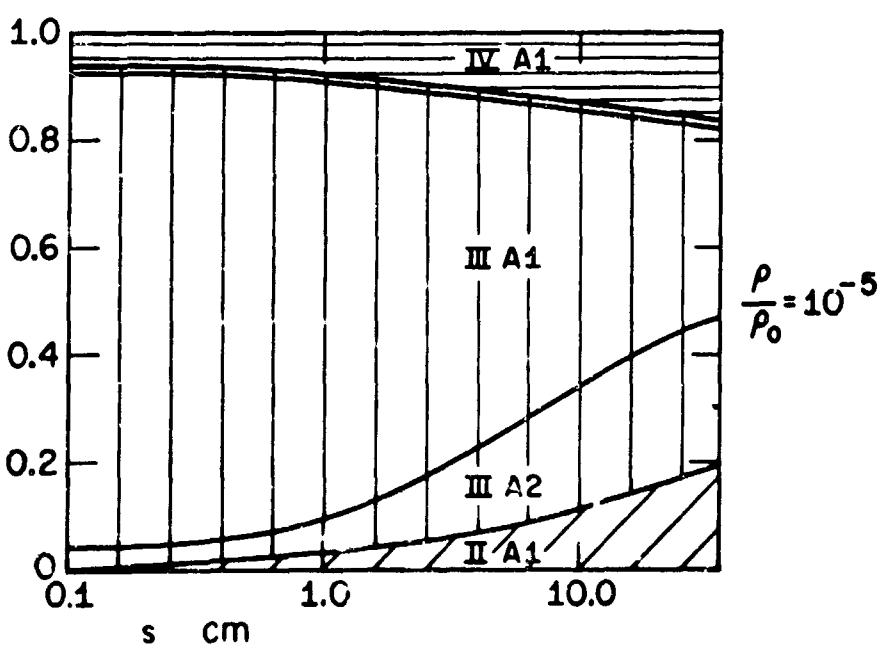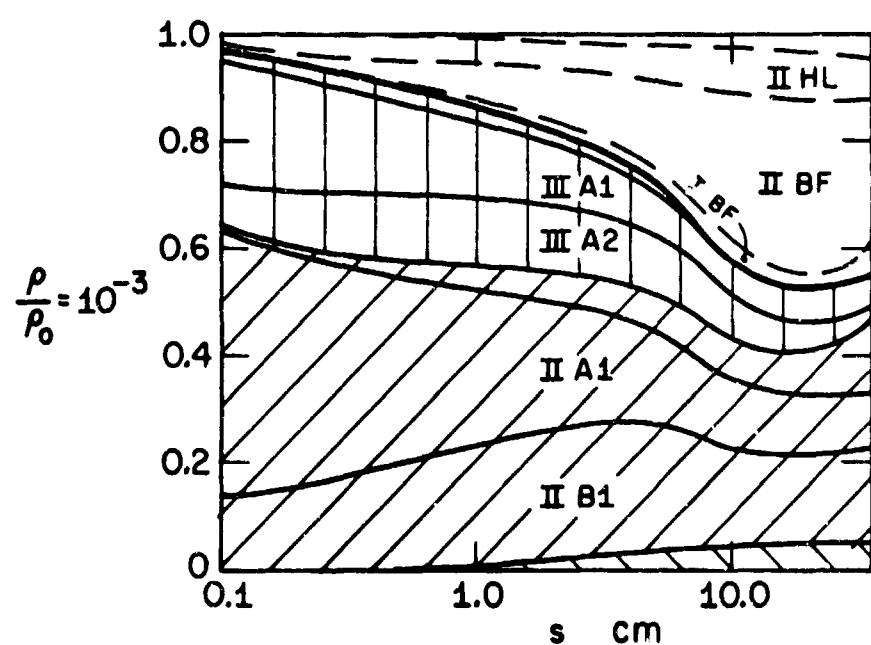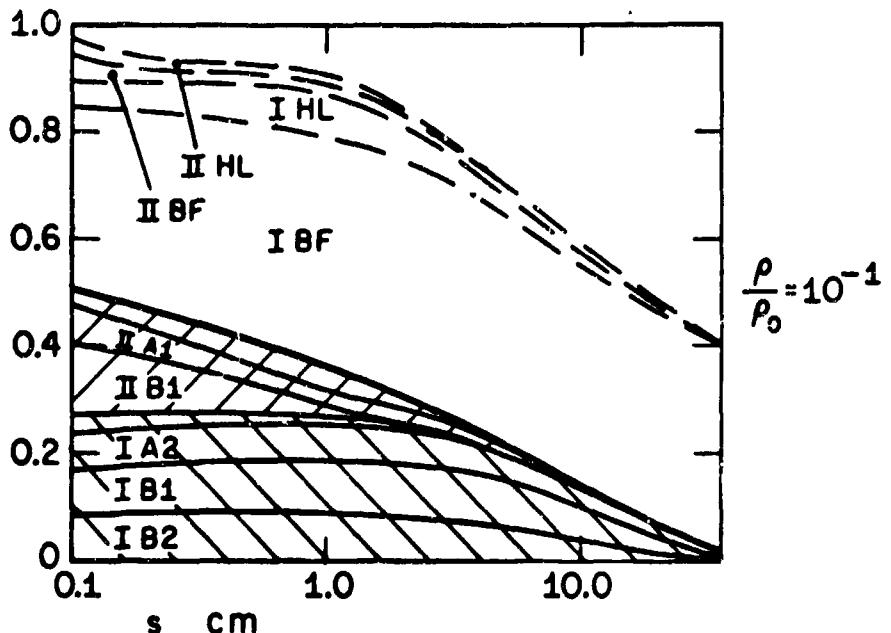
FIG. 9d T = 30,000 °K
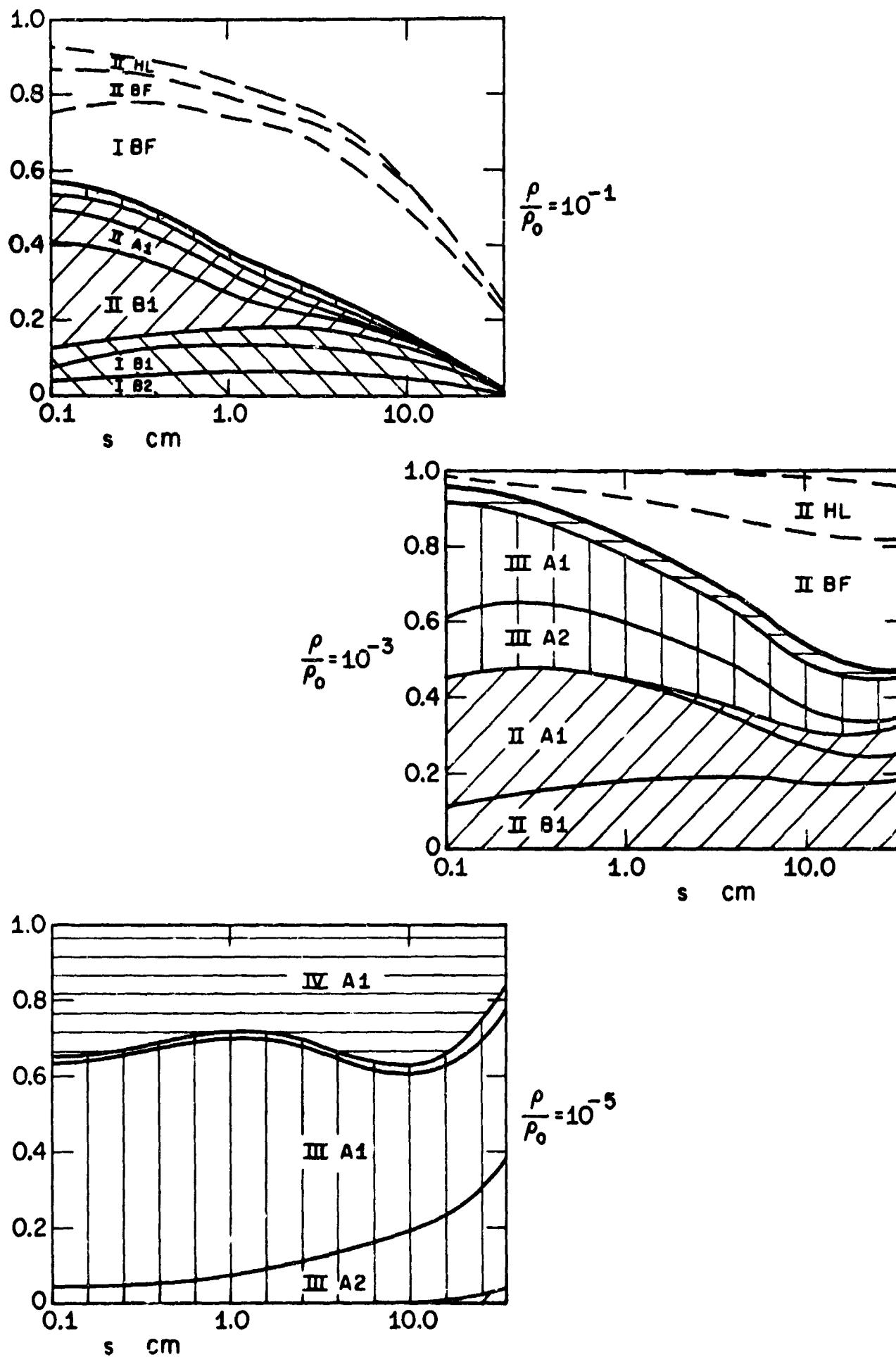
FIG. 9e T = 35,000°K
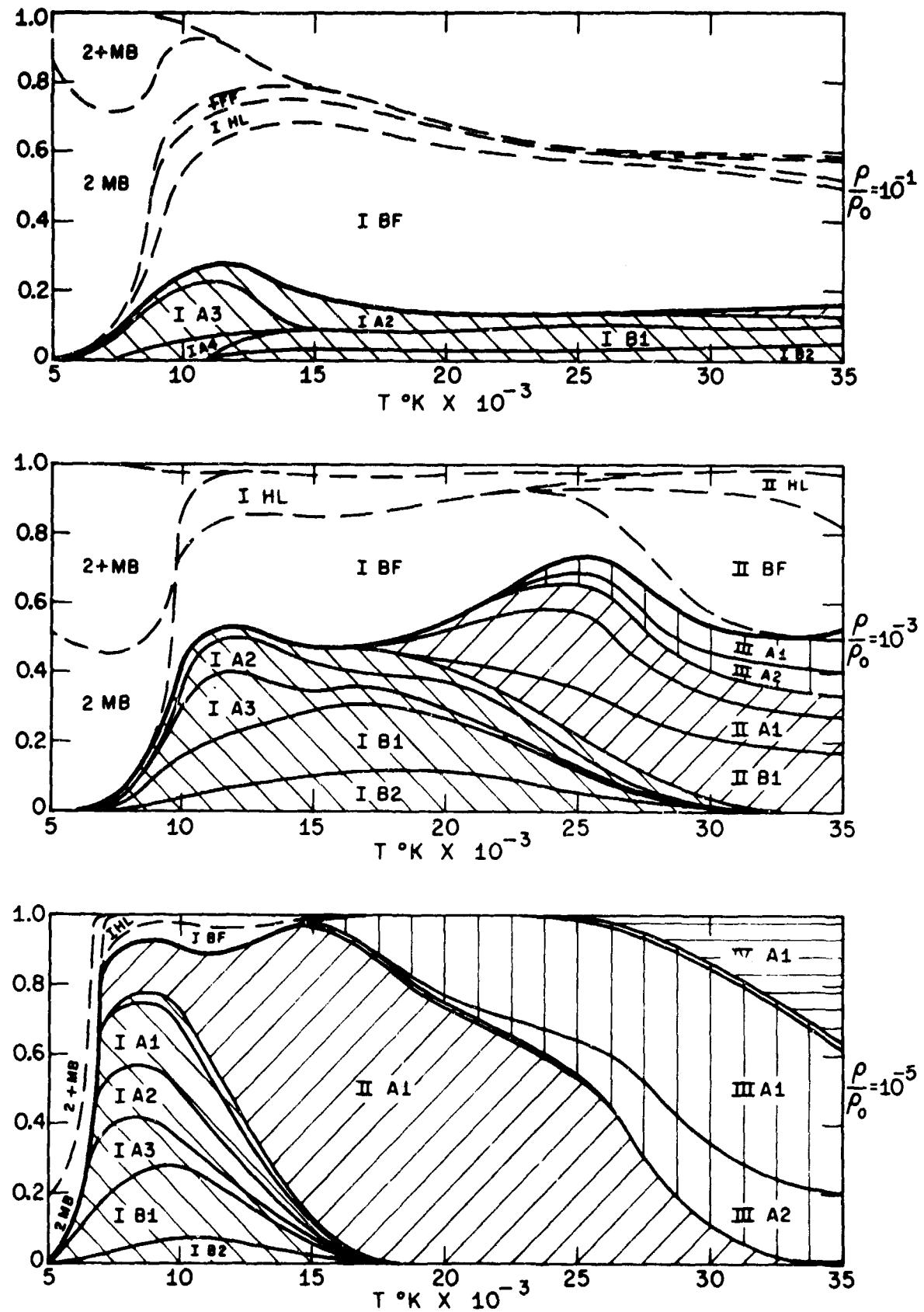
FIG. 10 DISTRIBUTION OF RADIATIVE INTENSITY
OVER INDIVIDUAL CONTRIBUTORS AS A
FUNCTION OF TEMPERATURE FOR
PATH LENGTH, s = 10 cm
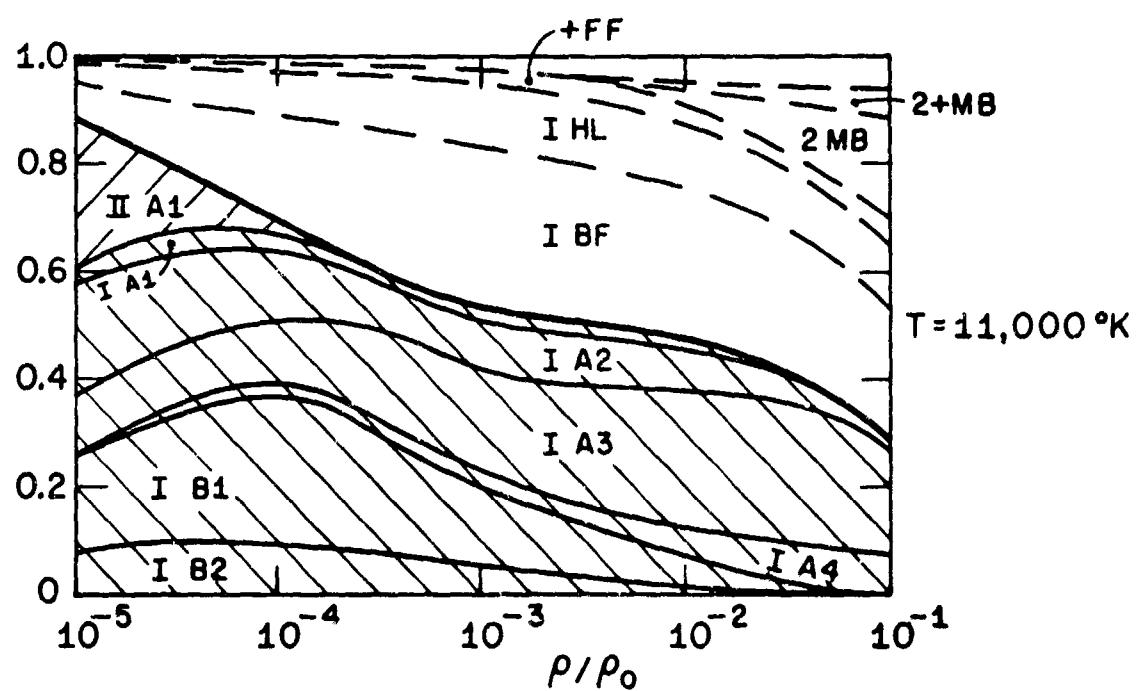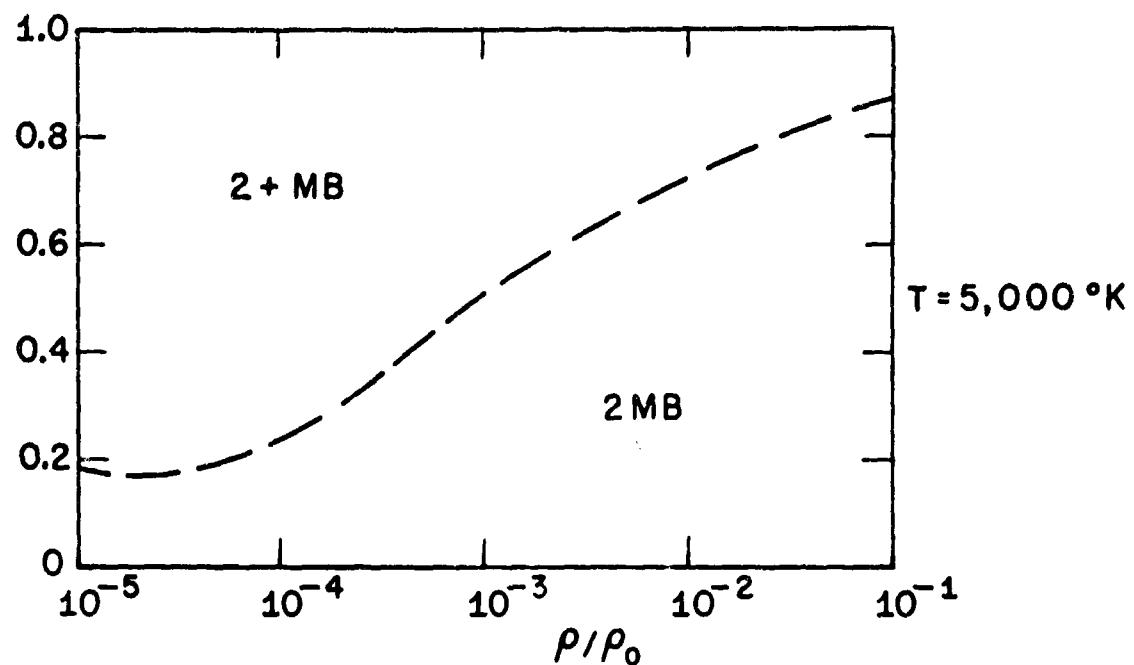
FIG.II DISTRIBUTION OF RADIATIVE INTENSITY
OVER INDIVIDUAL CONTRIBUTORS AS A
FUNCTION OF DENSITY FOR
PATH LENGTH, s = 10 cm
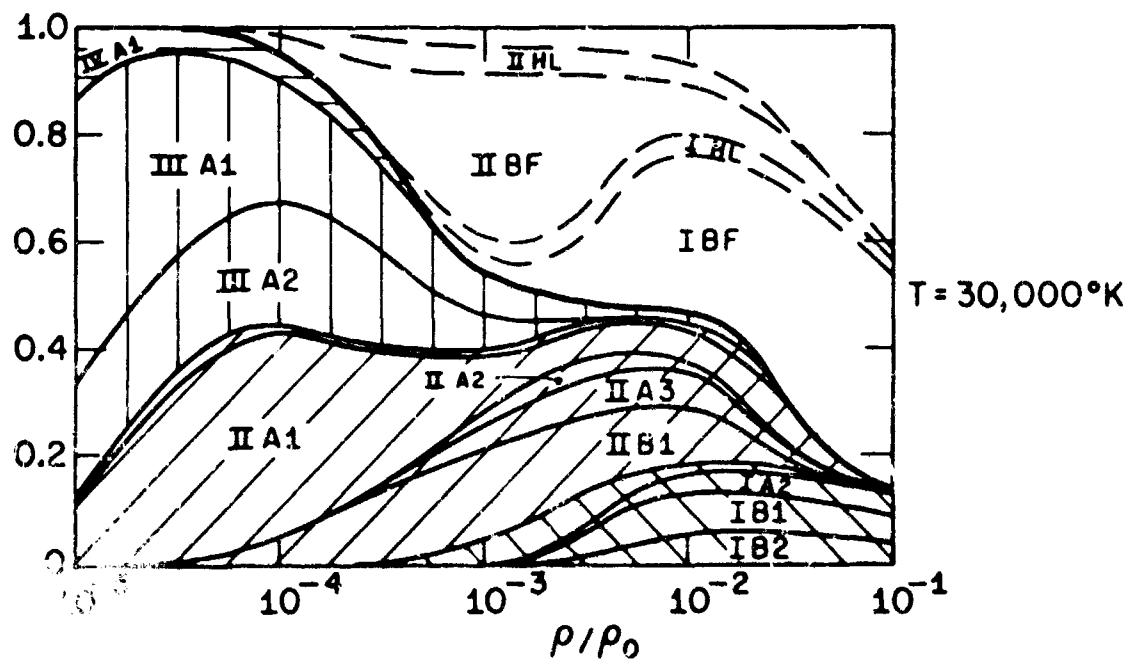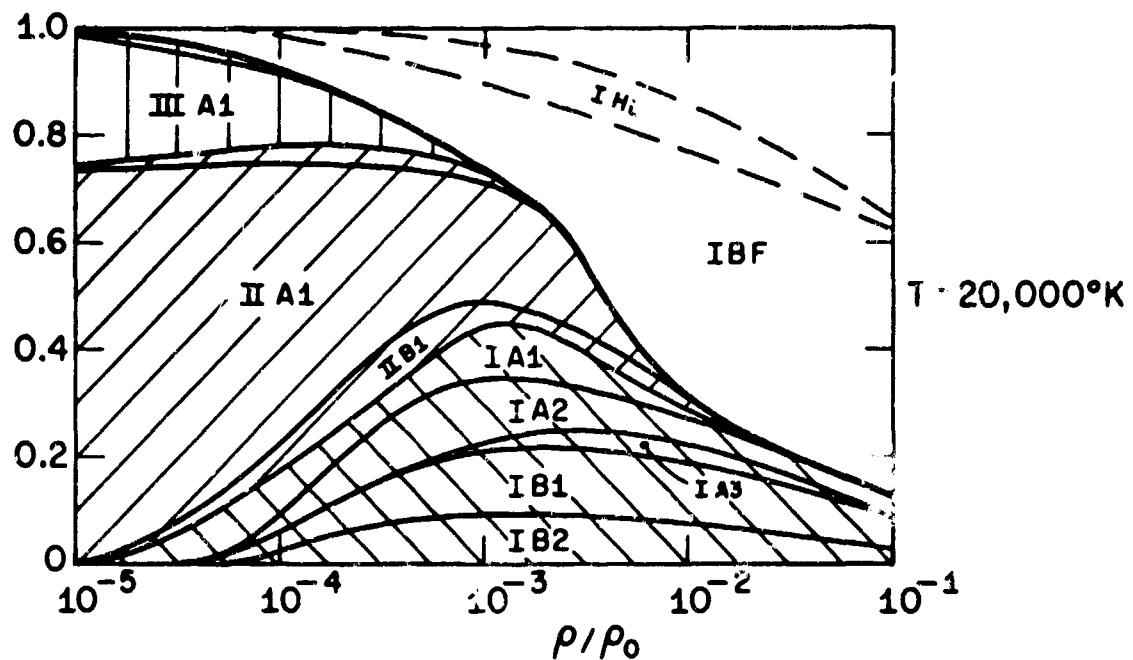
FIG. 11 (continued)

115
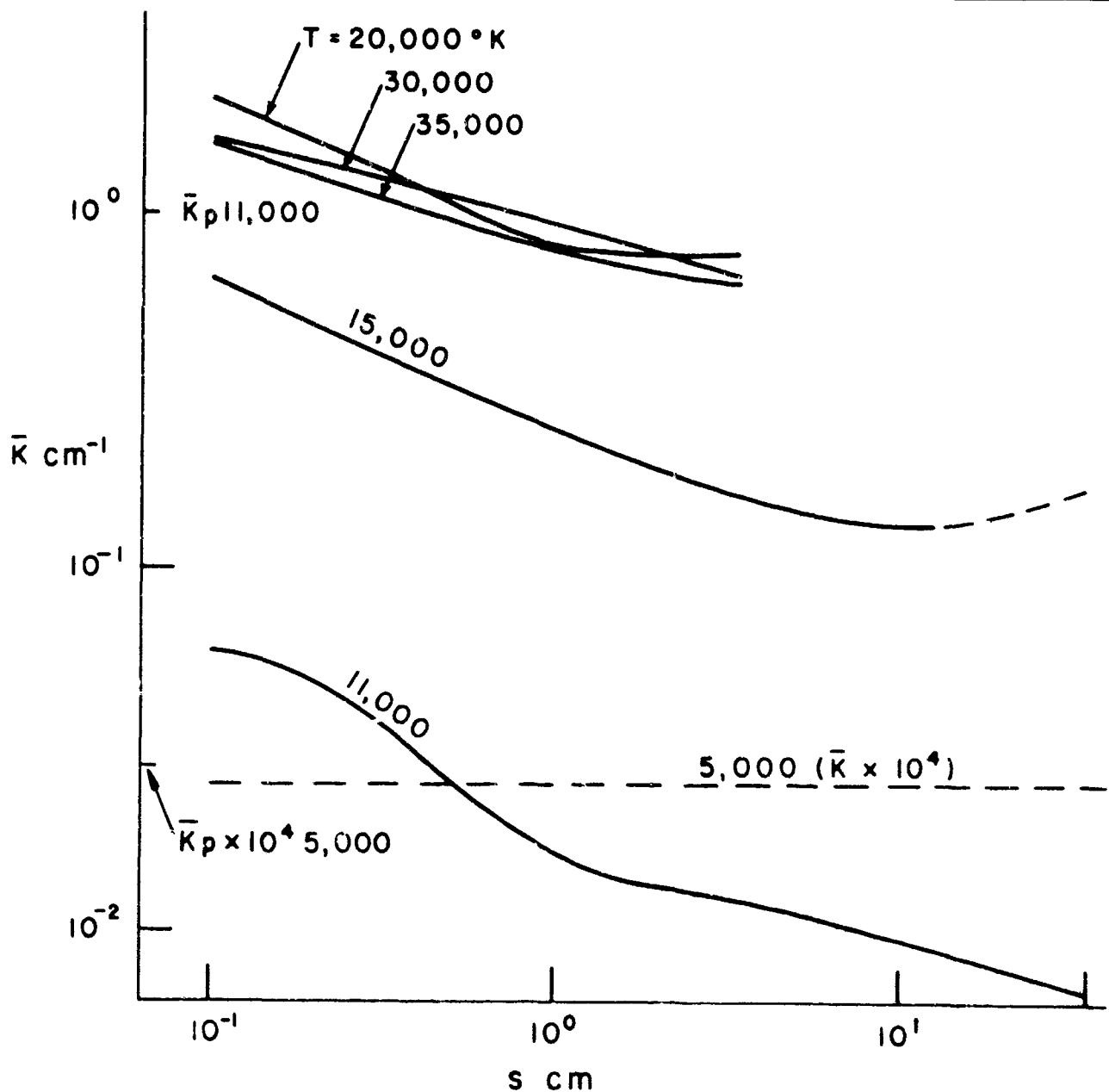
FIG. 12a ABSORPTION COEFFICIENT FOR AN
EQUIVALENT GRAY GAS AS A FUNCTION OF
PATH LENGTH.

$$\frac{\rho}{\rho_0} = 10^{-1}$$

VALUES OF PLANCK MEAN ABSORPTION COEFFICIENT

| T°K	5,000	11,000	15,000	20,000	30,000	35,000
K_p cm^{-1}	6.56×10^{-8}	8.60×10^{-3}	2.63×10^{-2}	6.35×10^{-2}	1.63×10^{-1}	1.42×10^{-1}
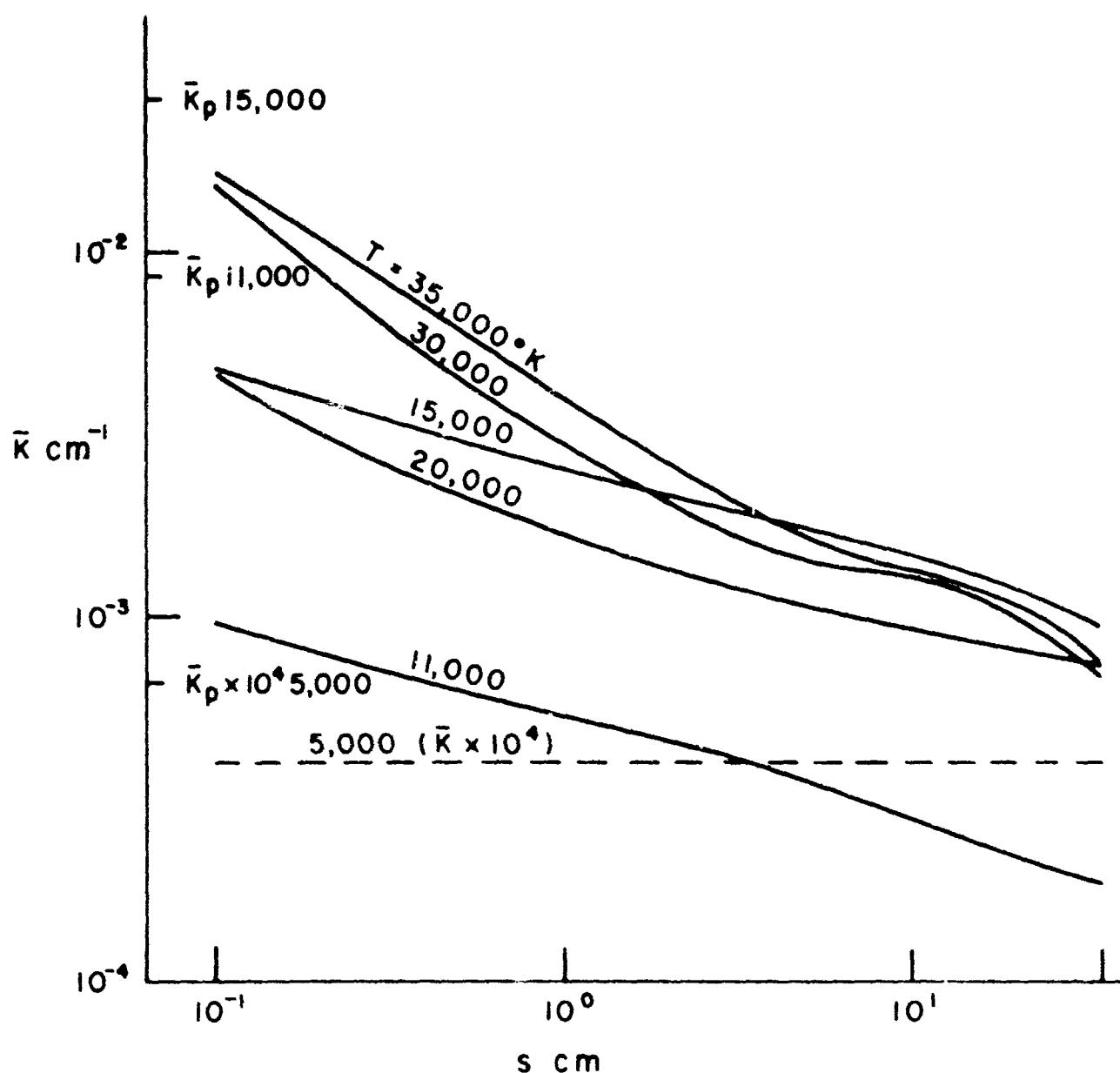
FIG. 12 b $\dfrac{\rho}{\rho_0} = 10^{-3}$

VALUES OF PLANCK MEAN ABSORPTION COEFFICIENT

| T °K	5,000	11,000	15,000	20,000	30,000	35,000
$\bar{K}_p$ cm^{-1}	2.28×10^{-9}	3.62×10^{-5}	1.88×10^{-4}	5.65×10^{-4}	1.30×10^{-3}	1.55×10^{-3}
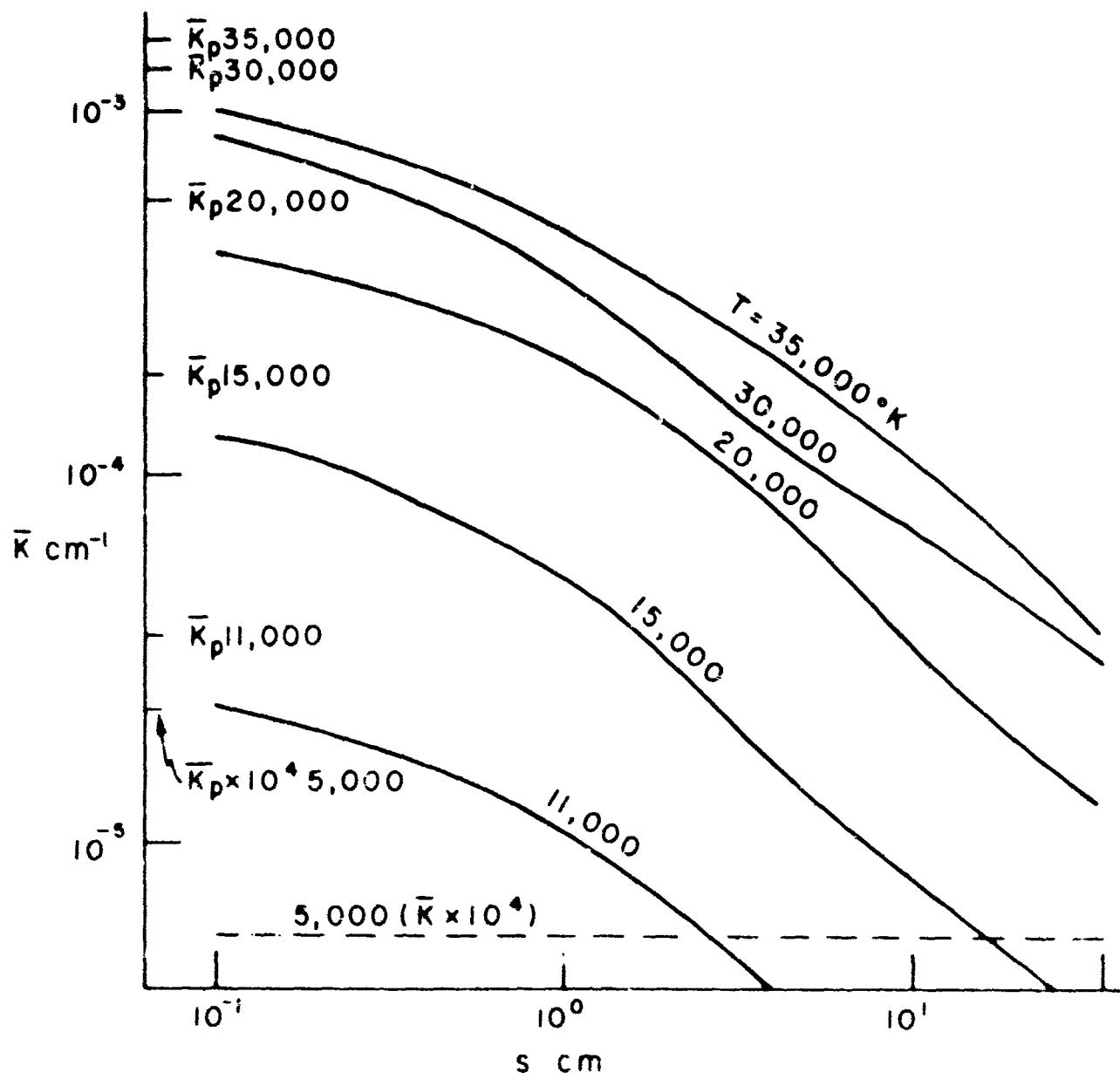
FIG. 12 c $\dfrac{\rho}{\rho_0}=10^{-5}$
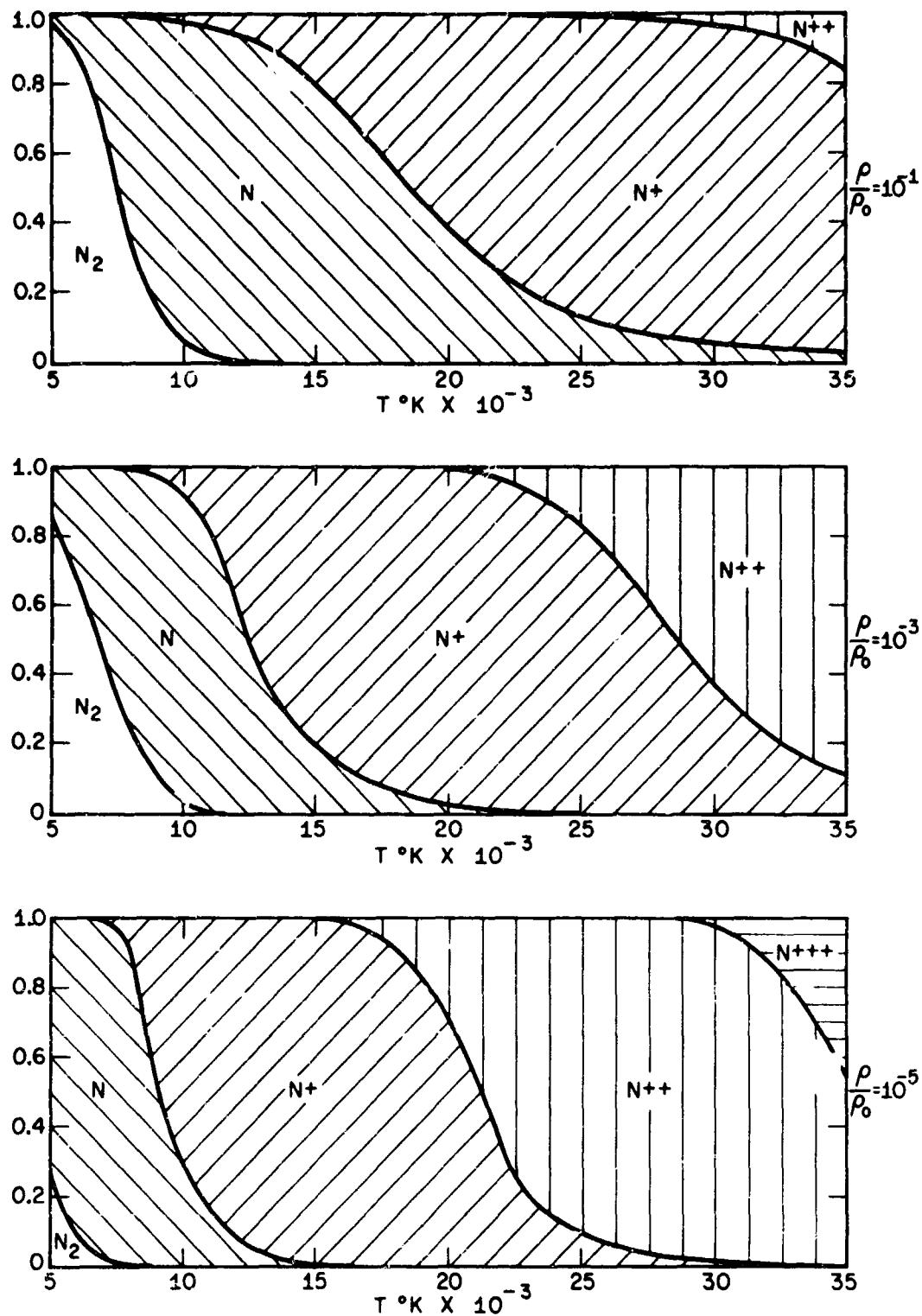
FIG. 13 DISTRIBUTION OF PARTICLE NUMBER
DENSITIES OF RADIATING SPECIES OVER
INDIVIDUAL CONTRIBUTORS AS A
FUNCTION OF TEMPERATURE.

NOTE: THE PARTICLE NUMBER DENSITY OF
N_2^+ IS NEVER SUFFICIENTLY HIGH TO APPEAR
ON THIS REPRESENTATION
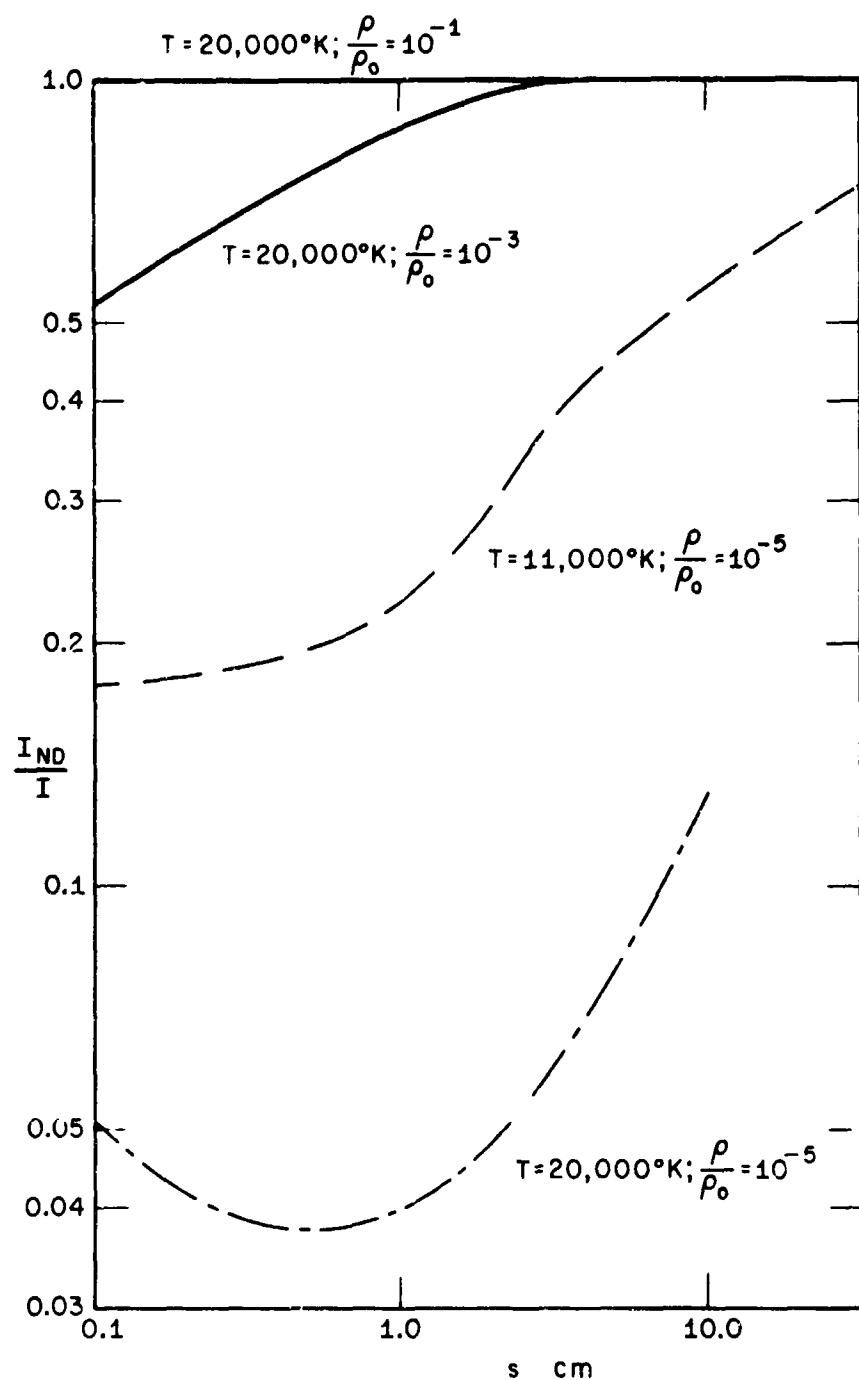
FIG. 14 THE INFLUENCE OF DOPPLER
BROADENING ON THE TOTAL
INTENSITY FROM NITROGEN GAS.
I_{ND} IS THE TOTAL INTENSITY
WHEN DOPPLER BROADENING OF
THE LINES IS OMITTED.
I IS THE TOTAL INTENSITY WHEN
DOPPLER BROADENING OF THE
LINES IS INCLUDED.

DOCUMENT CONTROL DATA - R&D		
(Security classification of title, body of abstract and indexing annotation must be entered when the overall report is classified)		

1 ORIGINATING ACTIVITY (Corporate author)	2a. REPORT SECURITY CLASSIFICATION
	Unclassified
Brown University, Providence, R. I. 02912	2b GROUP

3. REPORT TITLE

RADIATIVE TRANSFER IN A GAS OF UNIFORM PROPERTIES
IN LOCAL THERMODYNAMIC EQUILIBRIUM
PART 3:   A DETAILED CALCULATION FOR NITROGEN

4. DESCRIPTIVE NOTES *(Type of report and inclusive dates)*

5. AUTHOR(S) *(Last name, first name, initial)*

Hunt, Brian L. and Sibulkin, Merwin

6. REPORT DATE	7a. TOTAL NO. OF PAGES	7b. NO. OF REFS
December, 1966	119	32

8a. CONTRACT OR GRANT NO.	9a. ORIGINATOR'S REPORT NUMBER(S)
Nonr 562(35)	
b. PROJECT NO.	Nonr 562(35)/18
Task NR 061-132	
c.	9b. OTHER REPORT NO(S) *(Any other numbers that may be assigned this report)*
d. ARPA Project Code Number 2740	

10. AVAILABILITY/LIMITATION NOTICES

11. SUPPLEMENTARY NOTES	12. SPONSORING MILITARY ACTIVITY
	Advanced Research Projects Agency and Office of Naval Research

13 ABSTRACT

This report describes a calculation of radiative transfer in nitrogen. The
gas is uniform and in local thermodynamic equilibrium. The temperatures and
densities used in the calculations range from 5,000°K to 35,000°K and from 10^{-5}
atmospheres to 10^{-1} atmospheres respectively. Radiative transfer due to the lines
is computed by techniques developed in Part 1 of this series of reports. The
lines are classified into various groups and the contribution of each group to
the overall radiation from the gas is distinguished. The reduction in line
intensity due to the background continuum is allowed for. The intensity due to
a combination of up to 18 types of continuum and pseudo-continuum processes is
computed with exact allowance for self-absorption. The results for the total
intensity and the relative contributions of selected groups of contributors are
presented graphically. In addition, an equivalent gray gas absorption coefficient
is defined and the values presented. The results of the calculation demonstrate
that, in most cases, the atomic and ionic lines are the most important contribu-
tors. When the gas is highly ionized, the dominant contributors are a few strong
lines arising from same-shell transitions which have low-lying initial energy
levels and are situated in the near ultra violet. A further interesting and
unexpected result is that the intensities of the strongest lines are often
significantly influenced by Doppler broadening of the line profiles.

DD FORM 1473
1 JAN 64

14. KEY WORDS	LINK A		LINK B		LINK C	
	ROLE	WT	ROLE	WT	ROLE	WT
Nitrogen						
Radiative transfer						
Self-absorption						
Spectral lines						

INSTRUCTIONS

1. **ORIGINATING ACTIVITY:** Enter the name and address of the contractor, subcontractor, grantee, Department of Defense activity or other organization (*corporate author*) issuing the report.

2a. **REPORT SECURITY CLASSIFICATION:** Enter the overall security classification of the report. Indicate whether "Restricted Data" is included. Marking is to be in accordance with appropriate security regulations.

2b. **GROUP:** Automatic downgrading is specified in DoD Directive 5200.10 and Armed Forces Industrial Manual. Enter the group number. Also, when applicable, show that optional markings have been used for Group 3 and Group 4 as authorized.

3. **REPORT TITLE:** Enter the complete report title in all capital letters. Titles in all cases should be unclassified. If a meaningful title cannot be selected without classification, show title classification in all capitals in parenthesis immediately following the title.

4. **DESCRIPTIVE NOTES:** If appropriate, enter the type of report, e.g., interim, progress, summary, annual, or final. Give the inclusive dates when a specific reporting period is covered.

5. **AUTHOR(S):** Enter the name(s) of author(s) as shown on or in the report. Enter last name, first name, middle initial. If military, show rank and branch of service. The name of the principal author is an absolute minimum requirement.

6. **REPORT DATE:** Enter the date of the report as day, month, year; or month, year. If more than one date appears on the report, use date of publication.

7a. **TOTAL NUMBER OF PAGES:** The total page count should follow normal pagination procedures, i.e., enter the number of pages containing information.

7b. **NUMBER OF REFERENCES:** Enter the total number of references cited in the report.

8a. **CONTRACT OR GRANT NUMBER:** If appropriate, enter the applicable number of the contract or grant under which the report was written.

8b, 8c, & 8d. **PROJECT NUMBER:** Enter the appropriate military department identification, such as project number, subproject number, system numbers, task number, etc.

9a. **ORIGINATOR'S REPORT NUMBER(S):** Enter the official report number by which the document will be identified and controlled by the originating activity. This number must be unique to this report.

9b. **OTHER REPORT NUMBER(S):** If the report has been assigned any other report numbers (*either by the originator or by the sponsor*), also enter this number(s).

10. **AVAILABILITY/LIMITATION NOTICES:** Enter any limitations on further dissemination of the report, other than those imposed by security classification, using standard statements such as:

(1) "Qualified requesters may obtain copies of this report from DDC."

(2) "Foreign announcement and dissemination of this report by DDC is not authorized."

(3) "U. S. Government agencies may obtain copies of this report directly from DDC. Other qualified DDC users shall request through

_____ ."

(4) "U. S. military agencies may obtain copies of this report directly from DDC. Other qualified users shall request through

_____ ."

(5) "All distribution of this report is controlled. Qualified DDC users shall request through

_____ ."

If the report has been furnished to the Office of Technical Services, Department of Commerce, for sale to the public, indicate this fact and enter the price, if known.

11. **SUPPLEMENTARY NOTES:** Use for additional explanatory notes.

12. **SPONSORING MILITARY ACTIVITY:** Enter the name of the departmental project office or laboratory sponsoring (*paying for*) the research and development. Include address.

13. **ABSTRACT:** Enter an abstract giving a brief and factual summary of the document indicative of the report, even though it may also appear elsewhere in the body of the technical report. If additional space is required, a continuation sheet shall be attached.

It is highly desirable that the abstract of classified reports be unclassified. Each paragraph of the abstract shall end with an indication of the military security classification of the information in the paragraph, represented as (*TS*), (*S*), (*C*), or (*U*).

There is no limitation on the length of the abstract. However, the suggested length is from 150 to 225 words.

14. **KEY WORDS:** Key words are technically meaningful terms or short phrases that characterize a report and may be used as index entries for cataloging the report. Key words must be selected so that no security classification is required. Identifiers, such as equipment model designation, trade name, military project code name, geographic location, may be used as key words but will be followed by an indication of technical context. The assignment of links, rules, and weights is optional.